and spelling to structure and coherence.

Of the colleagues at Saab, and for that part of anyone who have been involved in this project, Gunnar Olsson, having been my supervisor, being the project leader and constant supporter of this project, has been of paramount importance for this ever to lift from the ground. You are directing with a firm hand regardless if you need to sort out budget issues, technical details or setting the strategy and future of this project. Also many thanks to Youssef Ghoneim, you have been a great supporter and source of inspiration throughout this project. There are not many with your experience with chassis control applications in this entire industry, and having access to your knowledge is a true privilege. Further the fact that you always are available for a technical discussion has been a great contribution toward my development. Further many thanks to all the members of the chassis controls team at Saab and recently the AWD team of Anders Tysk. Being in an environment with so many experts and great colleagues in various fields cannot be valued enough.

On the cover of this thesis is the suspension and driveline of the Saab 9^3 XWD. Primarily I would like to acknowledge Magnus Rydell, who probably more than anyone was made that project happen. Thanks Magnus for allowing me to be part of the small team that did the ground work for this vehicle during early 2006. Part of that team was also Jim Hayes, who has been around since 1997 when I first joined Saab as a consultant, and who is still keeping me updated on world politics and the peaking of global oil production.

I further want to express my love and gratitude to Sara, my dear wife and friend-for-life. I have been nearly been studying as long as we have been married, and there are still a few more years to go. You are a big part of this work in all it's aspects! Tobias was born during this project and Lukas was not yet one year old when it started. You boys have been, and are, a great joy and blessing to both of us! Whenever you are able to read this, consider most that "the fear of the LORD is the beginning of knowledge", not writing a thesis.

Matthijs Klomp
Göteborg, 2007

Nomenclature

The nomenclature used in this work follows ISO standard 8855:1991 [21] for the vehicle dynamics terminology. The notations for the aerodynamic forces are adopted from SAE standard J1594 [54].

[1]Sum of wheels on that axle if force or stiffness or average of wheels on axle if angle
[2]Relative to vehicle, unless otherwise stated

Super-/subscript	**Description**
0	Reference
1	Front left wheel
2	Front right wheel
3	Rear left wheel
4	Rear right wheel
F	Front axle [1]
R	Rear axle
$\mathrm{F/R}$	Front to rear
$\mathrm{L/R}$	Left to right
i	Counter index
IN	Input from power source
lim	Value at which variable saturates or peaks
ss	Steady-state
X	Longitudinal, positive forward [2]
Y	Lateral, positive to left
Z	Vertical, positive upward
W	In wheel coordinate system
$\dot{.}$	Derivation of variable with respect to time
$\ddot{.}$	Second time derivative

Table 1: Indices

Variable	**Unit**	**Description**
α	[rad]	Tire slip angle
β	[rad]	Body slip angle
γ	[-]	Ratio between front and total roll stiffness
δ	[rad]	Wheel steered angle
δ_{H}	[rad]	Steering-wheel angle
δ_{D}	[rad]	Ackerman steering angle (l/R).
φ	[rad]	Roll angle
θ	[rad]	Pitch angle
ψ	[rad]	Yaw angle
τ	[s]	Time constant
κ	[-]	Longitudinal tire slip
μ	[-]	Ratio between peak tangential force and normal force; the friction coefficient.
σ	[-]	Relative tire slip
ξ	[-]	Ratio between front and total drive force
ω	[rad/s]	Rotational velocity
Ω	[rad/s]	Rotational velocity of (vehicle) reference frame relative to a inertial system.

Table 3: Greek variables

Variable	Unit	Description
A	n/a	Jacobian respect to state variables
a	[m/s^2]	Acceleration
b	[m]	Track width; distance between left and right wheel
B	n/a	Jacobian with respect to input(s)
C	n/a	State variables $\rightarrow$ output transformation matrix
C_α	[N/rad]	Cornering stiffness
c_α	[-/rad]	Cornering stiffness normalized with vertical force
d	[Ns/m] or [Nms/rad]	Damping
F	[N]	Force
F_D	[N]	Drag force
g	[m/s^2	Gravitational acceleration
i_S	[-]	Steering ratio
k	[N/m] or [Nm/rad]	Stiffness
K_US	[rad s^2/m^2]	Understeer gradient
M	[Nm]	Moment
l	[m]	Wheelbase; distance between front- and rear axle
l_F	[m]	Distance from front axle to center of mass (CoM)
l_R	[m]	Distance from rear axle to CoM
R	n/a	Transformation (rotation) matrix
R	[m]	Corner radius
h	[m]	Vertical distance from CoM to ground
h_0	[m]	Vertical distance from CoM to roll- & pitch axis
n	[-]	Gear ratio
$\boldsymbol{u}$	n/a	Input variable(s)
v	[m/s]	Speed
$\boldsymbol{x}$	n/a	State variables
$\boldsymbol{y}$	n/a	Output variables

Table 4: Latin variables

Table of contents

Chapter 1

Introduction

1.1 Background

Vehicle dynamics, is the theory of how tire and aerodynamic forces acting on a vehicle affect the vehicle's motion, response, stability, and other characteristics. Ever since motor vehicles started traveling on roads, this research field has increased in importance for road vehicles. In its infancy, the main focus was on improving brakes and tires due to the demands of increased vehicle speed. Early developments include preventing the rear wheels from locking prior to the front wheels (a common cause of vehicle instability up to that point) through brake proportioning. Later, electronic control of the vehicle dynamics was introduced through anti-lock braking systems (ABS), which prevented the wheels to lock during hard braking thereby improving stability and shorter braking distance, as well as permitting the driver to maintain steer-ability. From ABS systems, traction control systems (TCS) were developed, which prevent wheel spin while accelerating. This is particularly useful on surfaces with different friction on each driven wheel. This electronic control of the brake system eventually lead to electronic stability control (ESC) systems. ESC uses autonomous brake intervention to steer the vehicle with the brakes in a situation when too large a deviation from the intended direction is detected by the system.

In its most recent development, vehicle dynamics has expanded to include active control of steering, driveline, and suspension sub-systems. Among these, this thesis focuses on the the study of controlling active all-wheel drive (AWD) systems. Even though AWD systems are almost as old as the automobile itself, they have so far been passive, i.e. not electronically controllable. Moreover, the purpose of these systems have changed from a pure traction aid for off-road conditions to the introduction in passenger cars for the improved use of the available grip on standard roads [28]. One current development in the field of drive force

distribution, is the advent of electronically controlled driveline systems. These active driveline systems enable the drive force distribution to be optimized for a much wider range of operating conditions when compared to passive systems with fixed characteristics.

As much as active driveline control offers opportunities to change and improve the vehicle characteristics, it is an area which has not been systematically analyzed to any great extent, as is discussed further in this chapter. This present work is motivated by the need to further explore the subject of combined longitudinal (drive/brake) and lateral (cornering) forces for the purpose of improving the control and design of active driveline systems.

1.2 The Importance of Understeer and Lateral Grip Limits of Road Vehicles

The subject of vehicle dynamics is of great interest to the development of road vehicles in general and also for its active subsystems. In the field of vehicle dynamics, vehicle handling deals with the study of a vehicle's response to input(s) from the driver. Two important aspects in the field of vehicle handling are the understeer and lateral grip limits of a vehicle. The understeer of the vehicle can be defined as how much the driver needs to change the steering input to maintain a constant radius as the vehicle speed is increased. Understeer is therefor an important feedback to the driver. A different way of viewing the understeer, but leading to the same result as with the previous definition, is how much the cornering radius changes with vehicle speed when the steering input is held constant. The understeer of the vehicle itself is determined by the rate at which the lateral forces are generated at the tire contact patches of each axle and are limited by tire/road capacity, the latter defined as the grip or friction limit. Furthermore, as much as the understeer is important for the driver, the vehicle itself is limited by the utilizable lateral grip. The lateral grip is of great importance since it, for instance, determines if an obstacle can be avoided [6], or if the vehicle can successfully negotiate a given road curve.

For the purpose of vehicle control, it is essential to always know the desired (or target) vehicle behavior based on driver inputs. Hiemer [18] notes that the anticipation of average drivers to a vehicle's response to his/her input can be viewed as the handling characteristics of a vehicle where the tires are in the linear range of operation. This anticipation can be modeled with a linear dynamic model, often referred to as the linear bicycle model. This linear model has a constant understeer and no lateral grip limit. Many researchers and developers of active safety systems use this linear model as an interpretation of the drivers' intention based

on his/her steering input, so also in this work.

Even though constant understeer is desired, the understeer of real vehicle is generally *not* constant, but changes with speed and the amount of utilization of the lateral and longitudinal grip. To overcome this change in characteristics of a "passive" vehicle with a given understeer and maximum lateral grip, the grip limits and understeer can be changed by actively controlling the steering, suspension and traction/braking systems. ESC systems use the bicycle model as a reference to control the vehicle motion [67, 66, 13, 72, 51]. ESC systems work on an intervention basis, i.e. they only operate when a pre-set deviation from the desired system output is exceeded. In contrast to these intervention based systems, it can be shown that real vehicle behavior is able to follow the linear bicycle model up to the grip limit, by fully utilizing steering, suspension and traction/brake actuators.

In this research it is shown how active drive force distribution can be used to accomplish the aim of constant understeer. Apart from changing the vehicle's understeer, the grip limit can also be expanded by drive force re-distribution. This is possible since a passive vehicle cannot fully utilize all tires potential under all operating conditions. Also, the ways to optimize the lateral grip by active drive force distribution is dealt with in this work. The focus of this research is thus how drive force distribution can be used to improve lateral grip and provide consistent handling characteristics over a wide range of operation.

Drive forces have the primary purpose to accelerate the vehicle or to maintain a constant vehicle speed. However, when accelerating in a corner, there is a strong influence on the lateral grip and understeer of the vehicle. This influence is due to the acceleration itself but is also dependent on how the drive forces are distributed. For maximum lateral grip, (1) the lateral force capacity must be maximized while (2) maintaining a balance between the lateral force capacity from the front and rear axle. The second requirement is important, since an imbalance between the front and rear axle will either tend to increase or decrease the turning rate of the vehicle. The drive forces and how they are distributed on all four wheels influence the two factors mentioned previously. Of interest in this study is therefor to understand and describe this influence.

Concerning the understeer of the vehicle, a further motivation to adhere to predefined understeer for any given operating condition is that the often dramatic change in understeer near the grip limit could potentially lead to loss of directional control or loss of vehicle stability. Accidents which are a result of the driver having lost control are the type of accidents that ESC systems, mentioned earlier, have been known to reduce by 25-40% [46, 31]. Miura et al.[44], for instance, indicates that consistent understeer, regardless of the operating condition, is desirable from the perspective of driver comfort .

1.3 Existing Research on Drive Force Distribution

Given the importance of the influence of drive force distribution on vehicle handling for the control and design of active driveline systems, a thorough literature review was conducted in order to identify the state-of art in this field. Of the commonly used literature in this field, such as [2, 14, 26, 40, 41, 43, 49, 51, 74], none give details regarding the effect of the combined driving or braking with cornering on the understeer and lateral grip on a vehicle level. This fact may seem somewhat surprising since the effects of combined driving/braking and cornering are well described on a tire level in both the previously mentioned literature as well as recent work by Svendenius [63] and many others. One aim of this research is to make a contribution to closing this gap between the knowledge available on a tire level to its implication on vehicle level characteristics. The focus of this work is thereby to explain the implications of drive force, and drive force distribution to the specific and important vehicle characteristics, lateral grip and understeer.

Studying the available literature in more detail, an overview of various means to actively control the vehicle characteristics by means of steer angle, drive/brake force, and vertical load control can be found in [4, 30, 33, 75]. There are further scientific papers that study the cross-coupling between lateral and longitudinal handling properties such as Pacejka [48], Uffelmann [69], Abe [1], Shibahata et al. [62] and Furukawa and Abe (1997) [12]. These papers are, however, mainly limited to simulation results and the theory explaining the phenomena is brief. Shihabata et al.[62], nevertheless, noted how longitudinal acceleration and deceleration in a corner can be seen as a yaw-moment, ΔM_Z. Furukawa and Abe [12] further explains the result of Shihabata et al. by showing how this moment tends to increase or decrease the cornering radius from the longitudinal load transfer caused by braking or acceleration in a turn. Based on these findings, Shibahata et al. proposed a feed-forward control of the left/right brake proportioning to counteract this yaw moment. This load transfer is not generally considered in analytical studies of vehicle dynamics and is therefor an important expansion of the theory for the combined longitudinal and lateral motion.

Most studies of vehicle dynamics have focused on understanding the lateral dynamics of the vehicle decoupled from the longitudinal dynamics, as previously mentioned. Even though the cross-coupling between longitudinal forces and lateral forces is well understood on a tire level, methods on how to directly evaluate the influence of drive force distribution on the total vehicle characteristics are brief, incomplete or only based on empirical results.

As a conclusion, a considerable gap, concerning the theory available to describe the implications of drive force and drive force distribution, was identified when reviewing the available literature in this field. It is this gap which therefor should be addressed in this work.

1.4 Objectives of this Study

This following work was on one hand motivated by the gap indicated in the available literature and, on the other hand, by the relevance that this knowledge has for the design and control of active driveline systems. Based on this motivation, the objectives for this work were divided into,

- the problems to be addressed,
- the requirements on the solution to these problems,
- a proposed solution, supported with the supporting theory that solves the problems indicated, while fulfilling the stated requirements, and,
- the verification of the solution using computer simulations.

Based on the previously indicated areas of interest, the questions to be answered in this project could be formulated as:

- How is the lateral grip affected by drive forces and how they are distributed
  - front/rear and
  - left/right?
- What is the optimal front/rear and left/right drive force distribution? Optimality here defined as the distribution that provides the maximum possible lateral grip.
- How does the drive force distribution change the understeer of a vehicle?
- How is constant understeer maintained during different operating conditions by means of drive force distribution?
- What drive force distributions are produced in particular driveline configurations what implications do they have on the lateral grip and understeer?

In order to limit the scope of the project, and to further establish some minimum requirements for the solution to be valid, the following requirements are listed:

- The theory must be valid for steady-state trim conditions as well as steady-cornering combined with steady braking/acceleration.
- The solution should be usable for design of driveline hardware and the associated feed-forward control.

- The lateral grip limit should be predicted assuming that the tire forces and the friction are known. For work on friction estimation techniques, see for instance [3, 36, 34, 35].

Subsequently, the proposed solution, and supporting theory, should result in:

- a tool which graphically shows the effect of possible drive-force distributions on the lateral grip limit.
- a tool useful for the design a drive-force distribution that maximizes the lateral grip for any given condition.
- an analysis tool and expressions for the effect of the drive force distribution on the vehicle understeer.

Finally, the proposed solution is verified using computer simulations. These computer simulations are based on industry standard test procedures. The simulations are, first aimed at verifying the developed theory which is based on a simplified modeling approach to describe the phenomena of interest. The use of more sophisticated vehicle models can confirm to the assumptions of the simple models. A second use of the simulations was to identify the limits to which the simple models were valid. These simulations are based on

- Steady cornering test such as the ISO4138:2004 [23] test procedure with constant steering angle. This test intends to verify the predicted understeer and predicted lateral grip limit.
- Cornering tests with various levels of constant acceleration/braking such as [24, 25]. The purpose of these tests are the same as the previous test with the modification that the effect of the drive force and the drive force distribution is included.
- Transient maneuvers with step-steer such as [22]. The objective with this test is, to evaluate predictions of the steady-state limits, as well as limitations in the theory with regard to overshoots possibly exceeding the predicted limit. The limit is detected by successively increasing the amplitude of the steering input until the lateral acceleration no longer increases.
- Evaluate the generality and limitations of the developed theory with fully dynamic maneuvers such as the NHTSA[1] ESC test as defined in [47]. Since this test is designed to induce oversteer, a vehicle where the steady-state lateral grip is determined by the front axle will show a larger lateral acceleration than predicted by the steady-state theory in this test. The purpose of the test is to verify that assumption.

[1]National Highway Traffic and Safety Administration – http://www.nhtsa.gov

Apart from the tire/road capacity or friction, longitudinal forces generated by the tires are also limited by the engine's power. The drive force distribution is further determined by the driveline configuration. This work also investigated how a specific drive force distribution can be realized with some specific driveline configurations.

1.5 Delimitations

The boundaries and scope of this work are given by the conditions that

- the tire/road friction is assumed to be given.
- only vehicle level modeling of drive force distribution is investigated. Component level realization such as engine, transmission or driveline modeling are outside the scope of this work. However, the control authority of certain driveline concepts are discussed.
- the characteristics of the vehicle under steady-state cornering and constant longitudinal acceleration while cornering (quasi-steady state), are of primary interest. Transient and dynamic maneuvers are used to evaluate limitations in the design methods valid for steady-state conditions.
- the only limits which are considered are the tire friction limits. Limits which are imposed by engine performance and drag forces are only briefly discussed.
- The road surface is assumed to be equal on all four tires. In real situations, the surface could vary in transients, which is not a topic studied in this work.

The modeling delimitations are further discussed in Chapter 2.

1.6 Main Contributions

As previously mentioned, the subject of combined slip (combined lateral and longitudinal forces) for tires is throughly discussed in the literature. The objective of this research has been to explain the implications of traction/braking in general and the drive force distribution, specifically in combination with cornering on vehicle level characteristics, namely the lateral grip and understeer. The aim has been to simplify the theory so that, wherever possible, closed-form expressions between dependent and independent variables could be given. Further, the theory has been applied on specific hardware concepts or driving scenarios. The main outcome of this work can be summarized as

- Closed form expressions for lateral grip versus the longitudinal drive force are developed for four specific front/rear drive force distribution concepts.
- A lateral grip margin which is useful for the computation of the maximum lateral acceleration for a given drive force and drive force distribution.
- A developed lateral grip margin which can be used to optimize the drive force distribution for maximum lateral grip.
- The influence of the front/rear drive force distribution on the lateral grip and understeer. A mainly unknown method by Kato et al. [27][2], is further developed.
- It is shown how load transfer, due to longitudinal acceleration, has a large influence on both the understeer and lateral grip.
- The influence of left/right drive force distribution on the understeer and lateral grip as is shown using a further developed version of the classic "handling diagram" [48].
- The ability of a variable left/right wheel speed ratio on the rear axle to keep the understeer constant for operating conditions within the limits of the available speed ratio.

1.7 Thesis Outline

After this introductory chapter which was intended to provide background, motivation and objectives for this work, Chapter 2 introduces vehicle, tire and driveline models and associated theory and analysis methods for the vehicle dynamics and handling characteristics. The main contributions of this work are described in the subsequent Chapter 3, dealing with the influence of the drive-force distribution on understeer and grip limits as well as the lateral grip margin. The work is divided such that the influence of (1) front/rear and (2) left/right drive force distribution is separately presented. Further, the validity and limitations of the previously developed theory are verified by the means of computer simulations in Chapter 4, which contains the results of the evaluation of the developed drive-force distribution and lateral grip margin definition using various drive cases of some specific vehicle configurations. Finally in Chapter 5, issues which need further development are identified and some conclusions and final remarks are made.

[2]Cited only twice and only in other Mitsubishi papers according to Google Scholar. The paper is not even indexed in Web of Science, Scopus or Compendex

Chapter 2

Vehicle Modeling and Handling Analysis

The aim of any modeling should be to use the simplest possible model that still captures the relevant characteristics which are to be evaluated. The goal of the following study is to study the influence of the drive force distribution on the understeer and lateral grip in steady-state (SS) and quasi-steady-state (QSS) conditions. This study requires the modeling of the influence of drive force on

- the lateral grip and
- cornering stiffness of the front and rear tires,
- the equations of motion and
- the normal forces.

Further, when studying the influence of left/right distribution on understeer and lateral grip, the following additional effects need to be considered:

- yaw-moment produced by different left/right forces and
- the influence of a forced speed difference between left/right wheels.

Following the above requirements, the modeling is considering:

- The planar motion dynamics represented by the longitudinal, lateral and yaw degrees of freedom.
- The vertical forces on all four tires accounting for the lateral and longitudinal load transfer in SS and QSS conditions.

- The (non-linear) lateral force to slip angle relationship taking into the consideration the influence of longitudinal forces.
- The tire dynamics for transient maneuvers are modeled using a single-order low-pass filter on the steady-state tire outputs [17].

Again, based on the requirements stated previously, items which are not considered are for instance:

- Roll, pitch and heave dynamics
- Steering system compliance
- Driveline dynamics (inertia and compliance)
- Wheel dynamics (inertia)
- Suspension kinematic- or elasto-kinematic characteristics.

From the above list it can be concluded that some dynamic characteristics are left unmodeled. This is a consequence of the focus on SS- and QSS conditions. One aspect that could be considered in more detailed studies of the understeer is the steering system compliance, see for instance [69].

The term "operating conditions" refer to the road surface friction, μ and the amount of longitudinal- and lateral acceleration, a_X and a_Y respectively. At steady-state and quasi steady-state operating conditions, the assumptions are that $a_X \approx F_X^{\text{IN}}/m$ and $a_Y \approx v_X\dot{\psi} = v_X^2/R$. The curve radius is related to the state variables as $R = v_X/r$.

2.1 Tire Modeling

In this study, what is required from the tire modeling is to find the effect of the drive force on, (1) the cornering stiffness ($\partial F_Y/\partial\alpha$), and (2) the peak lateral force. The reason is that these two aspects of the tire level characteristics relate directly to the vehicle level properties which will be studied, namely understeer and lateral grip respectively. As a result, the following requirements for the tire model are that:

- $F_Y = C_\alpha\alpha$ as $\alpha \to 0$
- $F_Y = \mu F_Z$ as $\alpha \to \infty$
- the model shall be valid for combined longitudinal and lateral slip, with either the longitudinal force, F_X, or the longitudinal slip, κ as independent parameter.

Here, α is the tire slip angle, defined in Eq. (2.2).

2.1.1 Model A — Inputs: $\alpha, F_{X_W}, F_{Z_W}, \mu$. Output: F_{Y_W}

One of the tire model used in this research treats the longitudinal force F_{X_W} as an input. This is natural if the longitudinal force is directly controlled and is a common approach when studying quasi-steady state cornering [49]. The lateral force is then computed using the following simple relationship:

$$F_{Y_W} = \sqrt{(\mu F_{Z_W})^2 - F_{X_W}^2}\tanh\left(\frac{c_\alpha}{\mu}\alpha\right) \ , \tag{2.1}$$

where $F_{X_W} \leq \mu F_{Z_W}\cos(\alpha)$ and where the slip angle,

$$\alpha \triangleq -\tan^{-1}\left(\frac{v_{Y_W}}{|v_{X_W}|}\right) \ . \tag{2.2}$$

The change in sign convention compared to ISO8855:1991 [21], ensures that positive slip angles result in positive lateral force (along the Y_W-axis). The use of the absolute $|v_{X_W}|$ in the denominator will avoid numerical problems when v_{X_W} changes sign (vehicle is traveling backwards) and that only the sign of v_{Y_W} will determine the sign of the force. Additionally, this definition restricts the maximum possible slip angles to $\pm 90°$, which simplifies the tire model implementation.

Algorithm 1 $F_Y = \mathrm{f}_{\mathrm{tire}--\mathrm{A}}(\alpha, F_X, F_Z, \mu_0)$

1: Read tire parameters c_0, c_1, μ_1 and F_{Z0}.
2: $c = c_0[1 - c_1(F_Z - F_{Z0})]$
3: $\mu = \mu_0[1 - \mu_1(F_Z - F_{Z0})]$
Ensure: $F_X \leq \mu F_Z$
4: $F_Y = \sqrt{(\mu F_Z)^2 - F_X)^2}\tanh\left(\frac{c}{\mu}\alpha\right)$

2.1.2 Model B — Inputs: $\kappa, \alpha, F_{Z_W}, \mu$. Output: F_{X_W}, F_{Y_W}

The combined slip model using the longitudinal slip κ instead of the longitudinal force F_X is the one proposed in [5]. In the work herein isotropic tire properties are assumed, meaning that the friction and stiffness are equal in all directions. Even though the friction usually is about 10-30% greater in the longitudinal direction compared to the lateral, it is the lateral capacity (peak friction) which is of interest here. In this case it is convenient to limit the longitudinal capacity to be equal to the lateral capacity. With the slip angle α defined as in Eq. (2.2) and the longitudinal slip,

$$\kappa \triangleq \frac{v_{X_W} - v_{X_W}^0}{v_{X_W}^0} \ , \tag{2.3}$$

with $v^0_{X_W}$ being the speed of the free-rolling wheel. The combined slip quantities used to compute the forces are

$$\boldsymbol{\sigma} \triangleq \frac{1}{1+\kappa} \begin{bmatrix} \kappa \\ \tan(\alpha) \end{bmatrix} , \tag{2.4}$$

from which the tire forces are computed as:

$$\begin{bmatrix} F_{X_W} \\ F_{Y_W} \end{bmatrix} = \frac{\boldsymbol{\sigma}}{||\boldsymbol{\sigma}||} \mu F_{Z_W} \tanh\left(\frac{c_\alpha}{\mu}||\boldsymbol{\sigma}||\right) . \tag{2.5}$$

Algorithm 2 $[F_X, F_Y] = \mathrm{f}_{\mathrm{tire--B}}(\kappa, \alpha, \mu_0, F_Z)$

1: Read tire parameters c_0, c_1, μ_1 and F_{Z0}.
2: $c = c_0[1 - c_1(F_Z - F_{Z0})]$
3: $\mu = \mu_0[1 - \mu_1(F_Z - F_{Z0})]$
4: $\sigma_X = \kappa/(1+\kappa)$
5: $\sigma_Y = \tan^{-1}\alpha/(1+\kappa)$
6: $\sigma = \sqrt{\sigma_X^2 + \sigma_Y^2}$
7: $F = \mu F_Z \tanh(c\,\sigma/\mu)$
8: $F_X = F\sigma_x/\sigma$
9: $F_Y = F\sigma_y/\sigma$

Model B is a modified version of Model A where instead of the longitudinal force being given as an explicit input, the longitudinal slip is in combination with the slip angle used to compute both the lateral and longitudinal forces.

2.1.3 Tire model comparison

Many different ways to model the tire behavior are available in current literature. The method employed in Models A+B is a very simple one, but not readily found in the literature. In order to establish some credibility for the chosen method a comparison to more established methods are shown in Fig. 2.1. The results shown in this graph are for pure lateral slip conditions of the models in Section 2.1.1 and Section 2.1.2, and normalized with F_Z. Some of the industry standard models to which the "tanh-tire" model (Models A+B) is compared are, the brush tire model [49], the "magic tire" model [5], and an exponential function [76]. From this comparison it can be seen that the tanh model is a good compromise of the different accepted models.

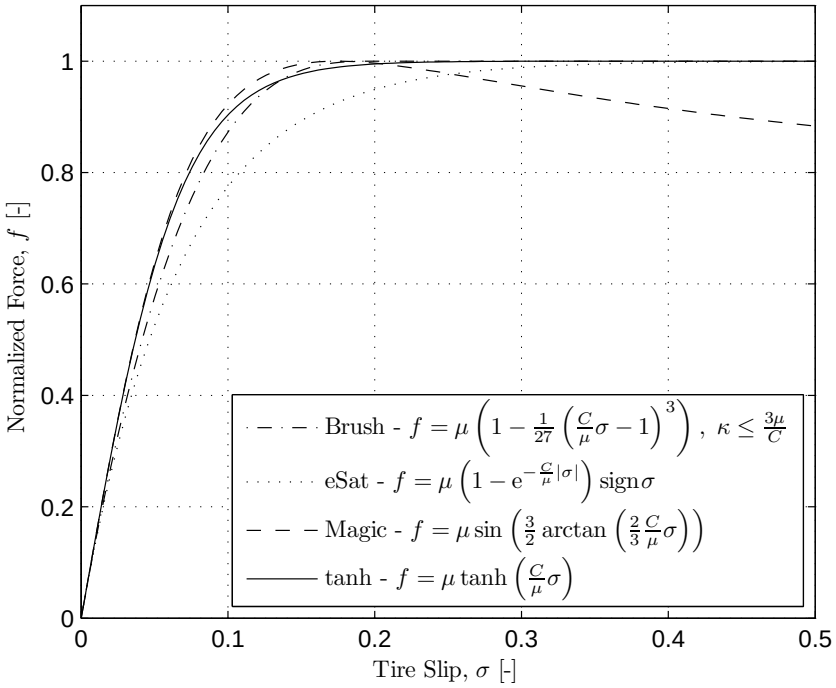

Figure 2.1: Comparison of the force/slip relationship of the "Tanh-tire" model to three other tire models

2.1.4 Tire/road properties

Both the tire cornering, rotational stiffness, and the peak tire force increase with normal force, but at a decreasing rate. In this work, the with F_Z normalized tire stiffness, c_α, is here computed as

$$c_\alpha = c_0[1 - c_1(F_Z - F_Z^0)] \tag{2.6}$$

which relates to the cornering stiffness

$$C_\alpha \triangleq \left.\frac{\partial F_Y}{\partial \alpha}\right|_{\alpha=0} = c_\alpha F_Z \ . \tag{2.7}$$

Further the peak friction coefficient (which is the peak tangential force divided by the normal force) is computed as

$$\mu \triangleq \left.\frac{F_X^{\max}}{F_Z}\right|_{F_Y=0} \equiv \left.\frac{F_Y^{\max}}{F_Z}\right|_{F_X=0} = \mu_0[1 - \mu_1(F_Z - F_Z^0)] \ , \tag{2.8}$$

where μ_0 and μ_1 are road condition and tire type dependent. In both cases, F_Z^0 is chosen as approximately equal to the average normal force of all tires.

2.1.5 Tire Dynamics

For the dynamic and transient simulations, reported in Chapter 4, the tire dynamics are modeled using a first order filter. In the Laplace domain this can be written as:

$$F_i = \frac{1}{\tau_i s + 1} F_i^{\text{ss}},\ i = X, Y \tag{2.9}$$

with

$$\tau_i = \frac{L_i}{v_X} \tag{2.10}$$

and L_i the dynamic relaxation length.

2.2 Vehicle Models

The complete vehicle model developed for this work, fulfilling the requirements as outlined in the introduction to this chapter, are described in this section. The main model nomenclature is presented in Fig. 2.2. For more complete nomenclature list in the beginning of this thesis.

2.2.1 Planar dynamics

The vehicle's planar dynamics has three degrees of freedom, two translational (longitudinal and lateral) and one rotational (yaw). Based on curve-linear motion of a vehicle-fixed coordinate system, where

$$\begin{aligned} a_X &= \dot{v}_X - v_Y \dot{\psi} \\ a_Y &= \dot{v}_Y + v_X \dot{\psi} \end{aligned} \tag{2.11}$$

are the equations of motion according to Newtons second law written on the state-space form $\dot{\boldsymbol{x}} = \mathrm{f}(\boldsymbol{x}, \boldsymbol{u})$ are

$$\frac{d}{dt} \begin{bmatrix} v_X \\ v_Y \\ \dot{\psi} \end{bmatrix} = \begin{bmatrix} \Sigma F_X/m + v_Y \dot{\psi} \\ \Sigma F_Y/m - v_X \dot{\psi} \\ \Sigma M_Z / I_{ZZ} \end{bmatrix} \triangleq \mathrm{f}(\boldsymbol{x}, \boldsymbol{u}), \tag{2.12}$$

with $\boldsymbol{u} = \delta$ and $\boldsymbol{x} = [v_X\ v_Y\ \dot{\psi}]^{\mathrm{T}}$. The driveline will require more inputs and states and will be discussed further.

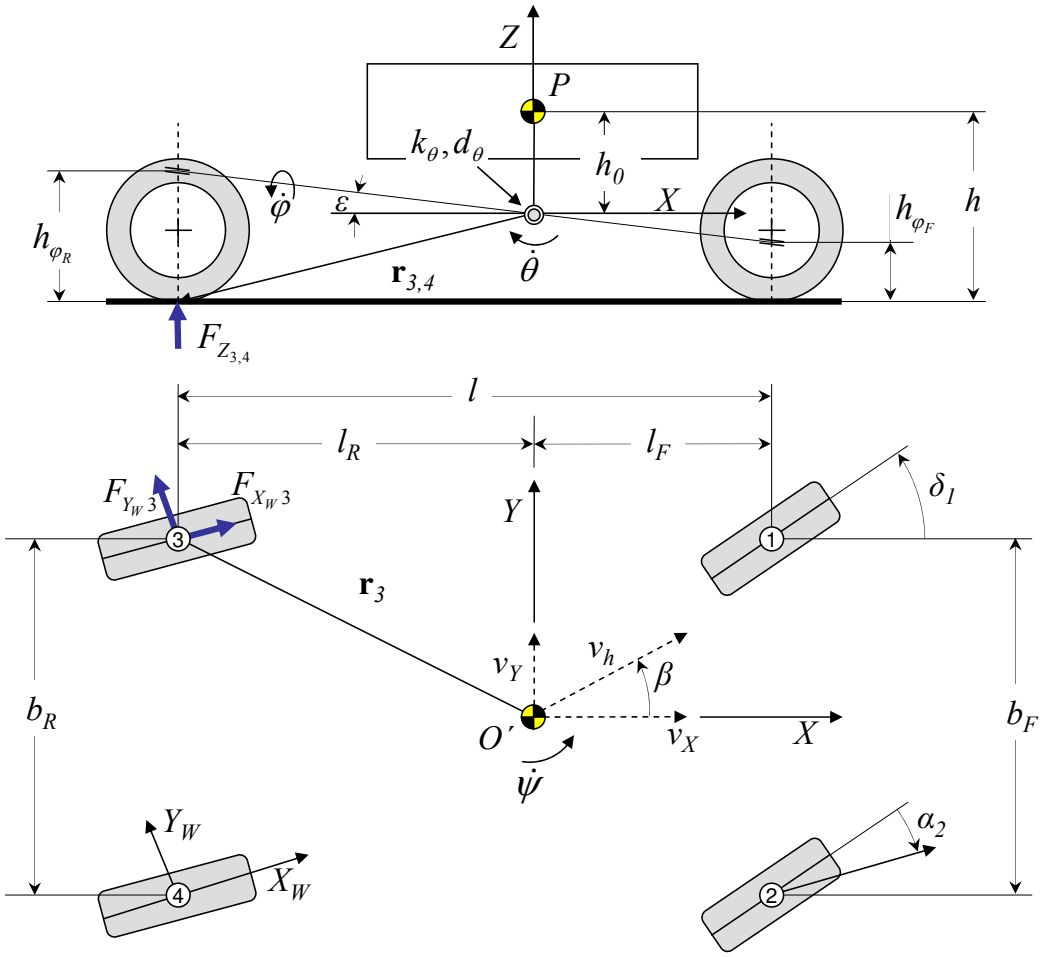

Figure 2.2: Two-Track Model

2.2.2 Quasi-steady state approximation

The application of the quasi-steady-state approximation (QSSA) involves the replacement of some of the differential equations by algebraic equations, by assigning some of the state variable derivatives ($\dot{\boldsymbol{x}}$) of the state-space model to zero [57, 58, 68]. The solution of this differential-algebraic system of equations should be real, positive, and in good accordance with the solution of the original system of ordinary differential equations.

From Eq. (2.12), we have a non-linear dynamic model with three state variables. Many of the vehicle characteristics such as stability, understeer and lateral limits are commonly studied for the steady-state case, i.e. $\dot{\boldsymbol{x}} = \dot{\boldsymbol{u}} = 0$. In this work, however, also constant longitudinal acceleration is considered, i.e. $\dot{\boldsymbol{x}} \neq 0$. It would therefor be useful if the theory developed for steady-state cornering could be expanded to cornering with constant braking or acceleration. In this case, the lateral dynamics are in this case assumed to vary slowly. This leads to the QSSA of the lateral state variables to be approximately zero. The QSSA has also been used previously in the study of the understeer and lateral grip with constant braking or acceleration while cornering [1, 8, 32, 69].

In summary, for this work, QSS cornering in this work is defined such that the states derivatives in the lateral and yaw direction are approximately zero during constant braking and/or acceleration, i.e. $\dot{v}_Y \approx 0$ and $\ddot{\psi} \approx 0$ in this case.

How well does this QSSA represent the real behavior during when accelerating the vehicle along the curvature of the vehicle path? In this case the yaw-rate increases proportional with the increase in speed if the curve radius is constant. In this work, the longitudinal (or rather, tangential) acceleration is assumed to be constant as being the definition of a QSS maneuver. One question for this research is if the lateral- and yaw- equations still can be considered as equilibrium conditions? First let's assume that the tangential acceleration is equal to the longitudinal acceleration (β is small). We have further that

$$\dot{\psi} = \frac{v_X}{R} \, . \tag{2.13}$$

Taking the time derivative of $\dot{\psi}$ and v_X in the body-fixed reference frame and further assuming that the curve radius, R, is constant, we have, together with Eq. (2.11), that

$$\frac{d}{dt}\dot{\psi} = \frac{a_X}{R} = \frac{\dot{v}_X - \overbrace{v_Y\dot{\psi}}^{\approx 0}}{R} \Rightarrow \ddot{\psi} \approx \frac{\dot{v}_X}{R} \, . \tag{2.14}$$

This yaw-acceleration multiplied with the yaw polar moment of inertia, I_{ZZ} and should be negligible compared to the yaw moment produced by the lateral forces if it can be ignored. The conclusion is, however, that the yaw acceleration is much

less than the change in vehicle speed since it is divided by the curve radius. As a result, it is therefor assumed in this work that $\ddot{\psi} = 0$. Even though it is not equally straightforward to evaluate the effect of a_X on $\dot{v}_Y$, this effect is also assumed to be small. One purpose in the final evaluation of a theory based on the QSSA is to ensure that the effect both $\dot{v}_Y$ and ψ are small compared to the other terms in Eq. (2.12).

2.2.3 Understeer Gradient

The *Understeer Gradient* is in ISO 8855:1991 [21] defined as

$$K_{\mathrm{US}} \triangleq \frac{\partial \delta_{\mathrm{H}}}{\partial a_Y} \frac{1}{i_S} - \frac{\partial \delta_{\mathrm{D}}}{\partial a_Y} = \frac{\partial (\delta - l/R)}{\partial a_Y} \,, \tag{2.15}$$

where δ_{D} is the so-called *dynamic reference steer* or the *Ackermann steering angle* and is $\delta_{\mathrm{D}} = l/R$, where R is the curve radius. It is essentially the radius the vehicle will turn at very low speed for a given steering angle.

2.2.4 Linear reference model

As indicated in the introduction, a model which represents the vehicle behavior in the tires' linear operating range, with a constant understeer gives the relationship between the drivers input and his/her expected output. This model can be derived from the model described by Eq. (2.12) by treating longitudinal velocity as an independent variable and assuming a linear relationship between lateral force the cornering stiffness and the tire slip angle. Additionally, the track widths are collapsed to zero, hence the name "bicycle" model, shown in Fig. 2.3. When

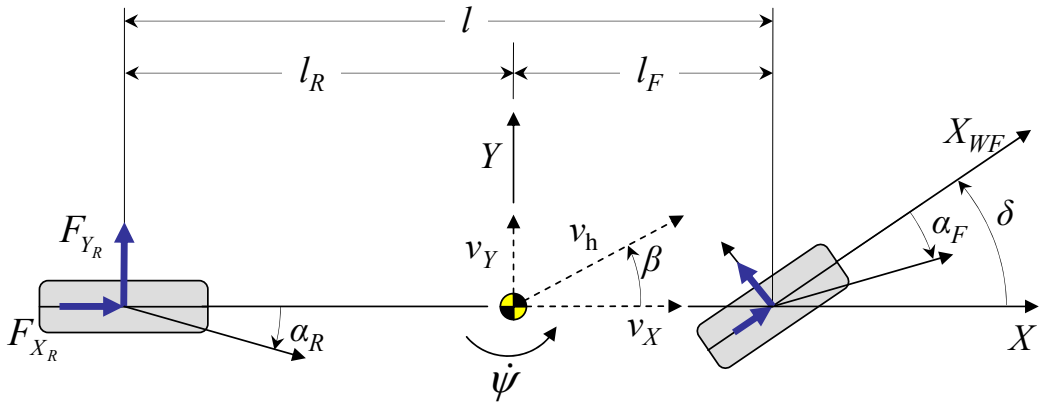

Figure 2.3: The "bicycle" model

assuming $\dot{v}_x \approx 0$, $\delta F_{X_F} \approx 0$ and $F_Y = C_\alpha \alpha$ in Eq. (2.12) the following model can be derived:

$$\underbrace{\begin{bmatrix} \dot{v}_Y \\ \ddot{\psi} \end{bmatrix}}_{\dot{\boldsymbol{x}}} = \underbrace{\frac{1}{|v_X|}\begin{bmatrix} m & 0 \\ 0 & \bar{I}_{ZZ} \end{bmatrix}^{-1}\begin{bmatrix} -C_{\alpha_R} - C_{\alpha_F} & l_R C_{\alpha_R} - l_F C_{\alpha_F} - m v_X^2 \\ l_R C_{\alpha_F} - l_F C_{\alpha_F} & -l_R^2 C_{\alpha_R} - l_F^2 C_{\alpha_F} \end{bmatrix}}_{A}\underbrace{\begin{bmatrix} v_Y \\ \dot{\psi} \end{bmatrix}}_{\boldsymbol{x}} + \underbrace{\begin{bmatrix} m & 0 \\ 0 & \bar{I}_{ZZ} \end{bmatrix}^{-1}\begin{bmatrix} C_{\alpha f} \\ l_F C_{\alpha_F} \end{bmatrix}}_{B}\underbrace{[\delta]}_{\boldsymbol{u}} \tag{2.16}$$

Rewriting to separate out the vehicle speed we rewrite the A-matrix as:

$$A = -\frac{1}{|v_X|}\begin{bmatrix} (C_{\alpha_F} + C_{\alpha_R})/m & (l_F C_{\alpha_F} - l_R C_{\alpha_R})/m \\ (l_F C_{\alpha_F} - l_R C_{\alpha_R})/I_{ZZ} & (l_R^2 C_{\alpha_R} + l_F^2 C_{\alpha_F})/I_{ZZ} \end{bmatrix} - \begin{bmatrix} 0 & 1 \\ 0 & 0 \end{bmatrix} v_X \tag{2.17}$$

For the analysis of the steady-state characteristics of the vehicle, the steady-state gain of the vehicle is of interest. From the input to state gain, conditions for stability and the relationship between the understeer and vehicle/tire parameters of can be derived.

The transfer functions from steering, δ, to the two states, v_Y and $\dot{\psi}$ are given by:

$$G = (sI - A)^{-1}B \ , \tag{2.18}$$

where s is the Laplace operator. The steady-state gain is found when $s = 0$ in Eq. (2.2.4) which gives that $\delta \rightarrow \dot{\psi}$ is

$$\frac{\dot{\psi}^{\text{ss}}}{\delta} = \frac{C_{\alpha_F} C_{\alpha_R} l v_X}{C_{\alpha_F} C_{\alpha_R} l^2 - (l_F C_{\alpha_F} - l_R C_{\alpha_R}) m v_X^2} \tag{2.19}$$

Since the steady-state lateral acceleration, a_Y^{ss} is $v_X \dot{\psi}$, we have that

$$\frac{a_Y^{\text{ss}}}{\delta} = \frac{\dot{\psi}^{\text{ss}}}{\delta} v_X \tag{2.20}$$

When re-writing Eq. (2.20) it can be found that the understeer gradient according to Eq. (2.15), expressed in tire and vehicle parameters, is

$$K_{\text{US}} = -\frac{m}{l}\frac{l_F C_{\alpha_F} - l_R C_{\alpha_R}}{C_{\alpha_F} C_{\alpha_R}} \ . \tag{2.21}$$

From this result follows that Eq. (2.19) can be rewritten as

$$\frac{\dot{\psi}^{\text{ss}}}{\delta} = \frac{v_X}{l + K_{\text{US}} v_X^2} \tag{2.22}$$

Finally, the steady-state gain $\delta \rightarrow v_Y$ is, according to ,

$$\frac{v_Y^{\text{ss}}}{\delta} = \frac{v_X}{l + K_{\text{US}} v_X^2} \left(l_R - \frac{m}{C_{\alpha_R}} \frac{l_F}{l} v_X^2 \right) . \tag{2.23}$$

From the three steady-state gain functions derived in this section, two important results are: (1) the relationship between the understeer gradient and vehicle/tire parameters, and (2) a stability criteria for $K_{\text{US}} < 0$, namely that $v_X < \sqrt{-l/K_{\text{US}}}$. This speed at which the steady gain goes to infinity is referred to as the critical speed, v_X^{crit} where the steady-state gain goes to infinity. These two results will be used in Chapter 3 when the influence of the drive force on the understeer, and further when the stability of the vehicle is discussed for cases when $K_{\text{US}} < 0$.

2.3 Driveline Modeling

Modeling a driveline is one step down from the abstraction on a vehicle level where each drive/braking force is treated individually. However, in order to understand how a given driveline concept realizes a specific drive force distribution, it was determined to elaborate on this issue in this section. The driveline of the studied vehicle configuration is assumed to have a single power source providing a force F_X^{IN} to the wheels. This drive force is distributed to the wheels with different types of hardware. The drive force is first distributed to the front and rear axles, and from there to each individual wheel.

2.3.1 Front/rear drive force distribution

The relationship between the drive force distribution and the longitudinal acceleration can be approximated as:

$$ma_X \approx F_{X_F} + F_{X_R} = F_X^{\text{IN}} , \tag{2.24}$$

which can be re-written as

$$F_X^{\text{IN}} = \underbrace{\xi F_X^{\text{IN}}}_{F_{X_F}} + \underbrace{(1-\xi) F_X^{\text{IN}}}_{F_{X_R}} , \tag{2.25}$$

if we define ξ as a parameter showing the front drive force relative to the total drive force

$$\xi \triangleq \frac{F_{X_F}}{F_{X_F} + F_{X_R}} . \tag{2.26}$$

In this work, four different specific front/rear drive force distributions are discussed in more detail. The first three of these can further be considered as basic configurations which, when combined, realize more general drive force distributions. One can note that the driveline configurations in Table 2.1 are not able

Driveline	**Drive force distribution**
Front wheel drive	$\xi = 1$
Rear wheel drive	$\xi = 0$
Locked center differential/clutch	$\xi \approx F_{Z_F}/(F_{Z_F} + F_{Z_R})$
Optimal drive force distribution that maximizes the lateral grip	$0 < \xi < 1$

Table 2.1: Driveline concepts for the distribution of drive force to the front- and rear axle.

re-distribute force *between* the front- and rear axles. In order to do this, the ratio between the front- and rear wheels should be variable, such as described by Tomari et al.[64] or as proposed by Wheals et al.[73]. In this work, only variable ratio between the left- and right rear wheels is considered, described in the next section.

Locked Center Differential

The special case which will be considered is when

$$\xi = \frac{\mu_F F_{Z_F}}{\mu_F F_{Z_F} + \mu_R F_{Z_R}} \approx \frac{F_{Z_F}}{F_{Z_F} + F_{Z_R}} \ , \tag{2.27}$$

which means that the drive force distribution is proportional to the size of the tire friction circles. In this work the friction circle is meant to be the maximum combined lateral and longitudinal *force*.

Taking into account the longitudinal load transfer, the normal forces are given by

$$\begin{aligned} F_{Z_F} &= m(l_R g - h a_X)/l \\ F_{Z_R} &= m(l_F g + h a_X)/l \end{aligned} \tag{2.28}$$

, which inserted in Eq. (2.27) simplifies to

$$\xi = \frac{l_R}{l} - \frac{h}{l}\frac{a_X}{g} \ . \tag{2.29}$$

The above case is interesting since this is the drive force distribution which is approximately achieved by forcing the front and rear wheels to rotate synchronously,

in this work referred to as rigid all-wheel drive. EIt is evident the wheel slip for this case must be equal since the average front and rear wheel speeds are equal. This is under the assumption that the effect of steering the front wheels is negligible. Secondly, the driving/braking stiffness ($\partial F_X/\partial\kappa$) changes approximately proportional to the normal load. If additionally the peak friction is nearly equal front/rear, the front/rear drive force distribution must follow the change in driving/braking stiffness which was proportional to the normal load.

2.3.2 Left/right drive force distribution

The left/right drive force distribution can be generalized by a *force* difference, it is in many cases more convenient to use the *speed* difference as parameter. For example when the wheel speed is known, but not the actual drive force distribution. The wheel speeds of each wheel are

$$\boldsymbol{v}_{X_W} = \begin{bmatrix} v_X - b\dot{\psi}/2 + (v_Y + l_f\dot{\psi})\delta \\ v_X + b\dot{\psi}/2 + (v_Y + l_f\dot{\psi})\delta \\ v_X - b\dot{\psi}/2 \\ v_X + b\dot{\psi}/2 \end{bmatrix}, \tag{2.30}$$

where the details are found in Section A.2. Using the definition of the wheel slip given in Eq. (2.3), we can find that when restricting the speed difference across the rear axle, there will be a positive slip on the inner wheel and a negative slip on the outer wheel. Superimposed on this slip is the applied longitudinal slip, κ_R, resulting from the drive torque on the rear drive shafts. If the ratio between the left and right wheels can be varied, the outer wheel could be forced to run faster than it's "nominal" speed as given by Eq. (2.30). It will then have a positive slip and the inner wheel will then have an equally large negative slip. Again, a drive torque on the rear axle will add a slip, κ_R, to the slip caused by the forced speed difference.

An open differential directs equal drive force between the left/right wheels, but imposes no restrictions on the wheel speed difference. A locked differential on the other hand forces both left and right wheels to rotate at the same speed, but imposes no restrictions on the *drive force* difference. A special type of differential is one that imposes a fixed speed difference (rather than zero speed difference) between the left/right wheels. These various concepts for free, restricted and superimposed wheel speed difference are given in Table 2.2.

The constraints imposed on the speed ratio of the concepts shown in Fig. 2.4 and an open differential are

$$n^{\mathrm{L/R}} \triangleq \omega_L/\omega_R \,. \tag{2.31}$$

Differential	**Condition**
Open	$F_{X_3} - F_{X_4} = 0$
Locked (eLSD)	$\boldsymbol{\kappa}_R = \kappa_R + b/(2R)[1\ -1]^{\mathrm{T}}$
Variable ratio (TV)	$\boldsymbol{\kappa}_R = \kappa_R + (b/(2R) - (1 - n^{\mathrm{L/R}}))[1\ -1]^{\mathrm{T}}$

Table 2.2: Driveline units that distribute drive force between the left- and right (rear) wheels

As mentioned, the concept shown left in Fig. 2.4 is a variable ratio TV-differential having a fixed left/right speed difference across two controllable clutches, which connect the left and right drive shafts [55, 56, 70] when engaged. When $(1 - n^{\mathrm{L/R}}) > b/(2R)$ the outer wheel has a higher slip than the inner wheel which enables force to be transferred from the inner wheel to the outer. The system shown in Fig. 2.4.a) re-distributes drive force between the left- and right wheels by controlling the speed difference across the differential by controlling one of two clutches. Locking one clutch imposes a fixed speed difference across the differential. Locking the other clutch gives an opposite in direction, and equally large, speed difference. If for example the nominal speed difference across the differential is 2%, and $F_X^{\mathrm{IN}} = 0$ ($\kappa_R = 0$) and the fixed speed difference imposed by the differential is further, say 10%, the wheel slip on the inner wheel becomes -4% and +4% on the outer wheel. This then means the inner wheel is braked and this brake force is transferred to the outer wheel as a driving force. This force pair generates a yaw moment in the direction of the turn, which could be called an oversteering moment, since it reduces the understeer of the vehicle. Shown in Fig. 2.4.b) is an electronic limited slip differential (eLSD). By engaging the eLSD clutch, the speed difference between the rear wheels can be eliminated. If from the previous example, the nominal speed difference (open differential) was 2%, the wheel slip on the outer wheel will become -1% and +1% on the inner wheel when this speed difference is eliminated. This will cause an understeering moment proportional to radius of the curve taken by the vehicle.

2.4 Vehicle Handling

Several methods, commonly used to assess vehicle handling, was evaluated as a background for this present work. The usefulness of these methods were evaluated based on the following criteria:

1. Does it show the lateral grip limit?

2. Can the method be used to evaluate the understeer gradient?

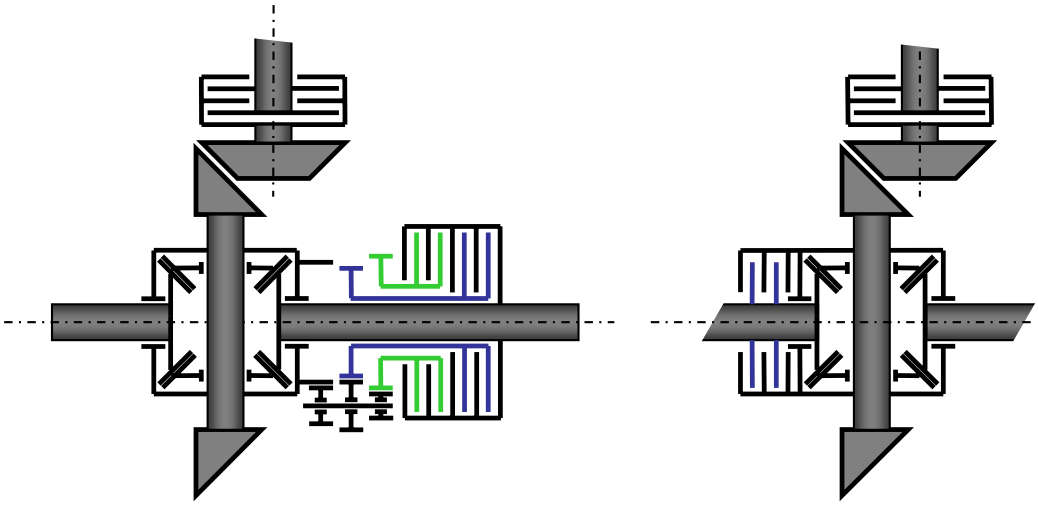

a.) Torque vectoring differential b.) Limited slip differential

Figure 2.4: Examples of two different rear differential units

3. Does it show the influence of the drive forces on 1 and/or 2?
4. Is the yaw moment required to fully utilize the lateral grip of all tires shown?

The methods which have been reviewed are listed in Table 2.3. In order to easier

Method	**Independent variable(s)**	**Dependant variable(s)**
Handling diagrams	a_Y	$(\alpha_F - \alpha_R)$
Phase plane diagram	Time	β & $\dot{\beta}$ or β & $\dot{\psi}$
MMM-diagram	δ & β	a_Y & M_Z
Beta method	δ	β & M_Z
Dynamic square	F_{X_F} & F_{X_R}	$a_Y^{\lim}$

Table 2.3: List of methods used to evaluate vehicle dynamic properties

compare the methods against each other, they are (when applicable) plotted for the same conditions.

2.4.1 Handling diagram

The method of the so-called handling diagram [48, 26, 49] is similar to the experimental results which are obtained from a vehicle test such as the ISO-4138 [23] steady-state cornering test. The handling diagram relates the difference in front-

and rear slip angles to the lateral acceleration. Instead of a vehicle experiment, the lateral force of each axle is normalized by the normal force and plotted versus the slip angle is the same diagram. From this diagram, the slip angle difference of the front- and rear axles is plotted versus the normalized lateral force, i.e. the lateral acceleration. The axle with the least friction (peak lateral force divided by the normal force) then also the maximum friction of the vehicle.

From Fig. 2.5 it can be seen that $\delta - l/R = \alpha_F - \alpha_R$. As can be seen from Eq. (2.15) the partial derivative of the difference in slip angle with respect to the lateral acceleration is the understeer of the vehicle and which can directly be seen in the handling diagram.

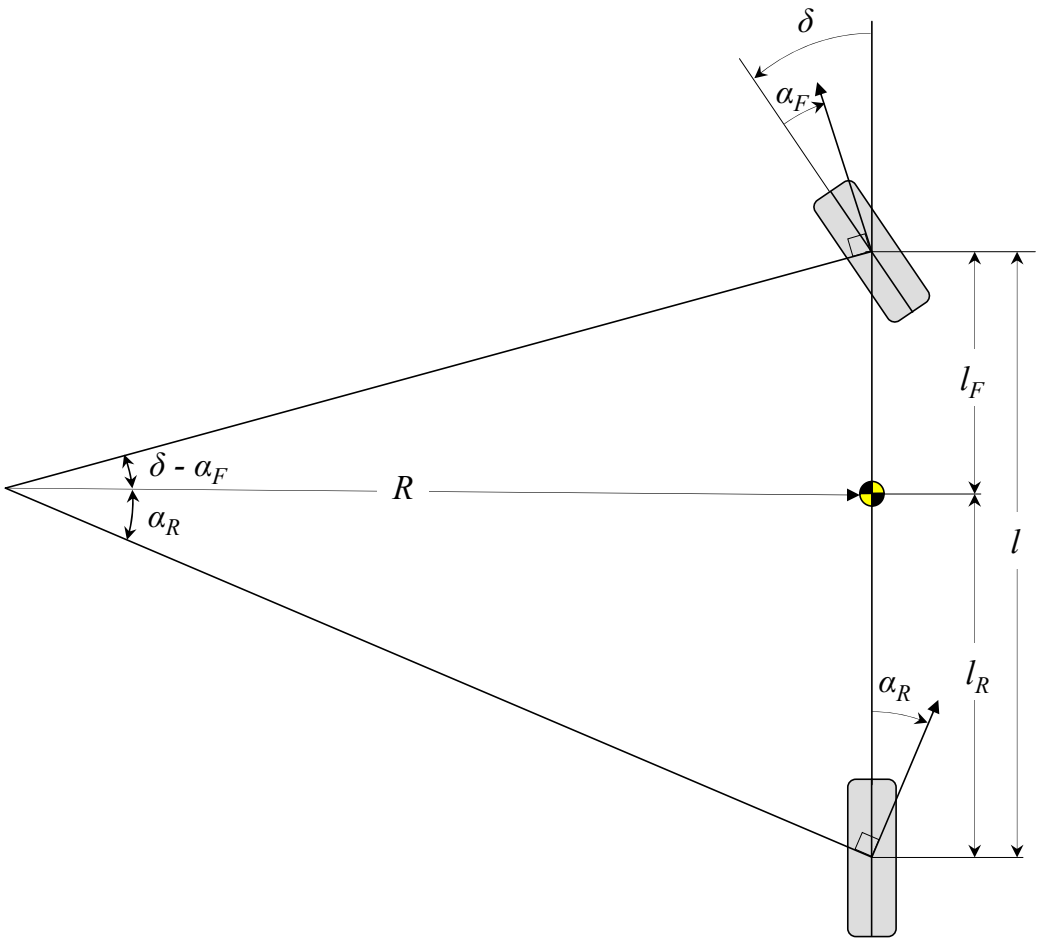

Figure 2.5: Relationship between wheelbase, slip angles, steering angle and the cornering radius

As shown in Fig. 2.6, both the understeer and the lateral grip limit are available from this test. It is therefor a method which reveals both of the variables of interest

in this study in a single diagram. Even though the yaw moment required to fully utilize both axles' lateral capacity is not explicitly shown in the diagram, from the left diagram the difference between the peak forces are shown. From the left diagram in Fig. 2.6 the yaw moment M_Z required to fully utilize both axles can be derived as

$$M_Z = l_F \mu_F F_{Z_F} - l_R \mu_R F_{Z_R} \ . \tag{2.32}$$

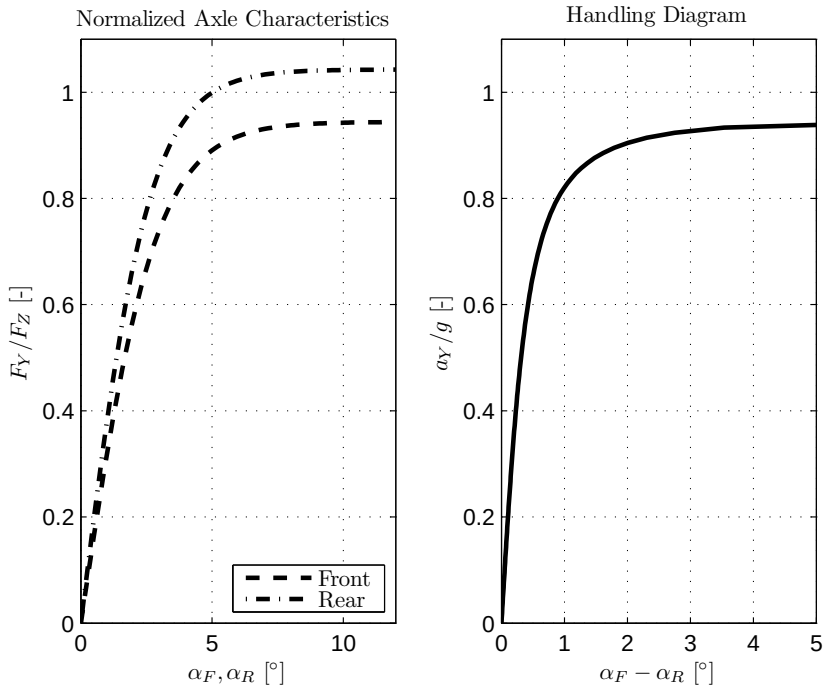

Figure 2.6: The handling diagram showing the understeer of the vehicle

One issue with the diagram in Fig. 2.6 is that it is not unique for various drive force distribution conditions. Recent work by Frendo et al. [11, 10] generalizes the method of the handling diagram to a wider range of operating conditions, such as locked differentials.

2.4.2 Phase plane diagrams

Phase plane diagrams are useful if one is interested to review all solutions of a specific operating condition (e.g. steering angle, speed) within a range of initial values of two state variables as shown in Fig. 2.7. This method does however not show the lateral grip limit of the vehicle and neither the understeer of the vehicle. The steady-state solution is simply a single point in this diagram. The method

could be refined to show how the steady-state solution (side-slip and yaw rate) moves with vehicle speed and steering angle. References to usage of this method can be found in [9, 15, 19, 20, 59, 65].

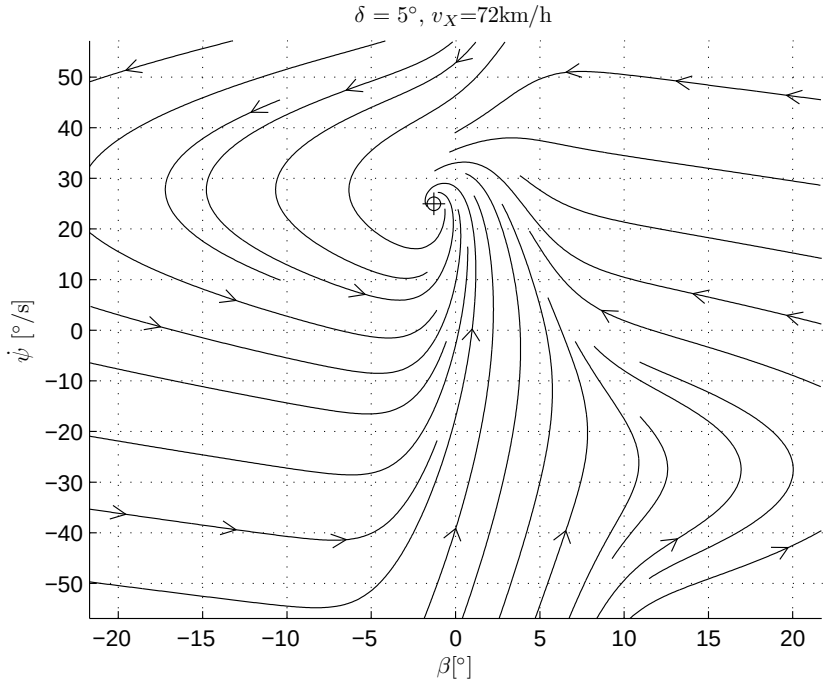

Figure 2.7: Phase-plane diagram

2.4.3 MMM diagram

The so-called Milliken Moment Method [39, 42] was developed during the 1970's, building on the research done during the 1950's at the Cornell Aeronautical Laboratory on behalf of General Motors. It applied existing aircraft dynamics theory to the dynamics of automobiles [38]. The purpose of this method was that by only performing a series of *static* tests (or simulations), the response to disturbances (stability) and steering angle (controllability) could be understood. From the diagram, it can be seen how much yaw moment a specific steering angle produces and at which steady-state lateral acceleration the vehicle will settle at (zero yaw moment). The maximum steady-state lateral acceleration is shown at the boundary of the diagram where it intersects the a_X-axis. Also, the limit behavior can be seen from the diagram. It can be seen that along the top edge of the diagram, the front axle saturates and the rear axle along the bottom edge. From this, the limit behavior can be seen from the diagram. Milliken describes vehicles where the

top edge intersects the a_X-axis as "final plowers", sometimes referred to as terminal understeer. Similarly, vehicles where the rear axle saturates prior to the front, i.e. where the bottom edge intersects the a_X-axis are denoted as "final spinners" and when the vertex lies on the a_X-axis they are called "final drifters". A natural question arises when reviewing the limits of the diagram: "Can an additional yaw moment be produced that allows the vehicle to utilize both axles for maximum lateral acceleration?". One answer to this question is torque vectoring, where longitudinal force is transferred from inner rear wheel to the outer rear wheel, or vice versa. These differential forces result in a yaw moment, moving the steady-state equilibrium to the point where both axles fully utilize their lateral capacity. For the purpose of evaluating the effect of front/rear drive force distribution, this is not a very efficient method since the diagram needs to be re-produced for every given drive force distribution and/or longitudinal acceleration. The diagram in Fig. 2.8 produced by computing the unbalanced yaw moment M_Z and the lateral acceleration a_Y for fixed angles while increasing the body slip angle β until rear axle saturates. The front- and rear slip angles and the body side-slip angle are related as

$$\begin{aligned} \alpha_F &= \delta - \beta - l_F/R \\ \alpha_R &= -\beta - l_R/R \end{aligned} \tag{2.33}$$

Fig. 2.8 is generated with $R \to \infty$ and with $F_X = 0$ using Eq. (2.12).

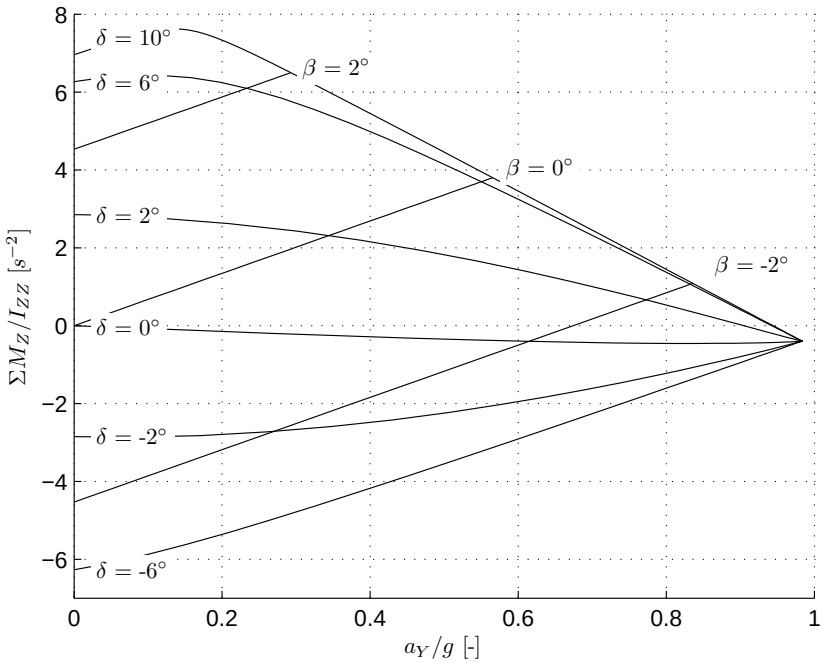

Figure 2.8: Milliken Moment Method diagram

2.4.4 Beta Method

The Beta Method was developed by Shibahata [61, 62, 60, 64] taking inspiration from MMM-method described in the previous section. In this method, rather than plotting the stabilizing yaw moment versus the lateral acceleration for various steering angles, the stabilizing yaw moment was plotted against the body slip angle β. From this beta diagram it can be seen that as the slip angle is increased, the unbalanced yaw moment first increases, but then saturates at a constant level. If the unbalanced yaw moment is positive and/or increases when the slip angle is positive, it stabilizes the vehicle, forcing it to return to steady-state (zero unbalanced yaw moment). In other words, the rear axle is in this case able to produce a larger yaw moment than the front. The yaw moment as a result of left/right drive force distribution which forces both axles to saturate simultaneously at steady-state is the unbalanced yaw moment which remains as $\beta \rightarrow \infty$. The understeer gradient is not directly available from this diagram, but can be derived as

$$K_{\mathrm{US}} = \frac{m}{lC_{\alpha_F}C_{\alpha_R}} \frac{\partial M_Z}{\partial \beta} \ . \tag{2.34}$$

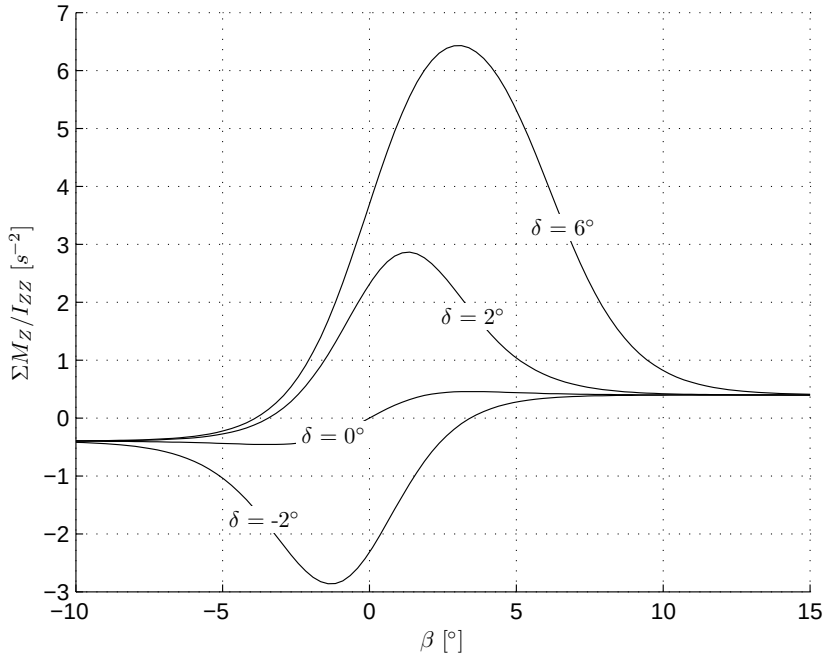

Figure 2.9: M_Z versus β diagram

This method could be used in this study to analyze the yaw moment required to balance both front- and rear axles. On the other hand, the properties of interest

in this study, the understeer and/or lateral grip limit are not readily given by this method. The conclusion is therefor that the method is not suitable for this work.

2.4.5 Dynamic Square

This method plots the available lateral acceleration as iso-curves in a diagram with the front and rear respective longitudinal force on each axle. It was a further development from a method well-known for brake proportioning. The method of a dynamic square was developed by Matsuo and Sekido [37] and Kato et al. [27] for AWD system development. The method is however, not found in any of the mainstream literature such as [14, 40, 74, 41, 2, 43, 26, 49, 51]. Only one more paper from Matsuno et al. [36] using this method was found by this author.

The dynamic square is composed by plotting the front/rear drive (or brake) force distribution which permits a given maximum lateral acceleration. Since the details of how to compute this diagram was left out in the above mentioned papers, an algorithm is given at the end of this section. A level curve of constant maximum lateral grip results in a quadrilateral in this diagram with the front- and rear drive force on the abscissa and ordinate axes, respectively. The quadrilaterals become deformed near the center of the diagram if the vehicle will saturate the front axle prior to the rear when $\mu_F \leq \sqrt{\mu_R^2 - (F_{X_R}/F_{Z_R})^2}$. Along the top and bottom edges of the quadrilateral, the rear axle saturates prior to the front axle. The opposite is true for the left and right edges. At the vertices, both axles saturate simultaneously. The front/rear drive force distribution which allows the maximum possible longitudinal acceleration for a given lateral grip is the top right vertex for acceleration and the bottom left vertex for braking.

An example of a complete dynamic square is shown in Fig. 2.10. The light gray areas shows where the rear axle will saturate first and the dark gray area where the front axle limits the lateral grip. Along the edge between the two areas, both axles saturate simultaneously, providing the best possible lateral grip for any given longitudinal acceleration. In a sense, the "optimal" drive force distribution is along these ridges.

The "normal" operating regions are the first quadrant for accelerating and the third quadrant for braking. The second and fourth quadrants combine braking on one axle with accelerating on the other which are not commonly utilized in applications. Also, the previous discussion about optimality is valid only in the first and third quadrants.

Shown in Fig. 2.10 are also diagonal lines where $F_{X_F} + F_{X_R} \approx ma_X$, along which the longitudinal acceleration is constant.

The dotted line is the drive/brake force distribution where $F_{X_F}/(\mu_F F_{Z_F}) = F_{X_R}/(\mu_R F_{Z_R})$. In other words, this line describes the drive/brake distribution which is proportional to size of the friction circle, μF_Z. This drive force dis-

tribution is closely followed when forcing the front- and rear wheels to rotate synchronously.

Since the topic of this research is on describing the influence of drive force distribution, only the first quadrant is considered in future discussions.

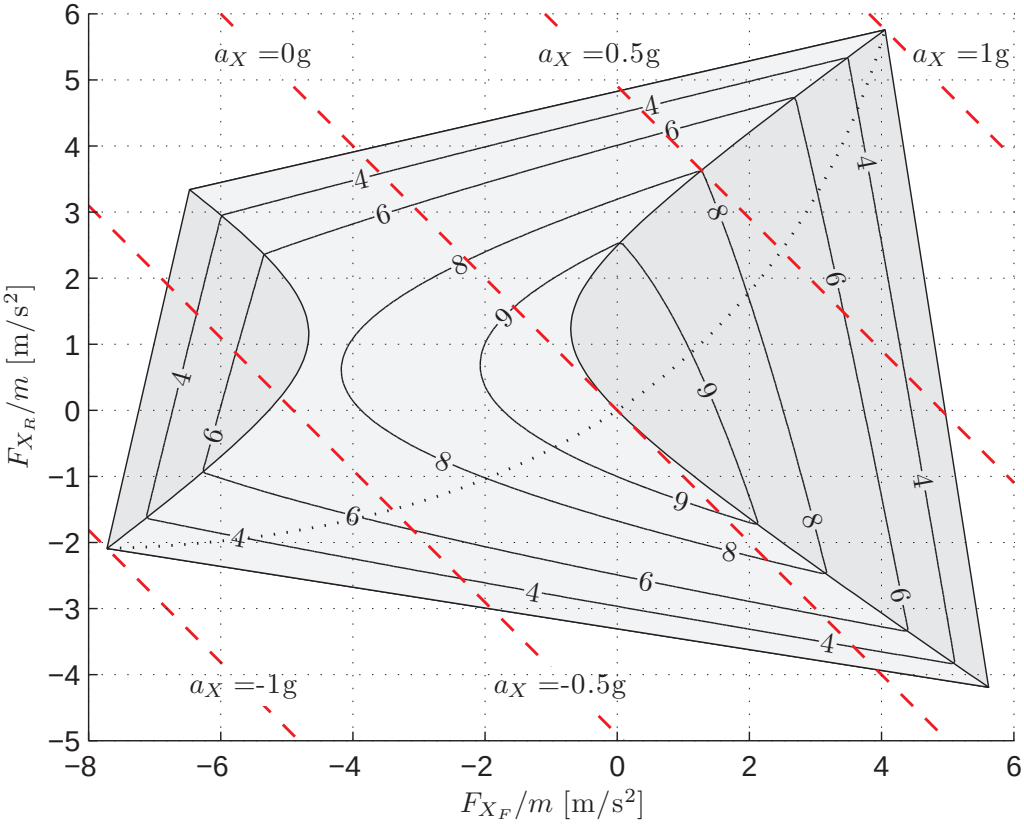

Figure 2.10: Dynamic square assuming constant and equal friction front/rear

2.4.6 g-g Diagram

The method of plotting the maximum possible longitudinal acceleration versus the lateral acceleration in a so-called g-g diagram [53, 52, 40], shown in Fig. 2.11, was developed prior to the dynamic-square method. As described in the introduction, this method is easy to understand, but reveals much less information than the dynamic square method. One can see the g-g diagram as a section through the dynamic square diagram. Since the g-g diagram does not add any more information than the dynamic square method it is not further used in this study. A typical g-g diagram for four different driveline configurations is shown in Fig. 2.11.

Algorithm 3 Dynamic square method, computing a matrix $\boldsymbol{a}_Y^{\lim}$ for range of front- and rear longitudinal forces from $F_X^{\min}$ to $F_X^{\max}$.

1: $\boldsymbol{F}_{X_F} = \begin{bmatrix} F_{X_F}^{\min} & \cdots & F_{X_F}^{\max} \\ \vdots & \ddots & \vdots \\ F_{X_F}^{\min} & \cdots & F_{X_F}^{\max} \end{bmatrix}^{n \times n}$

2: $\boldsymbol{F}_{X_R} = \begin{bmatrix} F_{X_F}^{\min} & \cdots & F_{X_F}^{\min} \\ \vdots & \ddots & \vdots \\ F_{X_F}^{\max} & \cdots & F_{X_F}^{\min} \end{bmatrix}^{n \times n}$

3: $\boldsymbol{F}_{Z_F} = (l_R mg - h(\boldsymbol{F}_{X_R} + \boldsymbol{F}_{X_R}))/l$

4: $\boldsymbol{F}_{Z_R} = (l_F mg + h(\boldsymbol{F}_{X_R} + \boldsymbol{F}_{X_R}))/l$

5: $\boldsymbol{\mu}_F = \mu_0(1 - \mu_1(F_Z^0 - \boldsymbol{F}_{Z_F}))$

6: $\boldsymbol{\mu}_R = \mu_0(1 - \mu_1(F_Z^0 - \boldsymbol{F}_{Z_R}))$

7: $\boldsymbol{F}_{Y_F}^{\lim} = \sqrt{(\boldsymbol{\mu}_F \bullet \boldsymbol{F}_{Z_F})^2 - (\boldsymbol{F}_{X_F})^2}$

8: $\boldsymbol{F}_{Y_R}^{\lim} = \sqrt{(\boldsymbol{\mu}_R \bullet \boldsymbol{F}_{Z_R})^2 - (\boldsymbol{F}_{X_R})^2}$

9: **for** $i = 1$ to n **do**

10: **for** $j = 1$ to n **do**

11: $M_Z^{\lim} = l_F \left(\boldsymbol{F}_{Y_F}^{\lim}\right)_{ij} - l_R \left(\boldsymbol{F}_{Y_R}^{\lim}\right)_{ij}$

12: **if** $M_Z^{\lim} < 0$ **then**

13: $(\boldsymbol{a}_Y^{\lim})_{ij} = l \left(\boldsymbol{F}_{Y_F}^{\lim}\right)_{ij} / (ml_R)$

14: **else**

15: $(\boldsymbol{a}_Y^{\lim})_{ij} = l \left(\boldsymbol{F}_{Y_R}^{\lim}\right)_{ij} / (ml_F)$

16: **end if**

17: **if** $(\boldsymbol{a}_Y^{\lim})_{ij} \in \mathbb{C}$ **then**

18: $(\boldsymbol{a}_Y^{\lim})_{ij} = 0$

19: **end if**

20: **end for**

21: **end for**

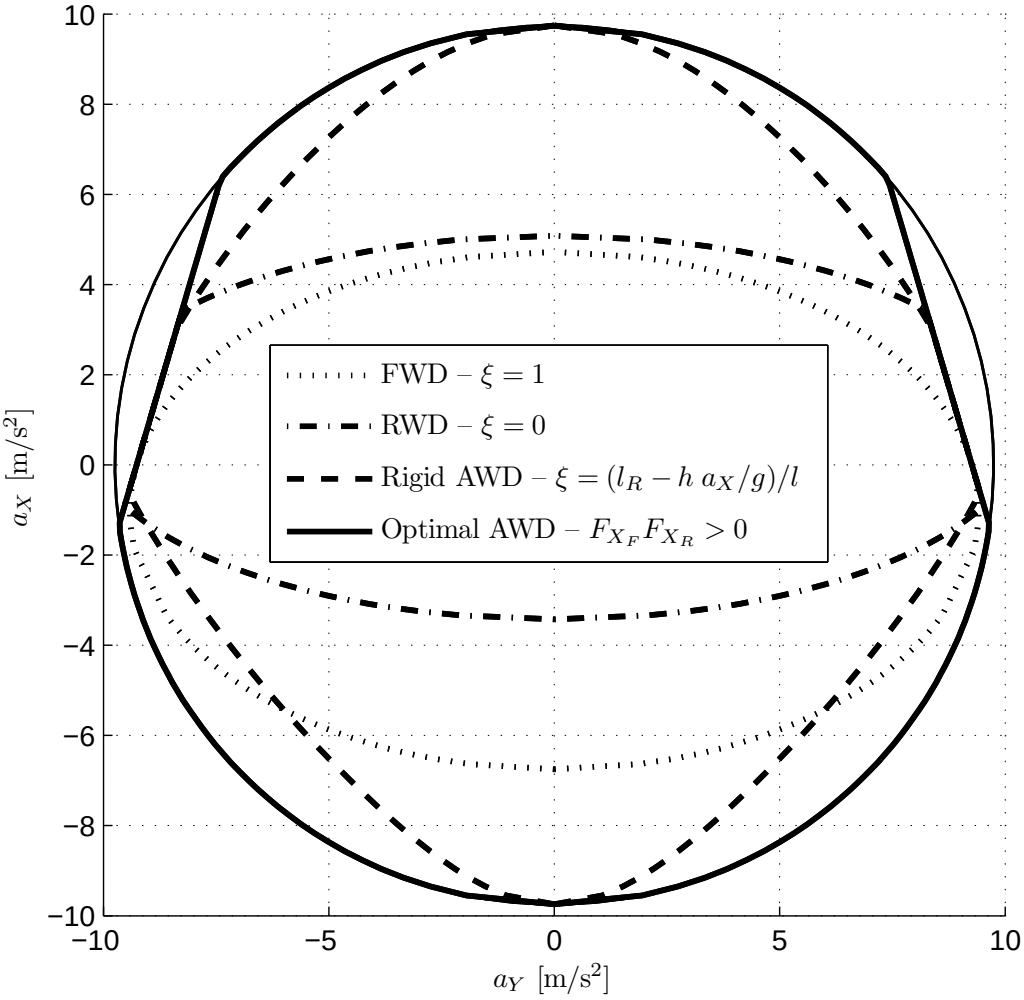

Figure 2.11: A g-g diagram showing $a_Y^{\lim}$ as function of a_X for four different drive-line configurations

2.5 Summary

This chapter first established some modeling and modeling considerations of tire, vehicle and driveline behavior. In the following chapter, these models will be used to describe the implications of the drive force distribution realized by the modeled driveline concepts on vehicle level characteristics based on tire level characteristics. Further, various (graphical) methods that could be used to show these relations were discussed. The dynamic-square method, for instance, was identified as useful to illustrate the implications of the front/drive force distribution on the lateral grip. In order to demonstrate the effect of the left/right force distribution, however, will require more development of the existing methods. Further, methods that illustrate the implications of the drive force distribution on the understeer, also require development. Combining the required modeling outlined in this chapter with the review of existing methods and their deficiencies in relation to the objectives of this work, a base for further development has been established.

Chapter 3

Effects of Drive Force Distribution on Lateral Grip and Understeer

In this chapter the main contributions of this study are presented. First the influence of the drive force on the tire characteristics are reviewed based on the tire modeling from Section 2.1. Secondly, a lateral grip margin is presented which can be used to evaluate the available lateral grip for a given drive force distribution. In the next section, this lateral grip margin is used to show how the lateral grip is related to the longitudinal acceleration for the driveline configurations modeled in Section 2.3.1. Additional to the effects of the front/rear drive force distribution, the influence of the left/right drive force distribution is described. Finally, the influence of the drive force distribution on the understeer of the vehicle is discussed. At the end of that section, it will be shown that the left/right drive force distribution has a large authority to change the understeer of the vehicle for any given operating condition.

As a further introduction to this chapter, the difference between *direct* and *indirect* actuators are defined. Andreasson [4], defined the influence of various actuators on the generation of lateral force in these two categories. Three items, where the item numbers refer to sub-figures a), b) and c) in Fig. 3.1 respectively, and which influence the lateral force generation, are

a.) – Slip angle, α, control – has a *direct* influence on the lateral force, F_Y through the tire's characteristics. Slip angle control is by Andreasson [4] confined to steering actuators. In this work, this definition extended to also include the effect of

   (a) different drive force left/right, $M_Z \propto \Delta F_X$;

   (b) or drive force on the steered wheels, $M_Z \propto F_X \delta$,

which really are "α"-effects.

b.) – Normal force, F_Z, control using suspension control – has an *indirect* effect on F_Y. This is because the peak lateral force and cornering stiffness is approximately proportional to change in F_Z. Even though Andreasson [4] in this context mainly mentions suspension actuators, the normal force control in this work is due to the load transfer caused by acceleration or braking.

c.) – Longitudinal force, F_X, control – an *indirect* influence on the lateral force given, by $F_Y \propto \sqrt{1-(F_X/(\mu F_Z))^2}$. This is a result of combined slip on the tire. This type of control is naturally directly related to this work.

The purpose of this discussion was to broaden the scope of drive force distribution control effects. Drive force distribution does not only influence the lateral force by reducing the cornering stiffness and peak lateral force. There is further the effect of load transfer which needs to be considered, and finally the explicit appearance of the drive force in the lateral and yaw equations of motion when considering different left/right drive forces and/or the lateral component of the drive force on the steered wheels ($F_X\delta$).

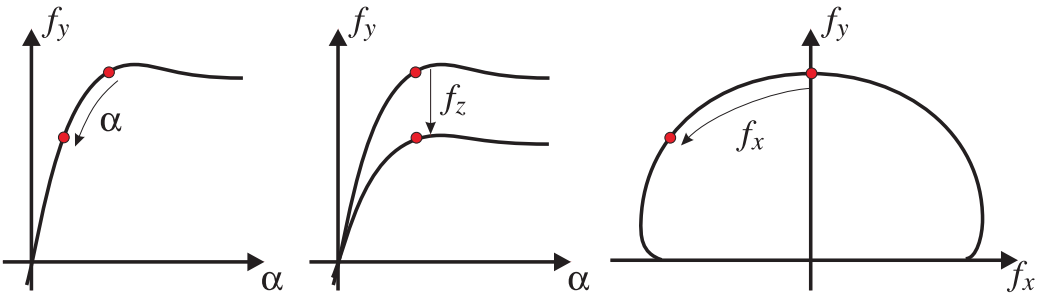

a.) slip angle control b.) normal force control c.) control of longitudinal force

Figure 3.1: Control of lateral force generation [4]

The influence of the drive force at a tire level are thus directly related to the effect on the vehicle level characteristics of interest for this study; understeer and lateral grip. Therefor, some basic principles on the influence of the drive force drive forces on a tire level are reviewed in more detail.

The lateral force versus slip angle is described in Section 2.1 and is modeled as a linear relationship, $F_Y = C_\alpha \alpha$ when the slip angle is near zero. Further, the tire is modeled to saturate or peak at a value of $F_Y = \mu_Y F_Z$, when the slip angle reaches a certain value ($\alpha \approx 10°$).

Both the cornering stiffness as defined in Eq. (2.7) and the peak lateral force are assumed to relate to the longitudinal force by the so-called friction circle con-

cept. This is illustrated in Fig. 3.2 which shows F_Y versus F_X for different levels of constant κ and α. The outer edge of this diagram illustrates the so-called friction circle, marking how the maximum possible lateral and longitudinal forces are related.

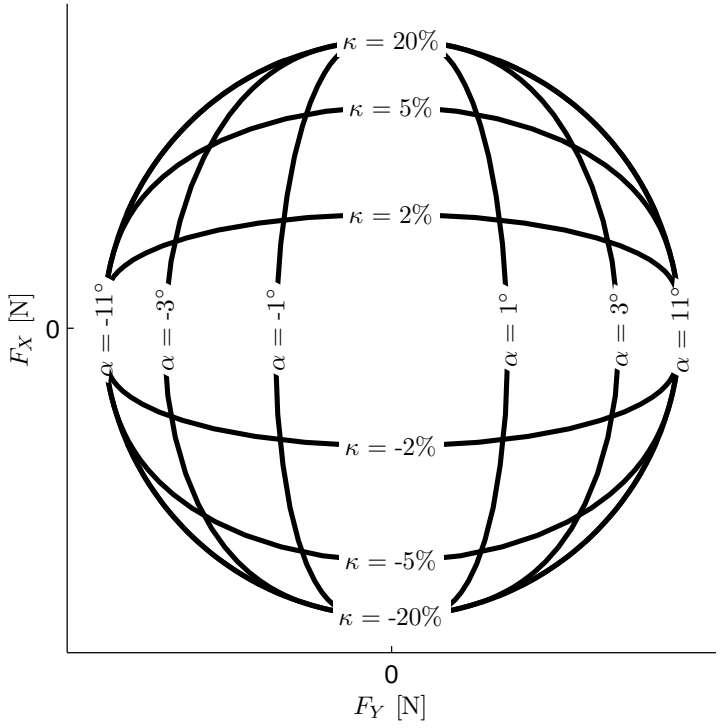

Figure 3.2: F_Y & F_X for different levels of constant κ and α

Alternatively, F_Y can be plotted vs α for various levels of constant F_X, which clearly shows the influence on the peak lateral force (saturation value) and the cornering stiffness (slope through zero) as shown in Fig. 3.3.

The effect of F_X on C_α influences the understeer of the vehicle as described in Section 3.3. Further, the effect of F_X on μ_Y has implications on the lateral grip as discussed in Section 3.2.

3.1 Lateral Grip Margin

In order to determine how much grip is utilized in relation to the maximum available grip (at a vehicle level), a lateral grip margin was envisioned. Examples of usage of the lateral grip margin are

- As a limitation for

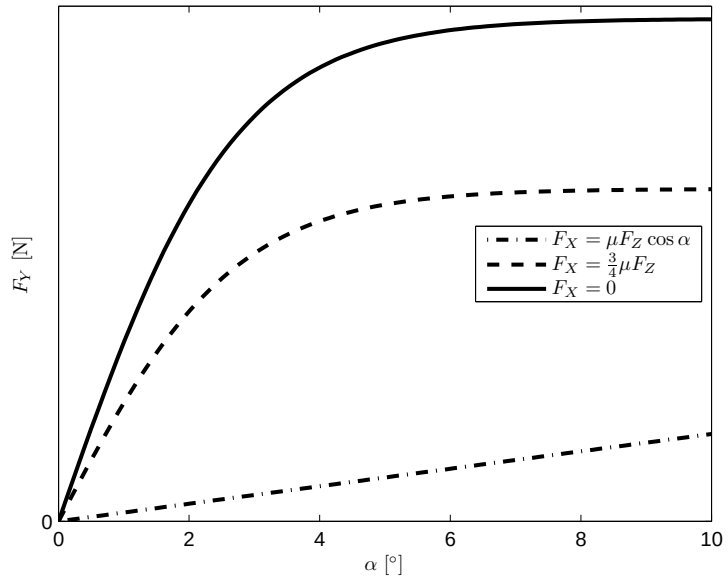

Figure 3.3: F_Y vs α for different levels of constant F_X

- maximum desired lateral acceleration (for model reference control) equal to maximum possible lateral acceleration;
- maximum lateral acceleration before warning the driver.

on a desired lateral acceleration

- As an optimization constraint to maximize the lateral grip with the way the drive force is distributed.

In previous work by this author [29] it was proposed that a lateral grip margin Λ should relate the current vehicle speed, v_X, to some limit speed $v_X^{\lim}$ as

$$\Lambda \triangleq 1 - \frac{v_X}{v_X^{\lim}} \tag{3.1}$$

which at steady state ($v_X = \sqrt{a_Y R}$) can be re-written as:

$$\Lambda = 1 - \sqrt{\frac{|a_Y|}{a_Y^{\lim}}} \tag{3.2}$$

It can be seen from Eq. (3.1) that $\Lambda = 1$ as $v_X = 0$ or $v_X^{\lim} \to \infty$. The latter condition occurs when going straight since $v_X^{\lim} = a_Y^{\lim}/\dot{\psi}$ and $\dot{\psi} \to 0$ when driving in a straight line. Further it can be seen that $\Lambda \to 1$ as $v_X \to v_X^{\lim}$. Fig. 3.4

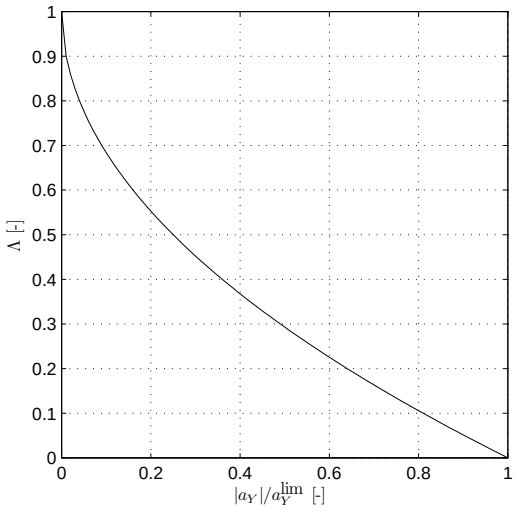

Figure 3.4: The proposed lateral grip margin, Λ, versus the absolute lateral acceleration, $|a_Y|$, normalized with the limit lateral acceleration, $a_Y^{\lim}$.

shows the relationship between the proposed lateral grip margin versus the lateral acceleration normalized with the limit lateral acceleration.

For the purpose of computing the limit lateral acceleration, it is of interest to understand if the front or rear axle is limiting the maximum lateral acceleration. In order to determine which axle is limiting the lateral acceleration, the limit yaw moment $M_Z^{\lim}$ is computed from the maximum possible lateral forces on the front and rear axle respectively as:

$$\begin{aligned} F_{Y_F}^{\lim} &\triangleq \sum_{i=1}^{2} \sqrt{(\mu_i F_{Z_i})^2 - F_{X_i}^2} \\ F_{Y_R}^{\lim} &\triangleq \sum_{i=3}^{4} \sqrt{(\mu_i F_{Z_i})^2 - F_{X_i}^2} \ , \end{aligned} \tag{3.3}$$

given that $F_{X_i} \leq \mu_i F_{Z_i} \cos(\alpha_i)$, which is the maximum longitudinal force possible. Further, the difference in all left and right longitudinal forces,

$$\Delta F_X \triangleq \sum_{i=1}^{4} (-1)^i F_{X_i} \text{sign}\, \dot{\psi} \ . \tag{3.4}$$

We can here note that Eq. (3.4) is positive for a curve to the left if the forces on the right side are greater than on the left; i.e. this quantity is positive if the difference in longitudinal forces produce a yaw moment in the direction of the turn. Next, using Eq. (3.3) and Eq. (3.4) the limit yaw moment,

$$M_Z^{\lim} \triangleq l_F F_{Y_F}^{\lim} - l_R F_{Y_R}^{\lim} + s \Delta F_X \ , \tag{3.5}$$

where $s = b/2$ (half track-width). Here $M_Z^{\lim}$ thus is the sum of the yaw moment contributions when saturating all tires in the direction of the turn, for a given drive force distribution. $M_Z^{\lim}$ indicates which axle is setting the limit for the lateral acceleration, since a yaw moment balance ($\Sigma M_Z = 0$) is required at steady-state. If the $M_Z^{\lim} > 0$ (terminal oversteer), the rear axle is limiting and the front axle is limiting if $M_Z^{\lim} < 0$ (terminal understeer) [39]. In order to determine the maximum lateral acceleration, the relationship between; the lateral forces at the front- and rear axle; and the lateral acceleration; needs to be established. For this purpose it is common to simplify Eq. (2.12) to the simple bicycle model as shown in Fig. 2.3. The dynamic equilibrium (quasi steady-state) equations for assuming small steer angles are here

$$\begin{cases} F_{X_F} + F_{X_R} = ma_X \\ F_{Y_F} + F_{Y_R} = ma_Y \\ l_F F_{Y_F} - l_R F_{Y_R} + s\Delta F_X = 0 \end{cases} \tag{3.6}$$

We now have two equations in Eq. (3.6) that establish the relationship between the lateral forces and the lateral acceleration. Now order to determine the limit lateral acceleration, $a_Y^{\lim}$, one more equation is required (two equations and three unknown, a_Y, F_{Y_F}, F_{Y_R}). We know, however, that at the limit one or both axles are saturated, i.e. $F_{Y_F} = F_{Y_F}^{\lim}$ and/or $F_{Y_R} = F_{Y_R}^{\lim}$. As indicated previously, the sign of $M_Z^{\lim}$ give the condition for which axle is limiting the lateral acceleration, i.e. $F_{Y_F} = F_{Y_F}^{\lim}$ if $M_Z^{\lim} < 0$ when $a_Y = a_Y^{\lim}$. Combining this insight with Eq. (3.6) we have that, in QSS conditions,

$$a_Y^{\lim} = \begin{cases} \left(lF_{Y_F}^{\lim} + s\Delta F_X\right)/(ml_R) & ,\text{if} M_Z^{\lim} < 0 \\ \left(lF_{Y_R}^{\lim} - s\Delta F_X\right)/(ml_F) & ,\text{if} M_Z^{\lim} > 0 \\ \left(F_{Y_F}^{\lim} + F_{Y_R}^{\lim}\right)/m & ,\text{if} M_Z^{\lim} = 0 \end{cases} \tag{3.7}$$

The above equations conclude this section on the lateral grip margin. In order to determine the lateral acceleration, a method that employs the concept of a limit yaw-moment was introduced. If the friction coefficient and the drive force distribution is known, these expressions provide a tool to compute the lateral grip margin. In the continuation of this chapter the influence of the front/rear- and left/right- drive force distribution is shown in detail, building on the methods introduced in this section. It will also be shown how the results in this section can be use to find the optimal drive force distribution.

3.2 Drive Force Distribution and Lateral Grip

The lateral grip has been defined as the maximum possible lateral acceleration, $a_Y^{\lim}$, at steady-state. It was seen that the lateral grip is not only dependent on the

maximum lateral grip of each individual tire, but also on the yaw-balance of the vehicle. At steady-state all moments around the vertical axis, yaw-moments, must result in a state of equilibrium. If the longitudinal forces are equal on the tires of each respective front and rear axle, the maximum possible lateral acceleration is determined by the axle which is able to produce the least amount of yaw moment from the lateral capacity of their tires. This is assumed to be the case in Section 3.2.1, and the influence of the drive force distribution on the lateral grip is described. If instead the longitudinal forces on either axle are not equal, the yaw moment contribution from the different drive/brake forces are able to force the axle with more lateral capacity to increase it's yaw moment. This can increase the lateral grip to the point where both axles fully utilize their lateral capacity as is further dealt with in Section 3.2.2

3.2.1 Effect of front/rear drive-force distribution

When analyzing the effect of the front- to rear drive force distribution, equal drive forces on the left and right wheels on each axle are assumed. From Eq. (3.6) and if $\Delta F_X = 0$, the lateral force on each axle is

$$\begin{aligned} F_{Y_F} &= \frac{l_R}{l} m a_Y \\ F_{Y_R} &= \frac{l_F}{l} m a_Y \end{aligned} \tag{3.8}$$

Further, neglecting the coupling between the lateral acceleration and the longitudinal load transfer as given by Eq. (A.10) we have:

$$\begin{aligned} F_{Z_F} &= \frac{m}{l}(l_R g - h a_X) \\ F_{Z_R} &= \frac{m}{l}(l_F g + h a_X) \end{aligned} \tag{3.9}$$

By combining Eq. (3.8) and Eq. (3.9) we can see that the utilized lateral friction, defined as F_Y/F_Z, is dependent on the longitudinal acceleration. This is an important result since it determines the over- and understeer of the vehicle and is not mentioned explicitly in the literature. By comparing the utilized lateral friction between the front and rear axle, we have that

$$\frac{F_{Y_F}}{F_{Z_F}} - \frac{F_{Y_R}}{F_{Z_R}} = -\frac{a_X a_Y h l}{(a_X h + g l_F)(a_X h - g l_R)} \, . \tag{3.10}$$

From the above result the conclusion can be drawn that the utilized friction is larger on the front axle compared to the rear axle when accelerating and vice versa for braking. If, for a moment, we assume that the lateral friction is not dependent on the longitudinal force (which is true for small longitudinal forces) the vehicle grip will be lost on the front axle prior to the rear when accelerating and vice versa for braking. This is the explanation why vehicles can spin-out close to the grip limit when subjected to sudden changes in normal force, for instance when releasing the accelerator pedal.

The so-called dynamic square mentioned in Section 2.4.5, is a useful tool to evaluate the influence of the drive-force distribution on the lateral grip limit. Building on the model introduced in this section, the friction can be less on the front axle than on the rear. This assumption is a modification of the results obtained in Section 2.4.5 and is typical for a front biased weight distribution.

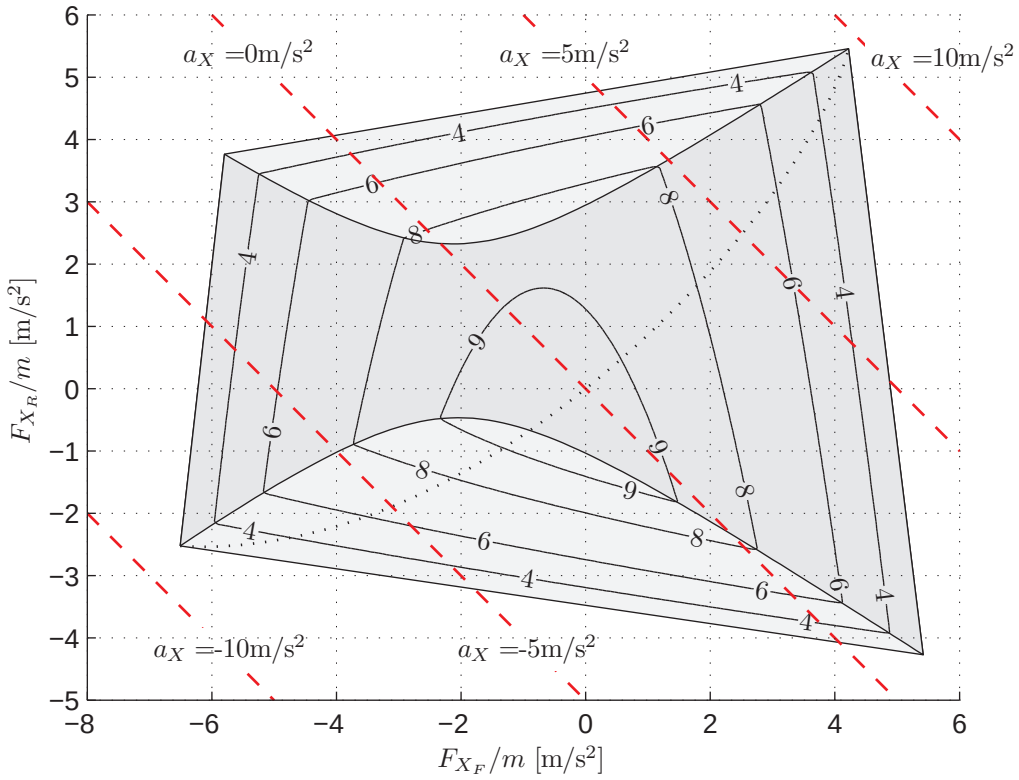

Figure 3.5: The Dynamic Square Method for evaluating the influence of front/rear drive (or brake) force distribution on the lateral grip margin

One question one could ask when studying the dynamic square diagram is: "Given a specific desired longitudinal acceleration, a_X, which front/rear drive force distribution results in the maximum possible lateral grip?" A section through

the dynamic square diagram for a constant $a_X \approx F_X^{\text{IN}}/m$ can be defined as $a_Y^{\lim}(\xi)\big|_{a_X=F_X^{\text{IN}}/m}$. The highest point on that section is the drive force distribution that maximizes $a_Y^{\lim}$, which is our definition of optimality. Thus, the front/rear drive force distribution, ξ, that minimizes

$$\min_{F_{X_F}\in\left[-\mu_F F_{Z_F},\mu_F F_{Z_F}\right]} - a_Y^{\lim}(F_{Y_F})\big|_{a_X=F_X^{\text{IN}}/m} \tag{3.11}$$

is the optimal drive force distribution. However, since this section is discontinuous where $M_Z^{\lim}=0$, it is not straightforward to solve Eq. (3.11). When studying Fig. 3.5 it can be seen that the maximum lateral grip for a given longitudinal acceleration is along the "ridge" between the area where the front axle first saturates (dark gray) and the area where the rear axle saturates first (light gray). Along the "ridge" between the two areas, both axles saturate simultaneously, where

$$a_Y^{\lim} = \sqrt{\bar{\mu}^2 g^2 - a_X^2}\ , \tag{3.12}$$

The optimal F_{X_F} for a given F_X^{IN} appear to be solutions where $M_Z^{\lim}=0$, except if $F_{X_F}F_{X_R}<0$, i.e. not both front and rear drive forces are positive. It thus appears that, the amount of front drive force F_{X_F}, that minimizes

$$\min_{F_{X_F}\in\left[-\mu_F F_{Z_F},\mu_F F_{Z_F}\right]} |l_F^2[(\mu F_{Z_F})^2 - F_{X_F})^2] - l_R^2[(\mu F_{Z_R})^2 - (\underbrace{F_X^{\text{IN}} - F_{X_F}}_{F_{X_R}})^2]| \tag{3.13}$$

is a candidate for the optimal drive force distribution. In the above distribution, Eq. (3.13) being zero can be interpreted as traversing the ridge in Fig. 3.5. On the other hand, it can be shown that the above condition does not give the optimal solution for small a_X. When reviewing Fig. 3.5 more closely we can, however, see that for small a_X, the optimal solution is *not* where $M_Z^{\lim}=0$.

It can be shown that all solutions of $F_{X_F}<0$ to Eq. (3.13) are non-optimal if $F_X^{\text{IN}}\geq 0$. Without exhausting this matter, it can be seen that point B in the Fig. 3.6 is where the constant longitudinal acceleration line (inclined dashed line) tangents the level curve where $a_Y^{\lim}=9\text{m/s}^2$ in Fig. 3.5. This tangent point results in the greatest $a_Y^{\lim}$ for a given longitudinal acceleration, i.e gives the optimal front/rear drive force distribution and which is when $F_{X_F}=0$. It also agrees with the intuition that as long as the front axle is limiting the lateral grip, i.e. $M_Z^{\lim}<0$, the optimal front/rear drive force distribution is to only drive the rear wheels ($\xi=0$) up to point C in the figure. The bold solid line in Fig. 3.6 shows the solution to Eq. (3.13) with constraint that F_{X_F} must be in the interval of $F_{X_F}\in[0,\mu_F F_{Z_F}]$. The bold dashed line shows the drive force distribution that arrises without this constraint, which gives in a lower $a_Y^{\lim}$ than would be the case if that constraint is added.

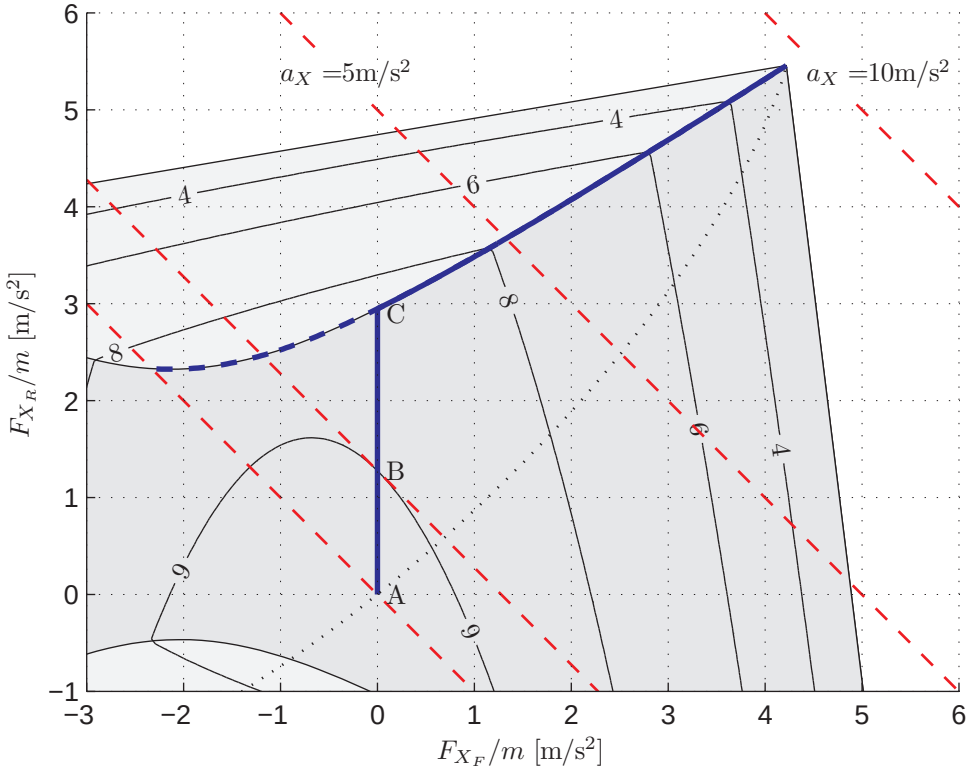

Figure 3.6: Optimal front/rear drive force distribution that minimizes $\min_{[F_{X_F} \in [0, \mu_F F_{Z_F}]}} |M_Z^{\lim}|$ shown with a bold solid line. Non-optimal solutions with $F_{X_F} < 0$ is indicated with bold dashed line.

A step further from the simple vehicle equilibrium as described in Eq. (3.6) is to also include the explicit effect of the front drive force in lateral force and yaw-moment balance. When assuming only front-wheel steer and small steering angles δ we have

$$\begin{array}{rrcrl} & F_{Y_F} + F_{X_F}\delta & + & F_{Y_R} & = m v_X \dot{\psi} \\ l_F & (F_{Y_R} + F_{X_F}\delta) & - & l_R F_{Y_R} & = 0 \end{array} \tag{3.14}$$

This effect can be included in the creation of dynamic squares when the steering angle is known. The effect is not further explored in this work, but it can be seen from the equations that a positive longitudinal force decreases the tendency for the front to saturate when steered in the direction of the turn. However, even at rather extreme steering wheel angles such as $\delta_{\mathrm{H}} = 180°$ the steered angle of the front wheels is only $\delta \approx 10° \approx 0.2$rad. This means that $\approx 20\%$ of the front drive force contributes to turning the vehicle.

3.2.2 Effect of left/right drive-force distribution

Following the study of the front/rear drive force distribution, the effect of the difference between the left- and right drive forces are studied in this section. It was shown in the previous section that for equal left/right drive forces, the yaw balance is primarily determined by the yaw moments caused by the lateral force of front- and rear axles. From this requirement of balanced yaw moments, the maximum possible lateral acceleration was determined by the axle which could provide the least yaw moment. It was also concluded previously that the maximum possible lateral acceleration is achieved if $M_Z^{\lim}$ is minimized for $\xi \in [0,1]$ for a given drive total drive force, F_X^{IN}. On the other hand, the best solution is if $M_Z^{\lim} = 0$ for $\xi \in [0,1]$, which was not reachable for small F_X^{IN}. The reason is that for small F_X^{IN}, the optimal drive force distribution is to only drive the rear wheels, but even when doing so, there is still unutilized lateral capacity at the rear axle. In order to achieve $M_Z^{\lim} = 0$ for all F_X^{IN}, one more control variable is needed; a additional yaw moment caused by different left/right forces. Since only one more degree of freedom is required, a decision is required, whether the left/right drive forces are to be varied on the front wheels, the rear wheels, or at both axles, with a single control? As previously concluded, the lateral grip limit for small F_X^{IN} and an optimal front/rear drive force distribution is determined by the front axle. Since the difference in drive forces reduce the lateral capacity, the rear axle is the better choice as long as $M_Z^{\lim} < 0$.

It can be shown, for a given front/rear drive force distribution $\xi \in [0,1]$ for which $M_Z^{\lim} \leq 0$; that the optimal difference in left/right drive forces, ΔF_{X_R} that solves

$$\begin{aligned}\arg_{\Delta F_{X_R}} & l_F \sum_{i=1}^{2} \sqrt{(\mu_i F_{Z_i})^2 - F_{X_F}^2/4} \\ & - \sum_{i=3}^{4} \left(l_R \sqrt{(\mu_i F_{Z_i})^2 - (F_{X_R}/2 + (-1)^i \Delta F_{X_R})^2} \right) + s\Delta F_{X_R} \equiv 0 \ ,\end{aligned} \tag{3.15}$$

given that

$$\Delta F_{X_R} < \sqrt{(\min(\mu_3 F_{Z_3}, \mu_4 F_{Z_4}))^2 - F_{X_R}^2/4} \ . \tag{3.16}$$

In order to find the optimal combined front/rear and left/right drive force distribution; first the $F_{X_F} \in [0, \mu_F F_{Z_F}]$ that minimizes $|M_Z^{\lim}|$ as given by Eq. (3.13) is found. Then if $M_Z^{\lim}$ after this first step still is less than zero, Eq. (3.15) is solved using the F_{X_F} found in the previous step, or otherwise. This final optimization step can also be used for systems that have limitations in the space of possible ξ that yield a $M_Z^{\lim} < 0$ for the minimum possible ξ.

3.2.3 Special cases

Based on more general method of computing $a_Y^{\lim}$ given in Section 3.1, $a_Y^{\lim}$ for the four different special cases given in Section 2.3.1 are given in this section. The special cases were:

- Front-wheel drive ($\xi = 1$)
- Rear-wheel drive ($\xi = 0$)
- Fixed all-wheel drive ($\xi \approx l_R/l - ha_X/(lg)$)
- Optimal all-wheel drive

By a fixed all-wheel drive is meant that the front- and rear differential units are fixed to rotate synchronously. This is commonly achieved for vehicles with a locked center differential, or a locked transfer clutch for hang-on all-wheel drive systems. For all configurations the assumption is that $\mu_F < \mu_R$ when $F_X = 0$.

Front-wheel drive

For a FWD vehicle it is assumed that $ma_X \approx F_{X_F}$, we then have that $M_Z^{\lim} < 0$, i.e. the front end of the front axle will saturate prior to the rear. From the Eq. (3.7) we can now derive the limit lateral acceleration for this vehicle configuration:

$$\begin{aligned} a_Y^{\lim} &= lF_{Y_F}^{\lim}/(ml_R) \\ &= \frac{l}{ml_R}\sqrt{(\mu_F F_{Z_F})^2 - F_{X_F}^2} \\ &= \frac{l}{ml_R}\sqrt{\left(\mu_F \frac{m}{l}(l_R g - ha_X)\right)^2 - (ma_X)^2} \\ &= \sqrt{\mu_F^2(g - a_X h/l_R)^2 - (a_X l/l_R)^2} \end{aligned} \tag{3.17}$$

under the condition that

$$|a_X| \leq \frac{\mu_F g l_R}{l + h\mu_F \operatorname{sign}(a_X)} \,. \tag{3.18}$$

The above condition restricts the longitudinal acceleration to be less or equal to the a_X that causes $a_Y^{\lim}$ in Eq. (3.17) reduce to zero, i.e. the maximum possible longitudinal acceleration.

Rear-wheel drive

Analogous to the FWD case, we can, derive $a_Y^{\lim}$ for a RWD vehicle $/ma_X \approx F_{X_R}$) as

$$a_Y^{\lim} = \sqrt{\mu_R^2(g + a_X h/l_F)^2 - (a_X l/l_F)^2}\ , \tag{3.19}$$

when $M_Z^{\lim} > 0$. However, $M_Z^{\lim} < 0$ for small F_{X_R} which for this case gives that

$$a_Y^{\lim} = lF_{Y_F}^{\lim}/(ml_R) = l\mu_F F_{Z_F}/(ml_R) = \mu_F(g - a_X h/l_R)\ . \tag{3.20}$$

From the above, we can see that $a_Y^{\lim}$ for the RWD case depends on which of Eq. (3.19) and Eq. (3.20) is valid, i.e. depends on the sign of $M_Z^{\lim}$. Combining these two equations it is evident that the limit lateral acceleration is given by the one that gives the least limit lateral acceleration:

$$a_Y^{\lim} = \min\left(\mu_F(g - a_X h/l_R), \sqrt{\mu_R^2(g + a_X h/l_F)^2 - (a_X l/l_F)^2}\right) \tag{3.21}$$

The limit for the maximum possible longitudinal acceleration is when $F_{X_R} = \mu_F F_{Z_R}$, which requires that

$$|a_X| \leq \frac{\mu_R g l_F}{l - h\mu_R \operatorname{sign}(a_X)}\ . \tag{3.22}$$

Synchronous front and rear differentials

As can be seen from Section 2.4.5 is that as long as $a_X < \mu g$, the front axle limits the maximum lateral acceleration for this configuration, i.e. $M_Z^{\lim} < 0\,\forall\, a_X < \mu g$. Now $ma_X \approx F_{X_F} + F_{X_R} = F_X^{\text{IN}}$ as introduced in Section 2.3.1 and the front/rear drive force distribution is approximately equal to the normal force distribution. From Section 2.3.1 we have that

$$F_{X_F} = \xi F_X^{\text{IN}} = \left(\frac{l_R}{l} - \frac{h}{l}\frac{a_X}{g}\right) F_X^{\text{IN}}$$

which inserted into Eq. (3.7) derives to

$$\begin{aligned} a_Y^{\lim} &= \frac{l}{ml_R}\sqrt{(\mu F_Z)^2 - F_{X_F}^2} \\ &= \frac{l}{ml_R}\sqrt{\left(\mu_F \frac{m}{l}(l_R g - h a_X)\right)^2 - (\xi m a_X)^2} \\ &= \frac{1}{l_R}\sqrt{\mu_F^2(l_R g - h a_X)^2 - (l_R g - h a_X)^2(a_X/g)^2} \\ &= \frac{l_R g - h a_X}{l_R g}\sqrt{\mu_F^2 g^2 - a_X^2}\ . \end{aligned} \tag{3.23}$$

Optimal front/rear distribution

In this section the optimal drive front/rear drive force distribution that fulfills Eq. (3.13) is shown. The restriction is on the drive force distribution which is required to be positive on both axles meaning $0 \leq \xi \leq 1$. This results in that the optimal drive force distribution is to drive only on the rear wheels up to the point when $M_Z^{\lim} = 0$. Thereafter the drive force is distributed to keep the limit yaw moment zero. Up to this transition point, the front wheels will set the limit for the lateral acceleration capacity due to the load transfer, off-loading the front wheels and increasing the normal force on the rear wheels. From Eq. (3.7) it thus follows that

$$a_Y^{\lim} = \min\left(\mu_F(g - a_X h/l_R), \sqrt{\bar{\mu}^2 g^2 - a_X^2}\right) \ , \tag{3.24}$$

given that the condition

$$\min_{F_{X_F} \in [0, \mu_F F_{Z_F}]} \left| M_Z^{\lim} \right| \tag{3.25}$$

is minimized for all $0 \leq a_X \leq \bar{\mu} g$.

Authority of some specific driveline configurations

The control authority of some driveline configurations which operate between the above special cases by controlling the slippage in one (or two) clutch(es) are described in Fig. 3.7, based on the previously described Dynamic Squares method. Table 3.1 describes configurations with one clutch. These configurations are of interest since they exist in a number of vehicle applications on the market today.

Description	**Clutch open**	**Clutch locked**	Subspace of possible ξ.
FWD $\Rightarrow$ Fixed AWD	$\xi = 1$	$\xi = F_{Z_F}/(mg)$	$\xi \in [F_{Z_F}/(mg), 1]$
RWD $\Rightarrow$ Fixed AWD	$\xi = 0$	$\xi = F_{Z_F}/(mg)$	$\xi \in [0, F_{Z_F}/(mg)]$
35:65[1] $\Rightarrow$ Fixed AWD	$\xi = 0.35$	$\xi = F_{Z_F}/(mg)$	$\xi \in [0.35, F_{Z_F}/(mg)]$

Table 3.1: Driveline configuration that operate between two different dirve force distributions by controlling a clutch.

The final configuration is not a configuration existing on any vehicle sold on the market, but is interesting since it operates between three different "modes" as given by Table 3.2

For all configurations in Fig. 3.7 it is important to consider the "rigid" AWD case, which was described in Section 2.3.1. In all these configurations, locking the front and rear axles together will yield the drive force distribution denoted as "Rigid" in the figure.

Front Clutch	**Rear Clutch**	**Drive force distribution**
Locked	Open	$\xi = 1$
Locked	Locked	$\xi = F_{Z_F}/(mg)$
Open	Locked	$\xi = 0$

Table 3.2: Driveline configuration that operate between three different drive force distributions by controlling two clutches

From Fig. 3.7.a it can now be seen that this vehicle, which is FWD in it's basic configuration (open clutch), can only operate at an optimal front/rear drive force distribution at upper right vertex of the diagram. However, this vehicle configuration is not able to accomplish a drive force distribution above the "rigid" line. This vehicle should therefor have excellent take-off capability, but could lack cornering capacity relative to an optimal AWD system under combined acceleration/cornering. The advantage of this system, however, is that it always operates in the "safe" area where $M_Z^{\lim} < 0$.

The configuration shown next in Fig. 3.7.b, on the other hand is a RWD based vehicle is the inverse of the previous case and has the authority to optimize the torque transfer to the front axle such that the optimization criteria given in Eq. (3.25) is fulfilled. On the other hand, operating in the light grey area where $M_Z^{\lim} > 0$, by improper control, can lead to instability.

The third configuration shown in Fig. 3.7.c is what often is called permanent AWD, with center differential providing a fixed front/rear drive force distribution. This system has no particular advantage over the system shown in Fig. 3.7.b when it comes to controllability. The advantage is mainly that the demand on the clutch is less, since only a smaller amount of the total torque is transferred through the clutch. This configuration one of the most common on AWD vehicles, when also vehicles without a controllable clutch are considered.

The final configuration, shown in Fig. 3.7.d is able to operate in the entire first quadrant of the dynamic square diagram (however, not in the second, unless the brakes are used) and is therefor an interesting concept. This system combines the benefits of both the configurations in Fig. 3.7.a) and Fig. 3.7.b). The disadvantage of this configuration is that two clutches are required and that both need to be packaged near the transmission. In vehicles with a transversely mounted engine with the configuration in Fig. 3.7.a), the clutch is often located near the rear axle where there is more package space. In these vehicles, it is often not possible to package two clutches near the transmission.

The results of $a_Y^{\lim}$ as function of a_X for these four configurations are also shown in a g-g diagram. This method shows, as described in Section 2.4.6, sections through the dynamic square for special drive force distributions. These re-

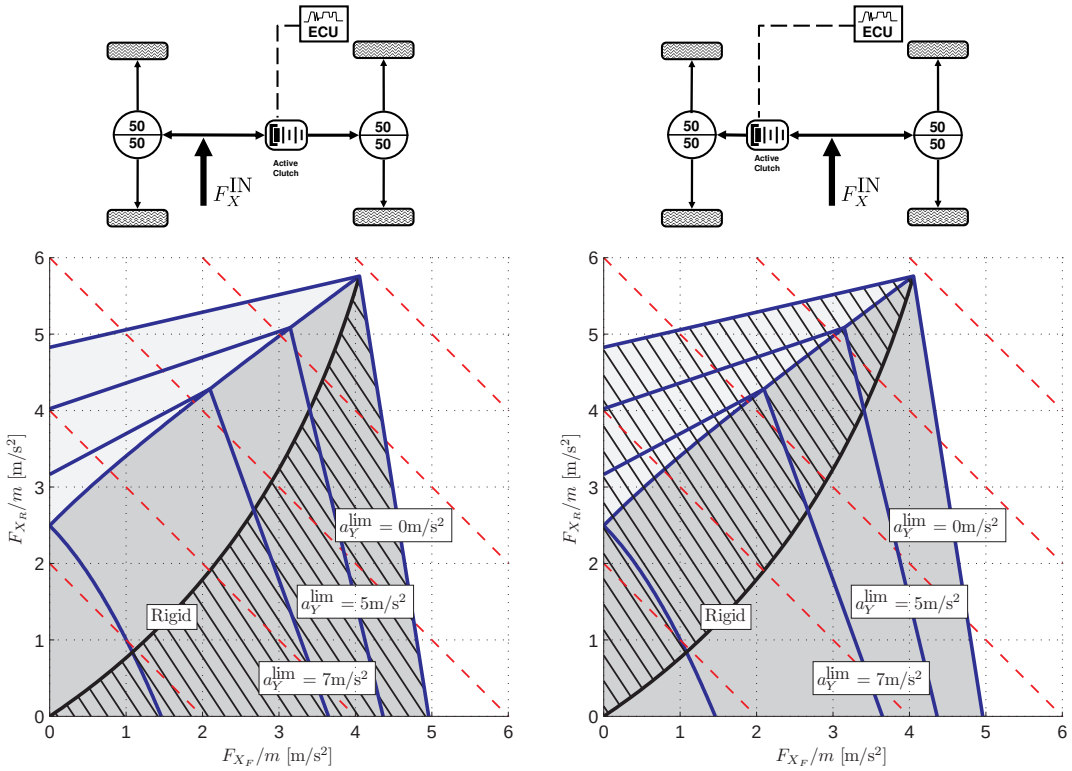

a.) FWD w. rear axle torque transfer control

b.) FWD w. front axle torque transfer control

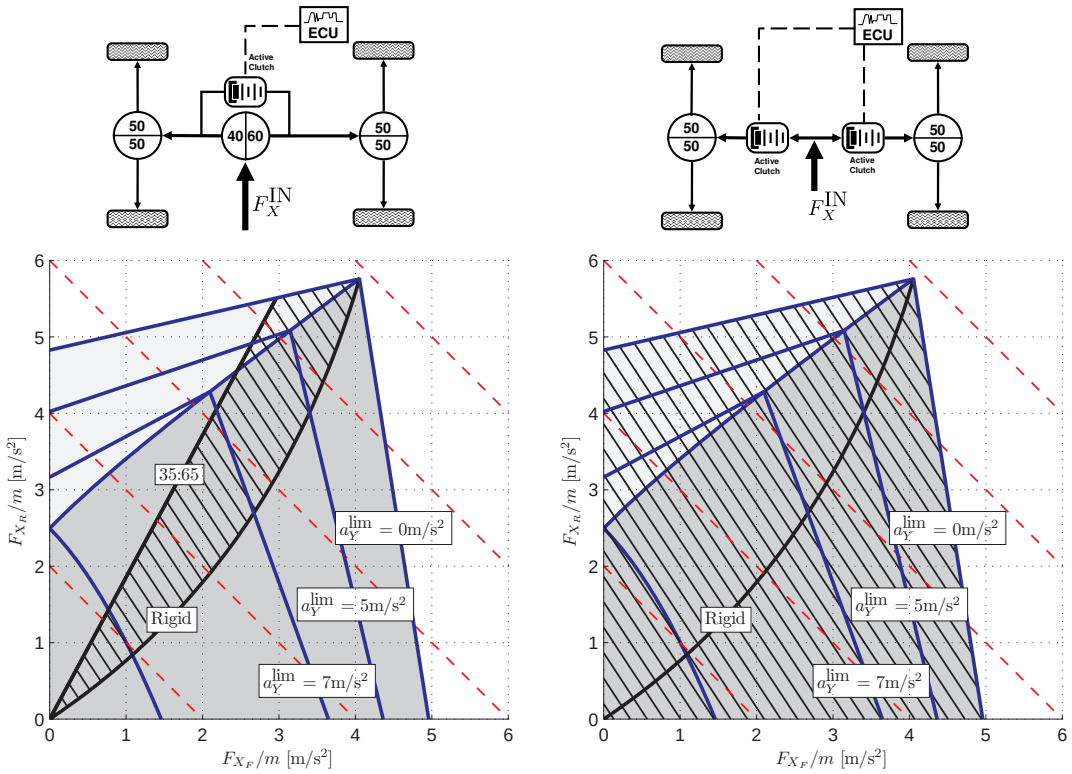

c.) Permanent AWD w. center diff. control

d.) Front and rear axle torque control

Figure 3.7: Authority shown as a hatched area for four different configurations. Rigid in the Dynamic Square diagrams means a locked center clutch.

sults are shown in Fig. 3.8. As can be seen from Fig. 3.8 for this particular

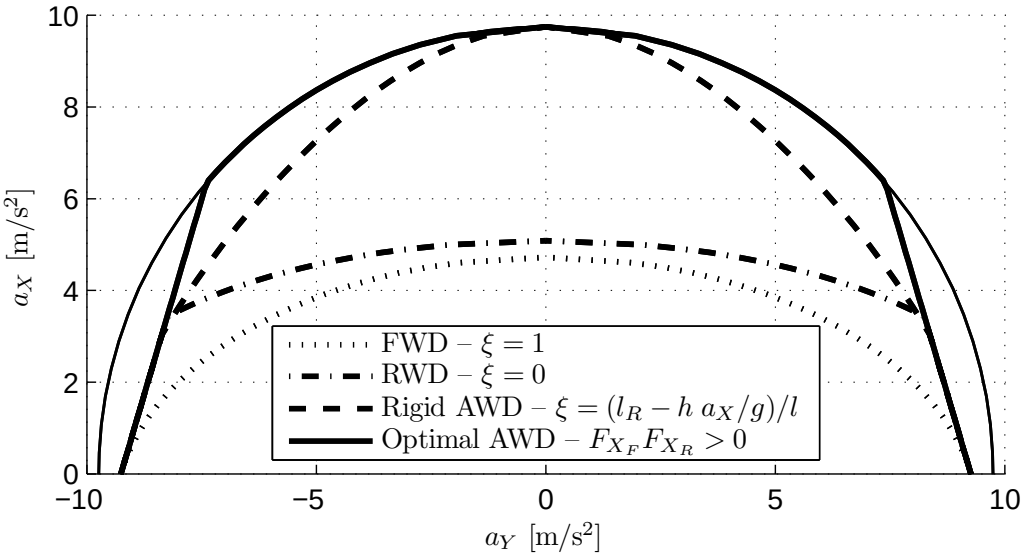

Figure 3.8: g-g diagrams for four different drive force distributions

weight distribution, the FWD vehicle has a larger longitudinal acceleration capability than the RWD vehicle. The acceleration capabilities for an arbitrary weight static front/rear weight distribution is shown in Fig. 3.9. The maximum lateral acceleration is given by the conditions Eq. (3.18) and Eq. (3.21) for the FWD and RWD vehicle respectively. In order to get a feel for these figures, it is often useful to take look at the extremes. For a FWD vehicle, the more weight on the front axle, the better the maximum forward acceleration under the condition that engine power is unlimited. The maximum weight possible would then be the entire weight of the vehicle, which is only possible if the center of mass would be placed in front of the front axle. Analogously for a RWD vehicle, more weight on the rear axle is better. Since the forward acceleration moves weight to the rear axle, there is a point where moving the center of mass even would cause the front wheels to lift from the ground when accelerating.

3.3 Drive Force Distribution and Understeer

This section describes the effect of the drive force distribution on the understeer of the vehicle. As earlier described in Section 2.2.4, the understeer gradient is

[1]Example of a fixed front/rear distribution

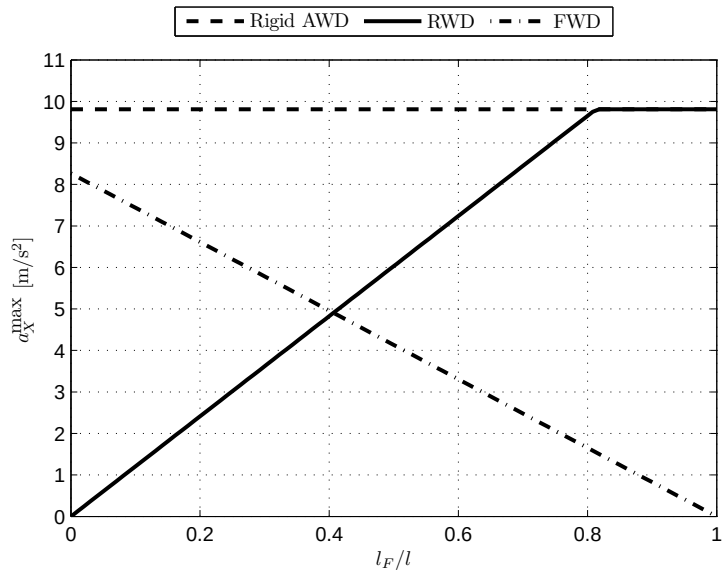

Figure 3.9: Maximum longitudinal acceleration versus the static front/rear distribution

defined in [21] as

$$K_{\mathrm{US}} \triangleq \frac{\partial(\delta - l/R)}{\partial a_Y} \equiv \frac{\partial(\alpha_f - \alpha_r)}{\partial a_Y} \ ,$$

It will be shown in this section that the front/rear the effects on the understeer can be divided in parts, namely the effect of the

- load transfer caused by acceleration or braking,
- drive force on the cornering stiffness and
- yaw moment caused by different left/right longitudinal forces.

The first two effects will be discussed in the Section 3.3.1 and the third effect in Section 3.3.2 dealing with the effect of left/right drive force distribution.

3.3.1 Effect of front/rear drive force distribution

For the study of effect of the front/rear drive force distribution on the understeer, we recall that the understeer in vehicle parameters as given by Eq. (2.21) is

$$K_{\mathrm{US}} = -\frac{m}{l}\frac{l_F C_{\alpha_F} - l_R C_{\alpha_R}}{C_{\alpha_F} C_{\alpha_R}} \ .$$

By introducing, C'_α, as the effective cornering stiffness for a given drive force F_X as

$$C'_\alpha \triangleq \left.\frac{\partial F_Y}{\partial \alpha}\right|_{\alpha \to 0} , \tag{3.26}$$

which combined with Eq. (2.1) becomes

$$C'_\alpha = c_\alpha F_Z \sqrt{1 - \left(\frac{F_X}{\mu F_Z}\right)^2} . \tag{3.27}$$

By replacing the normal force with the expression as given in Eq. (3.9) and by using that C_α is the cornering stiffness at the *static* normal force we have that

$$C'_{\alpha_F} = C_{\alpha_F} \left(1 - \frac{h}{l}\frac{a_X}{g}\right) \sqrt{1 - \left(\frac{F_{X_F} l}{\mu m (l_R g - h a_X)}\right)^2} , \tag{3.28}$$

which can be further simplified for small F_X as

$$C'_{\alpha_F} \approx C_{\alpha_F} \left(1 - \frac{h}{l}\frac{a_X}{g}\right) \tag{3.29}$$

and similarly

$$C'_{\alpha_R} \approx C_{\alpha_F} \left(1 + \frac{h}{l}\frac{a_X}{g}\right) . \tag{3.30}$$

By further replacing the cornering stiffness, C_α, in Eq. (3.3.1) with the approximations of the effective cornering stiffness, C'_α given by Eq. (3.29) and Eq. (3.30) we have that

$$\begin{aligned} K_{\text{US}} &= -\frac{m}{l}\frac{l_F C'_{\alpha_F} - l_R C'_{\alpha_R}}{C'_{\alpha_F} C'_{\alpha_R}} \\ &= -mg\frac{l_F C_{\alpha_F}(lg - h a_X) - l_R C_{\alpha_R}(lg + h a_X)}{C_{\alpha_F} C_{\alpha_R}(l^2 g^2 - h^2 a_X^2)} . \end{aligned} \tag{3.31}$$

This modified expression of the understeer is an important result and can be used to explain why a vehicle can become oversteered when braking ($a_X < 0$) and that acceleration ($a_X > 0$) explicitly increases understeer. By using the above result, Fig. 3.10 shows the understeer gradient as a function of longitudinal acceleration.

As the above result is a very simple way to take into account the load transfer caused by acceleration and braking, it does not take into account the drive force distribution. Since the dynamic-square method described in Section 2.4.5 is an effective way to show the influence of the drive force distribution on the lateral

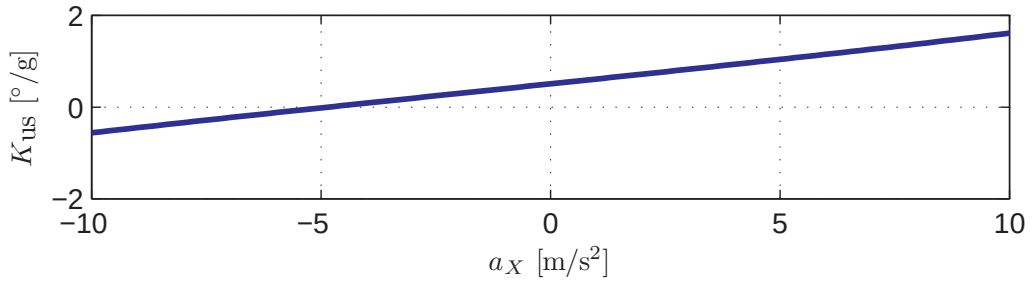

Figure 3.10: Understeer gradient as function of longitudinal acceleration

grip; the idea was that it also could be used to show the effect on the understeer. Given that proposal, the understeer was plotted versus all possible combinations of front/rear drive force distributions. The understeer gradient at $a_Y = 0$ is plotted under the assumption that the cornering stiffness changes according to Eq. (3.27).

In Fig. 3.11 the results of this modified dynamic square can be seen. The diagram shows the effect of the rear wheels saturating along the top- and bottom edges. Along these edges, $K_{\mathrm{US}} \rightarrow -\infty$ as $C'_{\alpha_R} \rightarrow 0$ because $F_{X_R} \rightarrow \mu_R F_{Z_R}$; similarly, along the left- and right edges where the front wheels saturate, $K_{\mathrm{US}} \rightarrow \infty$ as $C'_{\alpha_F} \rightarrow 0$ when $F_{X_F} \rightarrow \mu_F F_{Z_F}$. Further, the diagram is divided into three different areas; the light-gray areas at the top and bottom are areas where the understeer gradient is negative, i.e. oversteeer; conversely, the dark gray areas indicate (positive) understeer. Based on these discriptions, the edges between the dark and light areas mark the neutral steer boundaries, i.e. where $K_{\mathrm{US}} = 0$. Finally; as in the previous usage of the dynamic square, the dotted line is where the drive force distribution is proportional to size the normal force as given by Eq. (2.27).

3.3.2 Effect of left/right drive force distribution

Now having discussed the implications of the front/rear drive force distribution on the understeer of the vehicle; the next topic of interest is the effect of the left/right drive force distribution. Or rather, it is the effect of the difference between the left and right drive forces which are the subject of this section. In this research there was an interest to evaluate the effect of controlling the speed difference across the rear axle. By restricting the nominal speed difference of the rear axle $b\dot{\psi}$ (see Eq. (A.7)) by locking the differential, an understeering moment is added to the vehicle. If instead, a fixed speed difference $> b\dot{\psi}$ is imposed on the axle, the added moment decreases the understeer.

One further contribution of this research is to show how the handling diagram, described in Section 2.4.1, can be used to evaluate the effectiveness of an torque

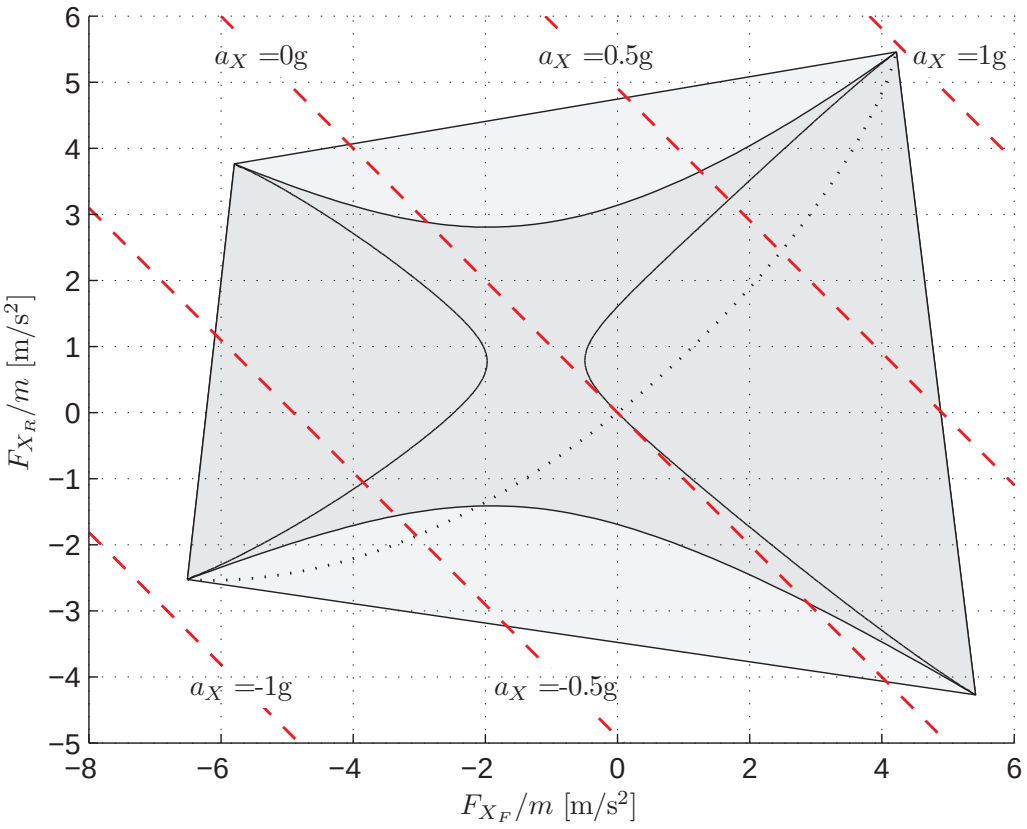

Figure 3.11: Modified Dynamic Square method which shows the influence of the drive force distribution on the understeer gradient, K_{US} at $a_Y = 0$.

vectoring differential or a limited slip differential. For this purpose, knowing the maximum speed difference which can be imposed by the torque vectoring differential when fully locked, the handling diagram for this configuration is drawn. The assumption in this research was that a constant understeer was desirable, so if the optimization criteria

$$\min_{n^{\mathrm{L/R}}\in\mathbb{R}} K_{\mathrm{US}} a_Y - \left(\sum_{i=1}^{2} \alpha_i - \sum_{i=3}^{4} \alpha_i \right) , \tag{3.32}$$

is minimized $\forall\ a_Y \leq a_Y^{\lim}$ the understeer is constant up to the lateral grip limit. Here K_{US} is a tuning parameter which here is assumed to be the understeer of the vehicle when $a_Y \to 0$ and $a_X \to 0$. The above result is based on the understeer definition Eq. (2.15), i.e. if the difference between the average slip angles on the front and rear axle increase linearly with the lateral acceleration, the understeer is constant.

3.3.3 Critical speed considerations

In Section 3.1 the limit speed, $v_X^{\lim}$, is computed for the speed at which the front or rear axle reach saturation. As briefly discussed in Chapter 3, the vehicle could become unstable at a lower speed than the saturation limit of the front and rear tires. One such a scenario is when the slip angles at the rear axle build up faster than at the front. This scenario defines an oversteered vehicle which will become unstable when reaching the *critical speed*. The vehicle stability is related to the understeer coefficient, K_{US}. From Section 2.2.3 we have that

$$\frac{\dot{\psi}^{\mathrm{ss}}}{\delta} = \frac{v_X}{l + K_{\mathrm{US}} v_X^2}, \tag{3.33}$$

from which it can be seen that the stability limit is when $K_{\mathrm{US}} v_X^2 = -l$, given that $K_{\mathrm{US}} < 0$. The speed at which this occurs is commonly referred to as the *critical speed*, which here is denoted as v_X^{crit}. Further the transfer function from $\delta \to v_Y$ is

$$\frac{a_Y^{\mathrm{ss}}}{\delta} = \frac{v_X^2}{l + K_{\mathrm{US}} v_X^2},$$

for which the same stability criteria as for $\dot{\psi}^{\mathrm{ss}}/\delta$ is valid.

The question is now, when is the $v_X^{\mathrm{crit}} \leq v_X^{\lim}$, i.e. when is the speed at which the vehicle becomes unstable is less or equal compared to the speed at which either axle saturates?

Since we have that at steady state that the critical speed,

$$(v_X^{\mathrm{crit}})^2 = -\frac{l}{K_{\mathrm{US}}},\ \text{if}\ K_{\mathrm{US}} < 0$$

and the in limit speed from Eq. (3.1);

$$(v_X^{\lim})^2 = a_Y^{\lim} R = a_Y^{\lim} \left| \frac{v_X}{\dot{\psi}} \right| ,$$

we are interested to see at when $v_X^{\text{crit}} \leq v_X^{\lim}$, namely when

$$K_{\text{US}} \leq -\frac{l}{a_Y^{\lim}} \left| \frac{\dot{\psi}}{v_X} \right| . \tag{3.34}$$

The solution to this issue is to analyze when $v_X \to v_X^{\lim}$. It should be noted that it is common for the critical speed to decrease very rapidly after K_{US} has changed sign from positive to negative. In order to maintain a safe distance of Δv_X between the vehicle speed and the critical speed, the condition is that

$$|v_X - v_X^{\text{crit}}| < \Delta v_X . \tag{3.35}$$

To summarize, if $K_{\text{US}} < 0$ it is not sufficient only to study the speed at which the lateral grip limit is reached. Concurrently, the critical speed must be computed based on the understeer of the vehicle. When the current speed is approaching the critical speed, the intersection between the two speeds will be the point where the vehicle becomes unstable.

3.4 Summary

In this chapter, the influence of longitudinal acceleration and the drive force distribution on the lateral grip and understeer was shown. The effects studied were limited to steady-state analysis with constant longitudinal acceleration, defined as quasi steady-state conditions. Further; drag forces, such as rolling resistance and aerodynamic drag; and steering effects, were neglected. The benefit of these simplifications were, however, that the often complex interaction between the longitudinal and lateral characteristics could in many cases be shown using close form expressions. In this way, the various effects could systematically be analyzed and quantified.

First, the change in normal force distribution due to (positive) longitudinal acceleration was shown to linearly decrease the lateral capacity on the front axle and increase the understeer gradient. The contribution of this work relating to this phenomena are the expressions which relate the longitudinal acceleration to the understeer. For braking, the results are opposite the acceleration case. Secondly there is an effect of the drive force itself on the lateral grip. This effect starts to dominate the influence on the lateral capacity and understeer when the drive

force is sufficiently large ($F_X \approx 0.4\mu F_Z$). Subsequently how the drive force is distributed on the front and rear axles is important to consider in the latter case.

A further area of contribution in this work is the development of a lateral grip margin was developed which could be used to evaluate the effect of the drive force distribution on the maximum possible lateral acceleration. From this lateral grip margin, conditions for optimality, were given separately for the front/rear drive force distribution as well as the left/right drive force distribution. Further, the results used to compute the lateral grip margin for a general drive force distribution was developed for four special cases; front-wheel drive; rear-wheel drive; all-wheel drive with synchronous front- and rear differentials; and finally, an optimal front/rear drive force distribution. Subsequently, the expressions that relate the longitudinal acceleration to the lateral acceleration limit were shown to be useful when generating g-g diagrams (showing $a_Y^{\lim}$ versus a_X) for the above mentioned special cases. Further, the it was shown that these g-g diagrams were sections in the dynamic square diagram, the latter showing the effect of the lateral acceleration capacity for an arbitrary front/rear drive force distribution. Expressions on the optimal left/right drive force distribution were shown and were related to previously derived conditions for the optimal front/rear drive force distribution. Based on these results, the conclusion is drawn that keeping the understeer constant while optimizing the lateral grip under all operating conditions, requires a combination of front/rear and left/right drive force distribution optimization. Finally, the implications of the change in understeer by means of drive force distribution on vehicle stability was discussed in the case the understeer becomes negative (oversteer).

Chapter 4

Simulations and Results

The purpose with the following simulations was to evaluate the validity and limitations of the theory developed in the previous chapter.

The evaluation was performed such that it starts with QSS conditions, for which the theory developed in Chapter 3 was valid, and which relates the drive force and drive force distribution to the lateral grip and understeer. The vehicle model in the simulations is, however, more comprehensive than the one for which this theory was developed. It was therefor expected that discrepancies between the predicted lateral grip and understeer and simulation results relate to these modeling simplifications. The purpose of the first part of this study was therefor to identify these shortcomings.

Continuing the evaluation, transient steering input was evaluated. For these simulations the lateral acceleration will after some time, for a stable solution, approach a steady state value. As the steering amplitude was increased until no further increase in lateral acceleration was possible, this maximum steady state value should correspond to the predicted lateral grip limit. Another purpose of this test was to evaluate if the lateral acceleration during the transient part of the maneuver can exceed the predicted lateral grip limit.

Finally, a dynamic maneuver was performed at increased steering input amplitude. During these maneuvers, the lateral acceleration never reaches steady-state and the theory developed in this work, should therefor not be valid in this case. The purpose of this part of the evaluation was to identify areas where the lateral grip margin computation could be improved to also identify the lateral grip limit during dynamic maneuvering.

Results are plotted in this chapter and further simulations results are provided in Appendix B.

4.1 Quasi–steady state cornering – fixed steering

The purpose of steady state cornering analysis was to evaluate the understeer, and lateral grip limit of the vehicle while cornering. The performed vehicle simulations are based on a modified version of the test procedure ISO4138:2004 [23]. According to the test procedure, they can be run in three different ways:

1. Constant radius – speed is slowly increased
2. Constant steering angle – speed is slowly increased
3. Constant vehicle speed – steering angle is slowly increased

Quasi–steady state (QSS) in this work means steady braking and acceleration while cornering with a fixed steering angle or constant curve radius as discussed in Section 2.2.2. This method is a natural extension of the steady-state cornering and is useful to evaluate the influence of the drive force distribution on the cornering behavior of the vehicle, which is the objective of this research. The idea of using constant braking and acceleration is that the analysis methods used for the steady-state cornering case are assumed to still hold, which they are not expected to do when doing dynamic steering maneuvers.

The simulations in this work, using the model described in Appendix A, were performed at various levels of constant drive forces; and on two different surfaces. The vehicle speed was then slowly increased until the either front- or rear axle saturated; while keeping the steering angle constant.

4.1.1 Results – front/rear drive force distribution

The front/rear drive force distribution configurations which are studied studied are:

- Front wheel drive
- Rear wheel drive
- All-wheel drive – synchronous front- & rear differentials

The test objectives were to evaluate the effects of the more comprehensive on the lateral grip computation given in Chapter 3. Additionally, the understeer of the vehicle was estimated based on the drive force distribution. The results of the understeer estimation, along with the lateral grip estimation, are shown in Fig. 4.1 and Fig. 4.2. In these figures, six different operating conditions are verified on two different surfaces; dry asphalt $(\mu_0 \approx 1)$ and snow $(\mu_0 \approx 0.4)$. The driveline configurations which are evaluated are the first three as given in Table 2.1. These

configurations were evaluated with two different levels of constant drive force, as given by the title of each subfigure. The inclined thin line is the predicted understeer; the vertical thin line is the limit lateral acceleration; and the circle the maximum lateral acceleration achieved in the detailed vehicle model.

In Fig. 4.1.e and Fig. 4.2.e it should be noted that the vehicle becomes unstable before reaching the lateral grip limit. This issue was discussed in Section 3.3.3. The circle in these sub-figures is therefor not a steady-state lateral acceleration, since the vehicle is unstable. The point of instability is indicated by a $\diamond$-character. At this point, the condition in Eq. (3.35) is violated. A different point indicated by a square is the point where

$$\begin{cases} \delta - l/R = 0 \\ K_{\mathrm{US}} < 0 \end{cases} . \tag{4.1}$$

Additional to the results shown in Fig. 4.1 and Fig. 4.2, a condensed parameter sensitivity study was performed. The conclusions from this parameter study together with the results shown in Fig. 4.1 and Fig. 4.2 are that:

- $a_Y^{\lim}$ is predicted to be approximately 10% more, on high-μ surfaces, than possible with the more comprehensive vehicle model used in the simulations. On low-μ surfaces this error is reduced to apprimately 3%. From the parameter study results shown in Appendix B, the conclusion is that the main descrepancy between the $a_Y^{\lim}$ computation and the actual maximum atainable lateral acceleration is the lateral load transfer, which reduces μ_F and μ_R.

- the longitudinal acceleration, a_X, and thereby the longitudinal load transfer is significantly influenced the following resistance forces,

  - $\delta F_{Y_F}/m$ for high lateral acceleration and
  - F_{D} where the aerodynamic drag dominates at high speeds (>50 km/h) and the rolling resistance at low speeds;

  both of which are attained at high-μ surfaces. For low-μ surfaces, the most noticeable factor is the rolling resistance, which can be up to 50% of the available friction. This reduction in a_X relative the predicted F_X^{IN}/m is significant for the computation of the lateral grip insofar that it influences the load transfer front/rear.

A final conclusion, which can be drawn from the results given in Appendix B, is that when the model with which the simulations were performed, was equal to the one for which the theory was developed (second “block” in these tables), the remaining difference in the results could be attributed to the QSS simplifications

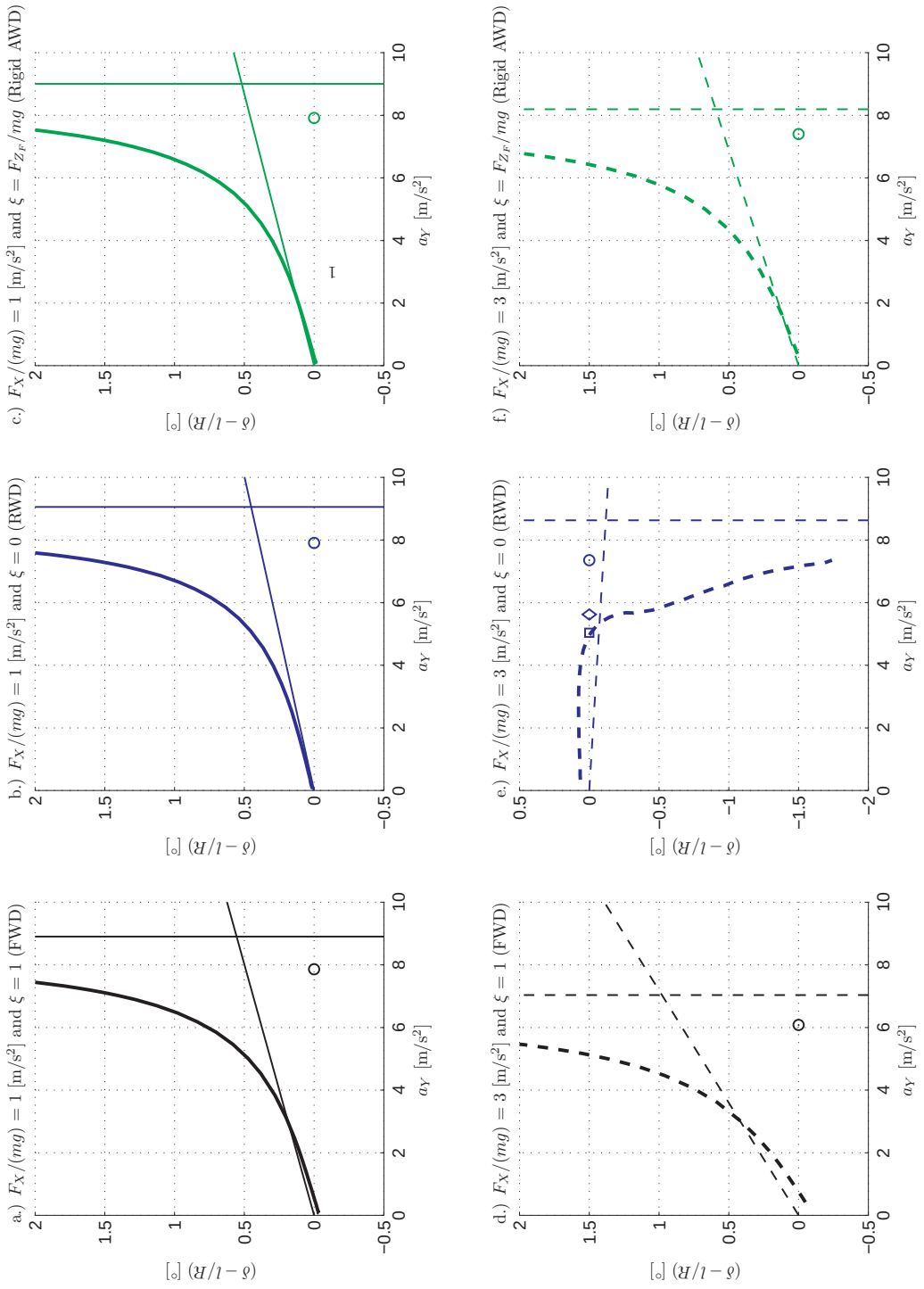

Figure 4.1: Plots of $\delta - l/R$ versus a_Y for constant steering ($\delta_{\mathrm{H}} = 80°$), constant longitudinal force starting at a low longitudinal speed. The surface is assumed to be dry asphalt ($\mu \approx 1$) and the figures show the results of three different drive force distributions and two different levels of constant drive force, as indicated by the headings of each sub-figure. The inclined thin line is the predicted understeer; the vertical thin line is the limit lateral acceleration; and the circle the maximum achieved lateral acceleration.

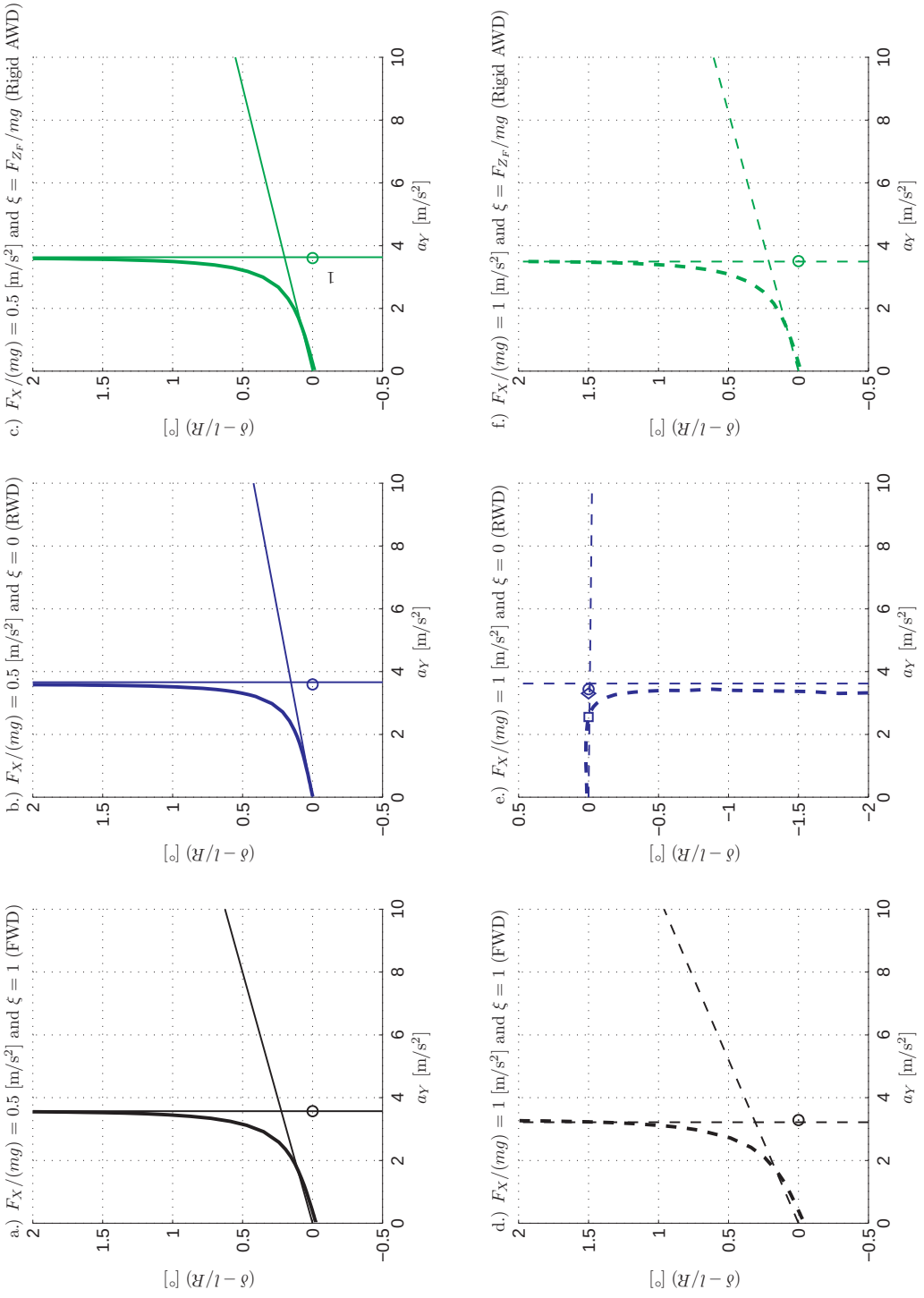

Figure 4.2: Plots of $\delta - l/R$ versus a_Y for constant steering ($\delta_{\mathrm{H}} = 80°$), constant longitudinal force starting at a low longitudinal speed. The surface is assumed to be packed snow ($\mu \approx 0.4$) and the figures show the results of three different drive force distributions and two different levels of constant drive force, as indicated by the headings of each subfigure. The inclined thin line is the predicted understeer; the vertical thin line is the limit lateral acceleration; and the circle the maximum achieved lateral acceleration.

discussed in Section 2.2.2. Based on the fact that the remaining differences are small, the conclusion is that the QSS assumptions hold for the simulated cases and as long as the vehicle was stable.

4.1.2 Results – left/right drive force distribution

Figure Fig. 4.3 shows the simulation results of the configurations that were discussed in Section 2.3.2, namely an

1. Open rear differential
2. Locked rear differential
3. Fixed positive ratio between inner and outer wheel
4. Variable L/R ratio which fulfills Eq. (3.32)

These results are plotted in a handling diagram first developed by Pacejka [48, 26, 49]. The handling diagram is an alternative way of presenting the results obtained from the cornering test described in this section. Further, this method can therefor be used to evaluate the understeer characteristics as well as the lateral grip limit for a given vehicle configuration. It can be then seen from the handling diagram that the understeer (the slope of the slip angle difference versus the lateral acceleration) increases with increased utilization of the lateral grip for a vehicle with equal left/right drive force distribution. If however the drive force is re-distributed from one side of the car to the other [55, 70, 16, 56, 64, 50] the understeer can be kept constant up to the grip limit. In addition to providing consistent handling, it can also be seen from the diagram that the maximum grip is increased by utilizing both axles to their maximum potential, whereas the front axle was limiting the lateral grip for the passive vehicle. Referring to the characteristics of a passive vehicle, the unaltered dynamics in combination with the increased lateral grip by using drive-force distribution could lead to a conflict between performance and consistent dynamics on the one hand and the need of driver feedback/warning on the other as previously described. The proposed solution to this conflict is a lateral grip margin which shows the relative distance to the lateral grip limit. When the lateral grip margin is reduced to a preset level, warning strategies could be executed to warn the driver. The details of these warning strategies are however outside the scope of this present work.

4.2 Transient cornering – step-steer

A step-steer maneuver according to ISO7401:2003 [22] reveals the vehicle's response, damping and steady-state gain for the given maneuver. In Fig. 4.5 the

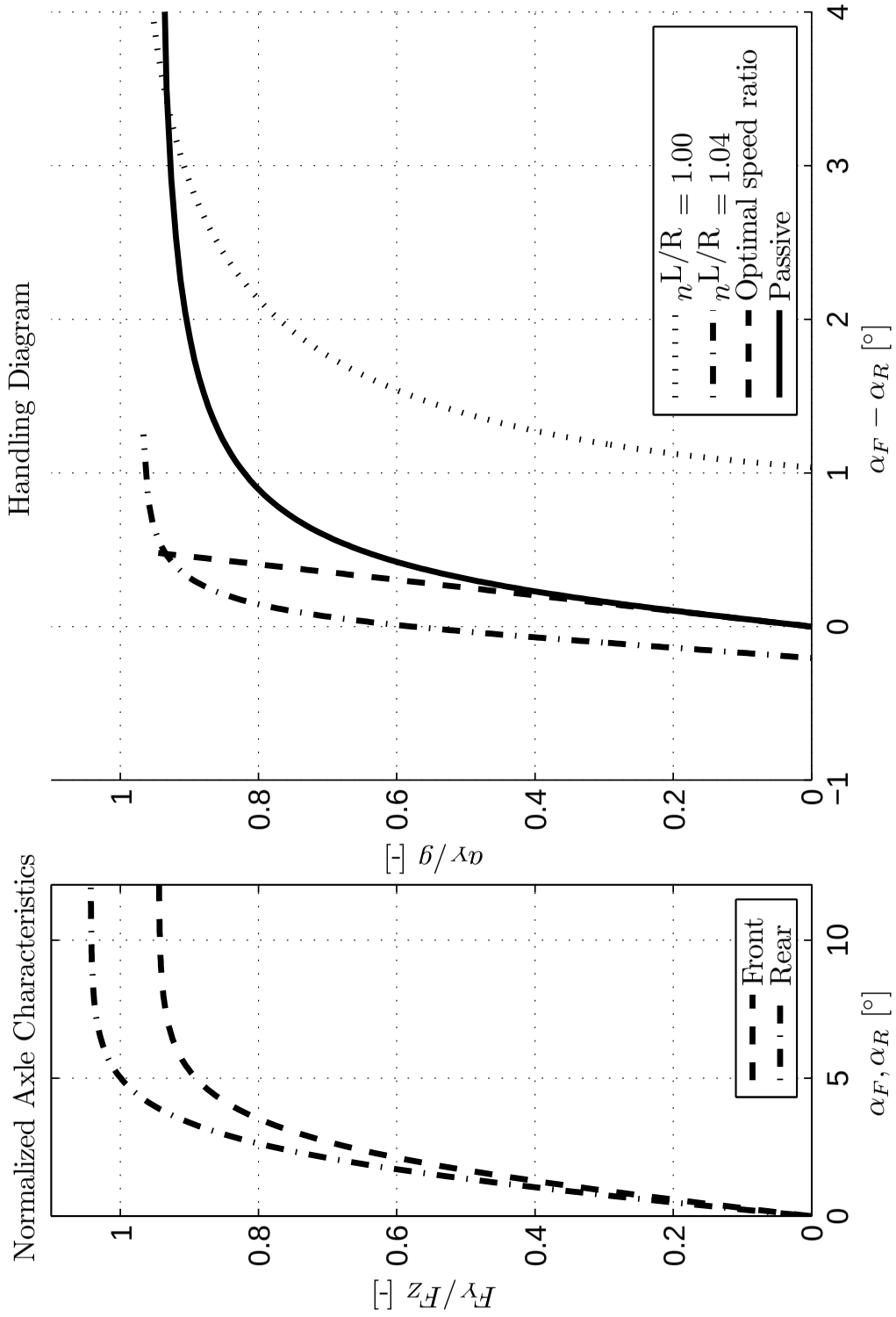

Figure 4.3: Handling diagram for various configurations

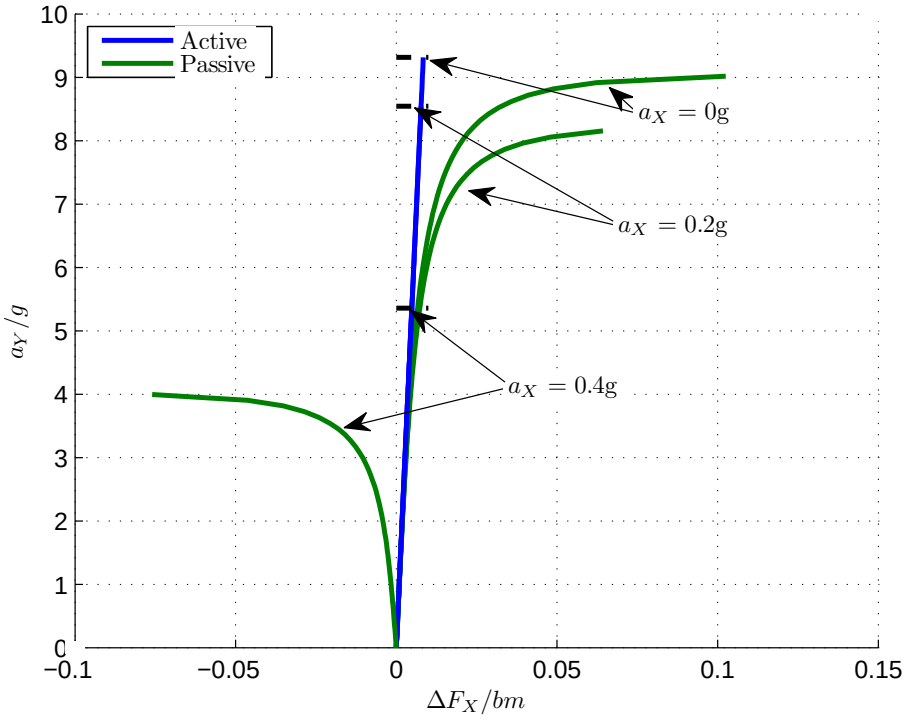

Figure 4.4: Example of how understeer increases with lateral acceleration for a passive vehicle but can be kept constant with torque vectoring (“active”) for any given longitudinal acceleration. Additionally, the maximum lateral lateral acceleration possible is increased.

yaw-response to a step-input of the steering wheel of three different amplitudes at $t = 0$ were evaluated. The drive force distribution in this study is $\xi = F_{Z_F}/mg$, i.e. fixed AWD. It can be seen that initially, there is no difference between the two vehicles, but as the yaw rate increases, so does the force difference between the left and right wheels for the vehicle with the locked differential. This force difference is against the turn and has a *yaw damping* effect. Further, the limit lateral acceleration using three methods are plotted as horizontal lines. These methods are

$$\begin{aligned} a_Y^{\max} &= (F_{Y_F}^{\lim} + F_{Y_F}^{\lim})/m \\ a_Y^{\lim}|_{\delta=0} &= lF_{Y_F}^{\lim}/(ml_R) \\ a_Y^{\lim}|_{\delta\neq 0} &= l(F_{Y_F}^{\lim} + \delta F_{X_F})/(ml_R) \end{aligned} \tag{4.2}$$

The first method, computing $a_Y \max$, is the lateral acceleration when both front- and rear tires are saturated simultaneously. This lateral acceleration is not possible at steady-state if $M_Z^{\lim} \neq 0$. In transients (such as a step in the steer command), however, the yaw-balance equation in Eq. (3.6) also includes the yaw acceleration, $\ddot{\psi}$, multiplied with the yaw inertia, I_{ZZ}. In fact, it can be shown that $a_Y^{\max}$ can be reached if $I_{ZZ}\ddot{\psi} = M_Z^{\lim}$. Now the second method in Eq. (4.2) is $a_Y^{\lim}$ as given by Eq. (3.7) under the condition that $M_Z^{\lim} < 0$. The results shown in Fig. 4.5, however, show a clear discrepancy between the steady-state lateral acceleration (a_Y as $t \to \infty$) and the estimated $a_Y^{\lim}|_{\delta=0}$. As discussed toward the end of Section 3.2.1, for large steering angles and large longitudinal forces on the front wheels, their contribution cannot be neglected. This is confirmed by the results shown in Fig. 4.5. The conclusions that can be drawn from this analysis is that

- The effect of δF_{X_F} should be included in the computation of $a_Y^{\lim}$ at large steering angles, as in the case of this study where the maximum steering amplitude was $\delta_{\mathrm{H}} = 180^\circ \to \delta \approx 0.2$rad. A simple modification to the lateral grip computation as proposed in Eq. (4.2) is one proposal to take this effect into account.

- As indicated, $a_Y^{\lim}$ is the steady-state maximum lateral acceleration. If yaw acceleration is sufficiently large, i.e. $\ddot{\psi} = M_Z^{\lim}/I_{ZZ}$, the lateral acceleration $a_Y = a_Y^{\max}$, can be reached.

4.3 Dynamic cornering – Sine with Dwell

From the previous study of the lateral acceleration in transients, it was seen that the maximum lateral acceleration attainable at steady-state can be exceeded when the

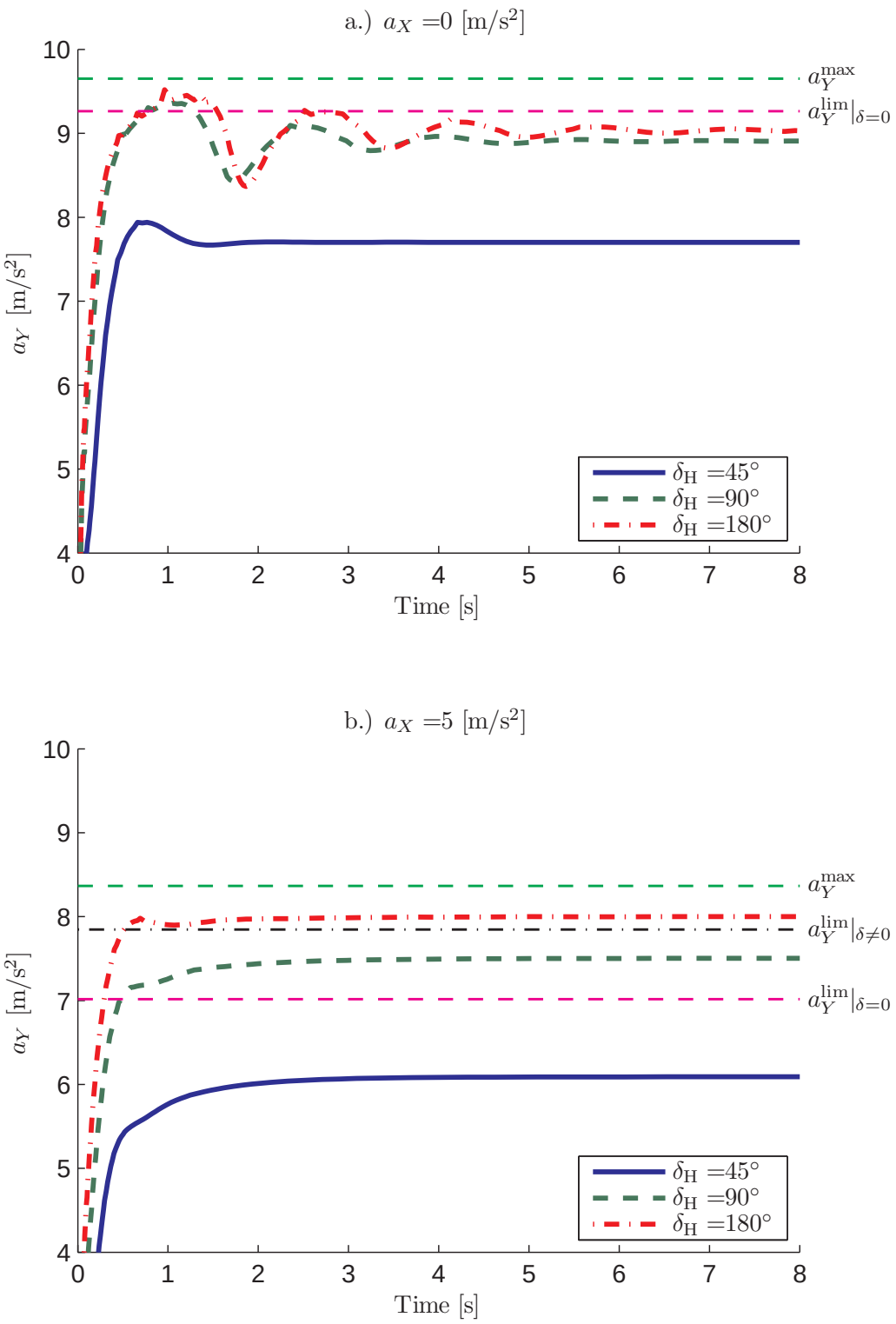

Figure 4.5: At $t = 0$ a steering input of three different amplitudes was applied at a speed of $v_X = 90$km/h. The four sub-figures show the results of four different levels of longitudinal acceleration. The drive force distribution, $\xi = F_{Z_F}/mg$, i.e. fixed AWD. Further, the limit lateral acceleration using three methods are plotted as horizontal lines.

yaw acceleration is large. The step-steer maneuver, however, does not reach $a_Y^{\max}$, as computed in Eq. (4.2) when the vehicle is accelerated. The National Highway Traffic Safety Administration in the United States has proposed an open-loop steering maneuver for evaluating ESC systems, described in the Federal Motor Vehicle Safety Standard (FMVSS) 126 [45]. This test-procedure called the "Sine with Dwell", described in [47], is designed to induce oversteer, which occurs when $\ddot{\psi} \geq M_Z^{\lim}/I_{ZZ}$. This maneuver should be a good candidate to generate sufficient yaw-acceleration to reach $a_Y^{\max}$, here designated as $a_Y^{\max_1}$.

Simulation results shown in Fig. 4.7 indicate a spin-out for high steering angles, since lateral acceleration is sustained even though the steering is zero (compare with Fig. 4.6). In dynamic maneuvers the lateral acceleration should therefor be able to reach $a_Y^{\max_1}$ shown by the thin horizontal dash-dotted lines. The lateral acceleration, however, never reaches this limit, so the $a_Y^{\lim}$ computations appears to have some limitations.

It can be shown that this limitation is, due to an assumption in this work that (with some abuse of notation)

$$F_Y^{\lim} = \sum \sqrt{(\mu_i F_{Z_i})^2 - F_{X_i}^2} \approx \sqrt{(\sum \mu_i F_{Z_i})^2 - (\sum F_{X_i})^2} \; . \tag{4.3}$$

In other words, the assumption is that the sum of the limit lateral forces on each tire on one axle can be computed by summing the normal load and longitudinal force separately. This simplification was done in order to remove the dependency which the lateral force has on the normal force. To estimate how large this simplification is, an attempt was made to compute $a_Y^{\max}$ which takes this effect into account. In short, the computation of a new $a_Y^{\max_2}$ as given by Eq. (4.2) involves now involves the solving of

$$\arg_{a_Y^{\max_2}} \; a_Y^{\max_2} - (F_{Y_F}^{\lim}(a_Y^{\max_2}) + F_{Y_R}^{\lim}(a_Y^{\max_2})/m \equiv 0 \; . \tag{4.4}$$

The results of the computation of $a_Y^{\max_2}$ in this way, is shown as dashed lines in Fig. 4.7. These new results show a good correlation between the actual maximum lateral acceleration and the estimated $a_Y^{\max_2}$ when $a_X = 0$. If, however, $a_X \neq 0$, there is again a deviation between the computed an actual and computed $a_Y^{\max_2}$.

As for the steady-state limit, $a_Y^{\lim_1}$ is computed as in Eq. (3.7). This method, as for $a_Y^{\max}$ in Eq. (4.2), does not take into account the effect of the load transfer. For this purpose, $a_Y^{\lim_2}$ is computed analogous to $a_Y^{\max_2}$. In Fig. 4.8 these two different limits, $a_Y^{\lim_1}$ and $a_Y^{\lim_2}$, are plotted as horizontal lines. As expected, $a_Y^{\lim}$ is never a good measure of the limit lateral acceleration for this maneuver, since steady-state cornering is never achieved.

The conclusions from this study is that

- $a_Y^{\lim}$ is not a valid measure in this maneuver which never reaches steady cornering.

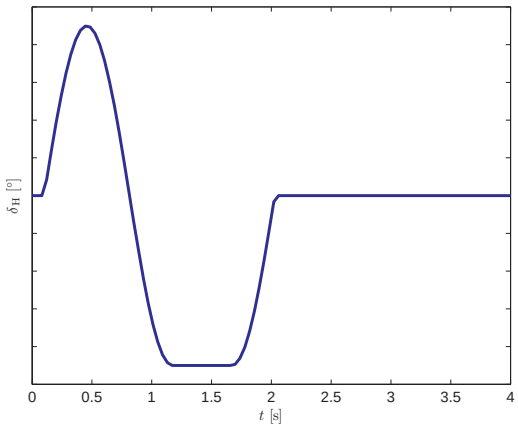

Figure 4.6: Open-loop steering input consisting of a 0.7Hz sine input with a 500ms dwell after 3/4 period. The steering amplitude is varied according to [47].

- The computation of $a_Y^{\max}$, as introduced in the previous section, requires further development since there is a significant lateral load transfer. This proposal is that each tire must be handled separately when computing $F_Y^{\lim}$ instead of computing $F_Y^{\lim}$ using the combined normal load and longitudinal force on the axle.

Finally, this study points the way to future work that needs to be done in order to create a more comprehensive understanding of the lateral grip limits.

4.4 Summary

In this chapter, the main purpose was to evaluate the theories introduced in Chapter 3. One objective of this study was therefor to evaluate the lateral grip estimation accuracy, given the modeling simplifications which were made. For this purpose, a more comprehensive vehicle model was used that took into account more factors than the bicycle model, which influence were of interest. Further, some transient and dynamic maneuvers were performed. The purpose of these simulations was to find limitations in the lateral grip estimations which are a result of the QSS assumption. Even though only a limited number of operating conditions and driveline configurations could be evaluated within the scope of this work, several areas for further development of the lateral results from Chapter 3 were identified. Additionally, further evaluations should include even more comprehensive vehicle models, and eventually real-world measurements. A main conclusion, however, is that the developed theory in Chapter 3 takes into account, and explains, most of the important factors influencing the lateral grip and understeer of the vehicle.

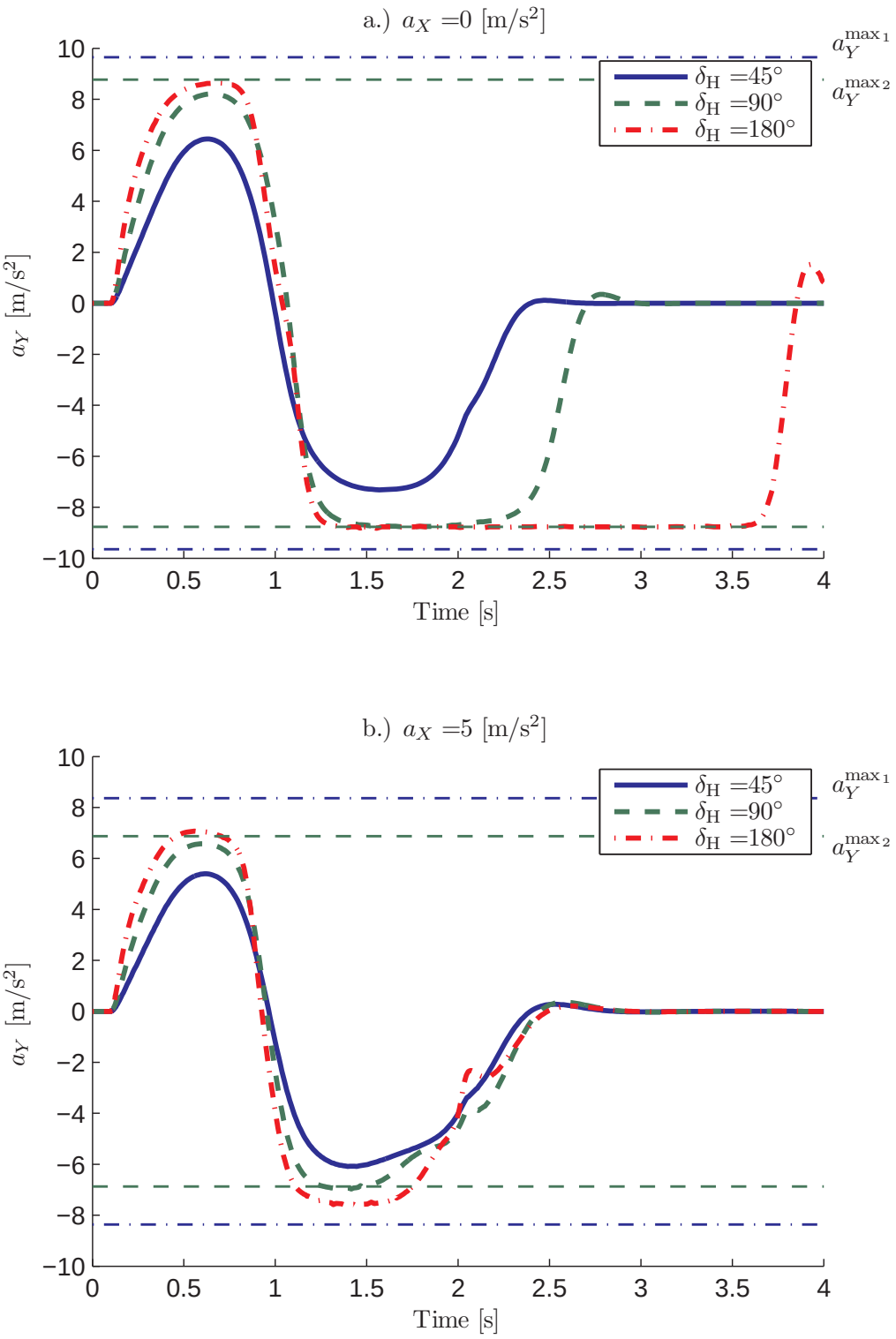

Figure 4.7: Lateral acceleration versus time for a sine-with-dwell maneuver for four different levels of constant drive force. Two different predicted lateral acceleration limits, $a_Y^{\max 1}$ and $a_Y^{\max 2}$ are shown as horizontal lines.

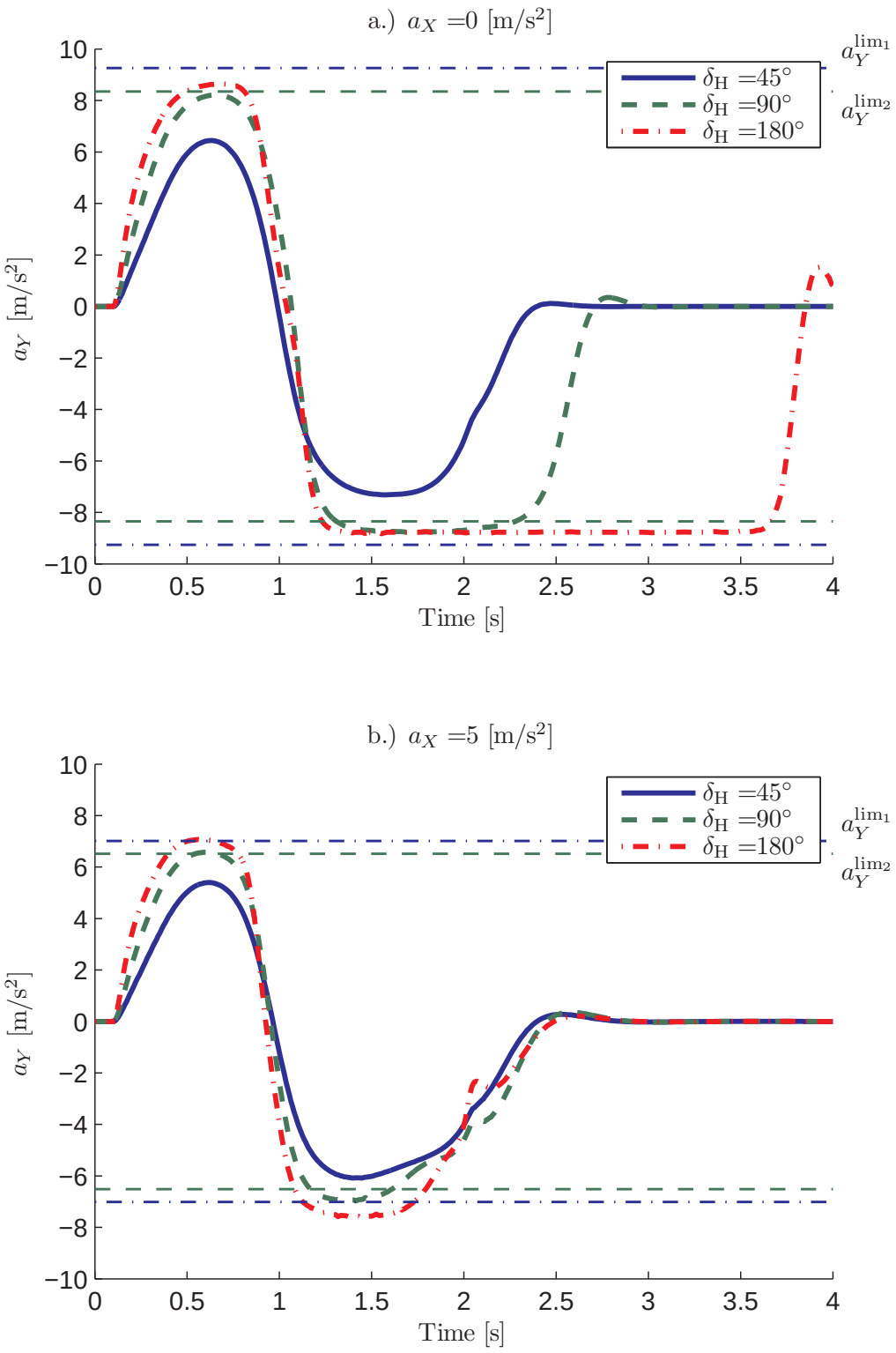

Figure 4.8: Lateral acceleration versus time for a sine-with-dwell maneuver for four different levels of constant drive force. Two different predicted steady state lateral acceleration limits, $a_Y^{\lim_1}$ and $a_Y^{\lim_2}$ are shown as horizontal lines.

The left/right drive force distribution was also shown to permit a constant K_{US} and increased lateral grip limit.

Chapter 5

Future Work and Conclusions

The objective of this study was to show the influence of the drive force distribution on the understeer and the lateral grip of passenger vehicles. It was expected that, if the drive force could be re-distributed freely, the understeer could be kept constant across an expanded range of operating conditions and that the maximum attainable lateral acceleration would be increased relative to a vehicle with fixed drive force distribution. One objective was further to develop a way to measure the lateral grip margin. This measure was aimed to predict the amount of utilization of the lateral grip in a given operating condition (cornering radius and longitudinal acceleration). Moreover, closing the gap in the existing knowledge regarding the influence of drive force distribution on the lateral grip and understeer was another major objective. This has lead the development of new- and enhanced methods which can be used to analyze the effects of front/rear and left/right drive force distribution on the understeer and the lateral grip of the vehicle. Knowing these effects naturally lead to conditions on the drive force distribution for maximum possible lateral grip.

Drivers are known to adapt the vehicle's speed to a limit where the control response (handling) is familiar [71, 7], therefor the vehicle speed would likely increase, if the range where the vehicle handling characteristics are constant is expanded. Since a gradual change in understeer as the grip limit is approached changes the response and damping of the vehicle [40], it can also be viewed as a driver feedback or warning [37]. How to develop this driver feedback is left to future work, but the lateral grip margin developed in this present work is assumed to be useful for this purpose.

As indicated, only the understeer and the lateral grip were studied in this thesis. Moreover, other handling characteristics such as yaw-damping and side-slip control, are not mentioned in great detail in this report. Apart from changing the lateral grip limits and understeer, drive force distribution can also be used to

change the response, damping and stability in transient and dynamic maneuvers. Future work should expand to also cover these aspects.

Summarizing the main contributions of this work, the drive force re-distribution was shown to allow the vehicle to perform consistent with the drivers expectation, i.e. constant understeer, under a large range of operating conditions. Furthermore, it was shown that the vehicle's performance in terms of the combined lateral- and longitudinal grip, by proper drive force distribution on all four wheels, is improved considerably under combined longitudinal acceleration and cornering when compared to two-wheel drive vehicles.

Moreover, the dynamic square (which is a fairly unknown, but useful method) was used to evaluate the influence of front/rear drive force distribution on the lateral grip of the vehicle was described in detail. How to create dynamic squares was namely not clearly described in the paper describing this method [27], but which is done in this work. The method was further developed for the purpose of showing the influence of front/rear drive force distribution on the vehicle understeer.

Another area which is unsatisfactorily described in current literature is a method to evaluate the capabilities of systems which are able to alter the drive force distribution between the left and right wheels. When controlling the drive-forces between the left and right wheels the lateral grip performance and understeer can be optimized for any given operating condition. For the purpose of evaluating these effects, this work proposed to expand the well-known handling diagram [48].

As a summary, the main findings related to effect of the drive force distribution in this work are that

- A lateral grip margin was developed which relating the drive force distribution to the lateral grip.
- Further, for the front/rear drive force distribution:
  - A method on how the drive force distribution influences the lateral grip margin when accelerating was developed from existing methods. The connection between so-called GG-diagrams and this method was also developed as part of this work.
  - Conditions for maximizing the lateral grip were given.
  - Closed-form expressions for four specific driveline configurations were derived from the developed lateral grip margin.
  - The control authority of a selection of hardware realizations of front/rear drive force distribution were shown.
- For the left/right drive force distribution:

- It was shown how the understeer coefficient could be kept constant up to the grip limit and which hardware realizations could achieve this aim.
- Increases the lateral grip to the average of the front and rear axle, rather than the axle that has the least grip.
- When the vehicle is tuned to understeer in steady state conditions, left/right drive force distribution is only required at the rear axle.
- Can, in contrast to front/rear drive force distribution, change the vehicle characteristics regardless of the desired longitudinal acceleration.

In order to estimate the lateral grip margin the following quantities are required to be known:

- The tire/road friction. The accuracy of this estimate is directly related to the accuracy of the lateral grip of the total vehicle. More information is available in [3], co-authored by this author.
- Normal force distribution, which can be estimated from the static load distribution combined with the load transfer due to longitudinal and lateral acceleration.
- The influence of the longitudinal force on the lateral characteristics are assumed be modeled by a friction circle concept, the influence starts to be significant when they start to become a large part of the total capacity. For example, 50% utilisation of the total capacity in the longitudinal direction means less than 14% reduction in the lateral capacity.

This research has had the aim to contribute to an improved understanding of the interaction between drive force distribution and vehicle characteristics. In fulfilling that objective, this work is another piece in the puzzle of understanding road vehicle dynamics, a quest which has been ongoing since the invention of road vehicles. As a further result the improved design and intelligently control driveline systems. As a result the vehicles equipped with these technologies would become increasingly capable and predictable, thereby further contributing to improved vehicle safety – an over-embracing motivation for this research.

Bibliography

[1] ABE, M., "A theoretical analysis on vehicle cornering behaviors in acceleration and in braking", in *9th IAVSD Symposium, Dynamics of Vehicles on Roads and on Tracks*, 1986.

[2] ABE, M., *Vehicle Dynamics and Control*. 2003.

[3] ANDERSSON, M., BRUZELIUS, F., CASSELGREN, J., GÄFVERT, M., HJORT, M., HULTÉN, J., HABRING, F., KLOMP, M., OLSSON, G., SJÖDAHL, M., SVENDENIUS, J., WOXNERYD, S., and WÄLIVAARA, B., "Road friction estimation", tech. rep., IVSS Project Report 2004:17750, 2007.

[4] ANDREASSON, J., *On Generic Road Vehicle Motion Modelling and Control*. PhD thesis, Royal Institute of Technology – Department of Aeronautical and Vehicle Engineering, 2006.

[5] BAKKER, E., NYBORG, L., and PACEJKA, H. B., "Tyre modelling for use in vehicle dynamics studies", in *SAE Technical Paper 870421*, 1987.

[6] BLANK, M. and MARGOLIS, D. L., "Minimizing the path radius of curvature for collision avoidance", *Vehicle System Dynamics*, vol. 33, no. 3, pp. 183–201, 2000.

[7] BOER, E. R., WARD, N. J., MICHAEL, P. M., and KUGE, N., "Driver-model-based assessment of behavioral adaptation", in *JSAE Annual Congress*, 2005.

[8] BRAYSHAW, D. and HARRISON, M., "A quasi steady state approach to race car lap simulation in order to understand the effects of racing line and centre of gravity location", *Proceedings of the Institution of Mechanical Engineers,*

Part D: Journal of Automobile Engineering, vol. 219, pp. 725–739, Jan. 2005.

[9] CHUNG, T. and YI, K., "A vehicle-simulator-based evaluation of combined state estimator and vehiclestability control algorithm", in *SAE Technical Paper 2005-01-0383*, 2005.

[10] FRENDO, F., GRECO, G., GUIGGIANI, M., and SPONZIELLO, A., "The handling surface: a new perspective in vehicle dynamics", *Vehicle System Dynamics*, vol. 45, no. 11, pp. 1001–1016, 2007.

[11] FRENDO, F., GRECO, G., and GUIGGIANI, M., "Critical review of handling diagram and understeer gradient for vehicles with locked differential", *Vehicle System Dynamics*, vol. 44, p. 431447, 2006.

[12] FURUKAWA, Y. and ABE, M., "Advanced chassis control systems for vehicle handling and active safety", *Vehicle System Dynamics*, vol. 28, pp. 59–86, 1997.

[13] GHONEIM, Y. A., LIN, W. C., SIDLOSKY, D. M., CHEN, H. H., CHIN, Y.-K., and TEDRAKE, M. J., "Integrated chassis control system to enhance vehicle stability", *International Journal of Vehicle Design*, vol. 23, pp. 124–144, 2000.

[14] GILLESPIE, T. D., *Fundamentals of Vehicle Dynamics*. SAE, 1992.

[15] GUO, K.-H., "A study of a phase plane representation for identifying vehicle behavior", in *Proc. of 9th IAVSD Symposium, Linköping*, 1985.

[16] HANCOCK, M., WILLIAMS, R., GORDON, T., and BEST, M., "A comparison of braking and differential control of road vehicle yaw-sideslip dynamics", *Proceedings of the Institution of Mechanical Engineers, Part D: Journal of Automobile Engineering*, vol. 219, pp. 309–327, Jan. 2005.

[17] HEYDINGER, G. J., GARROTT, W. R., CHRSTOS, J. P., and GUENTHER, D. A., "The dynamic effects of tire lag on simulation yaw rate predictions", *Journal of dynamic systems, measurement, and control*, vol. 116, pp. 249–256, 1994.

[18] HIEMER, M., *Model Based Detection and Reconstruction of Road Traffic Accidents*. PhD thesis, Universität Karlsruhe, Fakultät für Elektrotechnik und Informationstechnik, 2004.

[19] HOFFMAN, R., LOUCA, L., STEIN, J., and HUH, K., "Using the milliken moment method and dynamic simulation to evaluate vehicle stability and controllability", *ASME Dynamic Systems and Control Division*, vol. 73, pp. 173–180, 2004.

[20] INAGAKI, S., KSHIRO, I., and YARNARNOTO, M., "Analysis on vehicle stability in critical cornering using phase-plane method", *JSAE Review*, vol. 16, pp. 287–292, April 1994.

[21] ISO TECHNICAL COMMITTEE TC 22/SC9, "Vehicle dynamics and road-holding ability - vocabulary", in *ISO 8855*, 1991.

[22] ISO TECHNICAL COMMITTEE TC 22/SC9, "Lateral transient response test methods", in *ISO 7401*, 2003.

[23] ISO TECHNICAL COMMITTEE TC 22/SC9, "Steady-state circular driving behaviour", in *ISO 4138*, 2004.

[24] ISO TECHNICAL COMMITTEE TC 22/SC9, "Braking in a turn", in *ISO 7975*, 2006.

[25] ISO TECHNICAL COMMITTEE TC 22/SC9, "Power-off reaction of a vehicle in a turn", in *ISO 9816*, 2006.

[26] KARNOPP, D., *Vehicle Stability*. Marcel Dekker, Inc., 270 Madison Avenue, New York, NY 10016, USA: CRC Press, 2004.

[27] KATO, M., ISODA, K., and YUASA, H., "Study on vehicle dynamics in marginal condition using dynamic square method", in *SAE Technical Paper 958503*, 1995. SAE-958503.

[28] KLOMP, M., "Passenger car all-wheel drive systems analysis", tech. rep., University West - Division of Mechanical Engineering, 2005.

[29] KLOMP, M. and LIDBERG, M., "Safety margin estimation in steady state maneuvers", in *Proceedings of the 8th International Symposium on Advanced Vehicle Control*, 2006.

[30] LAINE, L., *Reconfigurable Motion Control Systems for Over-Actuated Road Vehicles*. PhD thesis, Chalmers University of Technology, Department of Applied Mechanics, 2007.

[31] LINDER, A., DUKIC, T., HJORT, M., MASTOMS, Y., MARDH, S., SUNDSTRÖM, J., VADEBY, A., WIKLUND, M., and ÖSTLUND, J., "Methods for the evaluation of traffic safety effects of antilock braking system (abs) and

electronic stability control (esc) - a litterature review", tech. rep., VTI report 580A, 2007.

[32] LUKOWSKI, S. A., TENER, D. R., CHU, M. L., and CLAAR, P. W., "Open-loop, fixed-control simulation of a vehicle undergoing steering and acceleration maneuvers", in *SAE Technical Paper 901658*, 1990.

[33] MANNING, W. J. and CROLLA, D. A., "A review of yaw rate and sideslip controllers for passenger vehicles", *Transactions of the Institute of Measurement and Control*, vol. 29, no. 2, pp. 117–135, 2007.

[34] MATSUNO, K. and KOGURE, M., "Estimation of tire-road friction coefficient", *SUBARU Technical Review*, pp. 125–130, 2007.

[35] MATSUNO, K., LE GRAND, R., and MICHAEL, E., "Method and system for road surface friction coefficient estimation", in *United States Patent 2007150156*, 2007.

[36] MATSUNO, K., NITTA, R., INOUE, K., ICHIKAWA, K., and HIWATASHI, Y., "Development of a new all-wheel drive control system", in *Seoul 2000 FlSITA World Automotive Congress*, 2000.

[37] MATSUO, Y. and SEKIDO, S., "Intelligent four-wheel drive system", in *SAE Technical Paper 930670*, 1993.

[38] MILLIKEN, W., WHITCOMB, D., and SEGEL, L., "Research in automobile stability and control and in tyre performance.", in *Proc.I.Mech.E. Auto. Div*, 1956.

[39] MILLIKEN, W. F., DEL'AMICO, F., and RICE, R. S., "The static directional stability and control of the automobile", in *SAE Technical Paper 760712*, 1976.

[40] MILLIKEN, W. F. and MILLIKEN, D. L., *Race Car Vehicle Dynamics*. SAE International, 1995. 1-56091-526-9.

[41] MILLIKEN, W. F. and MILLIKEN, D. L., *Chassis Design - Principles and Analysis*. SAE International, 2002.

[42] MILLIKEN, W. F., WRIGHT, P. G., and MILLIKEN, D. L., "Moment method - a comprehensive tool for race car development", in *SAE Technical Paper 942538*, 1994.

[43] MITSCHKE, M. and WALLENTOWITZ, H., *Dynamik der Kraftfahrzeuge*. Springer, 2004.

[44] MIURA, Y., TOKUTAKE, H., and FUKUI, K., "Handling qualities evaluation method based on actual driver characteristics", *Vehicle System Dynamics*, vol. 45, no. 9, pp. 807–817, 2007.

[45] NATIONAL HIGHWAY TRAFFIC SAFETY ADMINISTRATION (NHSTA, "Federal motor vehicle safety standards; electronic stability control systems; controls and displays; final rule", *Federal Register*, vol. 72, pp. 17235–17322, April 2007.

[46] NHSTA, "Notice of proposed rulemaking for electronic stability control systems", tech. rep., Docket No. NHTSA2006-25801, 2006.

[47] NHSTA, "Labratory test procedure for fmvss 126, electronic stability control systems", in *TP126-00*, 2007.

[48] PACEJKA, H. B., "Simplified analysis of steady-state behaviour of motor vehicles", *Vehicle System Dynamics*, vol. 2, pp. 161172, 173183, 185204, 1973.

[49] PACEJKA, H. B., *Tire and Vehicle Dynamics*. SAE, 2nd ed., 2005.

[50] PEDRINELLI, M. P. and CHELI, F., "Vehicle dynamics control system actuating an active differential", in *SAE Technical Paper 2007-01-0928*, 2007.

[51] RAJAMANI, R., *Vehicle Dynamics and Control*. Springer, 2006.

[52] RICE, R. S., "Measuring car-driver interaction with the g-g diagram", in *SAE Technical Paper 730018*, 1973.

[53] RICE, R. S. and ALIANELLO, D. A., "A driver characterization function - the g-g diagram", in *Cornell Aeronautical Laberatory Report No. VJ-2882-K*, 1970.

[54] SAE, "Vehicle aerodynamics terminology", in *SAE Standard J1594*, 1994.

[55] SAWASE, K. and SANO, Y., "Application of active yaw control to vehicle dynamics by utilizing driving/braking force", *JSAE Review*, vol. 20, pp. 289–295, 1999.

[56] SAWASE, K., USHIRODA, Y., and MIURA, T., "Left-right torque vectoring technology as the core of super all wheel control (s-awc)", *Mitsubishi Motors Technical Review*, vol. 18, pp. 16–23, 2006.

[57] SCHNEIDER, K. R. and WILHELM, T., "Model reduction by extended quasi-steady-state approximation", *WIAS Preprints*, no. 457, 1998.

[58] SEGEL, L. A. and SLEMROD, M., "The quasi-steady-state assumption: A case study in perturbation", *Study for Industrial and Applied Mathemathics Review*, vol. 31, pp. 446–477, September 1989.

[59] SHEN, S., WANG, J., SHI, P., and PREMIER, G., "Nonlinear dynamics and stability analysis of vehicle plane motions", *Vehicle System Dynamics*, vol. 45, pp. 15–35, Jan. 2007.

[60] SHIBAHATA, Y., ABE, M., SHIMADA, K., and FURUKAWA, Y., "Improvement on limit performance of vehicle motion by chassis control", *Vehicle System Dynamics*, vol. 23 (suppl), pp. 449–469, 1994.

[61] SHIBAHATA, Y., SHIMADA, K., and TOMARI, T., "The improvement of vehicle maneuverability by direct yaw moment control", in *International Symposium on Advanced Vehicle Control*, 1992.

[62] SHIBAHATA, Y., SHIMADA, K., and TOMARI, T., "Improvement of vehicle maneuverability by direct yaw moment control", *Vehicle System Dynamics*, vol. 22, pp. 465–481, 1993.

[63] SVENDENIUS, J., *Tire Modeling and Friction Estimation*. PhD thesis, Lund University, Department of Control, 2007.

[64] TOMARI, T., MORI, A., and SHIBAHATA, Y., "Development of sh-awd based on dyc (direct yaw control) concept", in *Proceedings of AVEC '06*, 2006.

[65] TRUE, H., "On the theory of nonlinear dynamics and its applications in vehicle systems dynamics", *Vehicle System Dynamics*, vol. 31, no. 5, pp. 393–421, 1999.

[66] TSENG, H. E., MADAU, D., B.ASHRAFI, BROWN, T., and RECKER, D., "Technical challenges in the development of vehicle stability control system", in *1999 IEEE International Conference on Control Applications*, 1999.

[67] TSENG, H. E., ASHRAFI, B., MADAU, D., BROWN, T. A., and RECKE, D., "The development of vehicle stability control at ford", *IEEE/ASME Transactions on Mechatronics*, vol. 4, pp. 223–234, September 1999.

[68] TURANYI, T., TOMLIN, A., and PILLING, M., "On the error of the quasi-steady-state approximation", *The Journal of Physical Chemistry*, vol. 97, pp. 163–172, 1993.

[69] UFFELMANN, F., "Automotive stability and handling dynamics in cornering and braking meanuevers", *Vehicle System Dynamics*, vol. 12, pp. 203–223, 1983.

[70] USHIRODA, Y., SAWASE, K., ANDKEIJI SUZUKI, N. T., and MANABE, K., "Development of super ayc", *Mitsubishi Technical Review*, vol. 18, pp. 73–76, 2003.

[71] VAN WINSUM, W. and GODTHELP, H., "Speed choice and steering behavior in curve driving", *Human Factors*, vol. 38, no. 3, pp. 434–441, 1996.

[72] VAN ZANTEN, A. T., "Bosch esp systems: 5 years of experience", in *SAE Technical Paper 2000-01-1633*, 2000.

[73] WHEALS, J. C., BAKER, H., RAMSEY, K., and TURNER, W., "Torque vectoring awd driveline: Design, simulation, capabilities and control", in *SAE Technical Paper 2004-01-0863*, 2004.

[74] WONG, J. Y., *Theory of Ground Vehicles*. John Wily & Sons, 3rd ed., 2001.

[75] YAMAMOTO, M., "Advice control strategy for improved handling and stability", in *SAE Technical Paper 911902*, 1991.

[76] ZUURBIER, J. and BREMMER, P., "State estimation for integrated vehicle dynamics control", in *Proceedings of the 6th International Symposium on Advanced Vehicle Control*, 2002.

Appendix A

Simulation Model

This chapter contains the details of the vehicle model used for simulations in this work.

A.1 Equations of motion

The planar dynamics have three degrees of freedom; two translational (longitudinal and lateral) and one rotational (yaw). The equations of motion according the Newtons second law become

$$\begin{aligned} m(\underbrace{\dot{v}_X - v_Y\dot{\psi}}_{a_X}) &= \sum_{i=1}^{4} F_{X_i} + F_{\mathrm{D}} \\ m(\underbrace{\dot{v}_Y + v_X\dot{\psi}}_{a_Y}) &= \sum_{i=1}^{4} F_{Y_i} \\ I_{ZZ}\ddot{\psi} &= l_F \sum_{i=1}^{2} F_{Y_i} - l_R \sum_{i=3}^{4} F_{Y_i} + \frac{b}{2}\sum_{i=1}^{4}(-1)^i F_{X_i} \end{aligned} \tag{A.1}$$

which can easily be re-writing to state-space form $\dot{\boldsymbol{x}} = \mathrm{f}(\boldsymbol{x}, \boldsymbol{u})$, where $\boldsymbol{u} = \delta$ and $\boldsymbol{x} = [v_X \; v_Y \; \dot{\psi}]^{\mathrm{T}}$ for simulation implementations an where the front and rear longitudinal forces expressed in the wheel coordinate system $X_W - Y_W$ are when projected onto the vehicle reference frame $X - Y$ for small δ are

$$\begin{aligned} \sum_{i=1}^{4} F_{X_i} &= \sum_{i=1}^{4} F_{X_{Wi}} - \delta \sum_{i=1}^{2} F_{Y_{Wi}} \\ \sum_{i=1}^{4} F_{Y_i} &= \sum_{i=1}^{4} F_{Y_{Wi}} + \delta \sum_{i=1}^{2} F_{X_{Wi}} \end{aligned} \tag{A.2}$$

The drag force, F_{D} can be divided into rolling resistance and aerodynamic drag as

$$F_{\mathrm{D}} = C_{\mathrm{RR}} mg \mathrm{sign}\, v_X + \frac{1}{2}\rho_{\mathrm{air}} A_F C_{\mathrm{D}} |v_X| v_X; . \tag{A.3}$$

For practical implementations, the sign function can be replaced with the $\tanh$ function to avoid numerical issues.

A.2 Wheel Speeds

The wheel speeds of each wheel given in the vehicle reference frame are:

$$\begin{aligned} v_{X_i} &= \begin{bmatrix} 1 & 0 & 0 \end{bmatrix} R_i (\boldsymbol{v}_{O'} + \boldsymbol{\Omega} \times \boldsymbol{r}_{W_i}) \\ &= \begin{bmatrix} 1 & 0 & 0 \end{bmatrix} R_i \left(\begin{bmatrix} v_X \\ v_Y \\ 0 \end{bmatrix} + \begin{bmatrix} 0 \\ 0 \\ \dot{\psi} \end{bmatrix} \times \boldsymbol{r}_{W_i} \right) , \end{aligned} \tag{A.4}$$

where $\boldsymbol{r}_{Wi}$ for each respective wheel ($i = 1, 2, 3, 4$) in the chassis frame is

$$\begin{aligned} \boldsymbol{r}_{W_1} &= \begin{bmatrix} l_F & b_F/2 & 0 \end{bmatrix}^T \\ \boldsymbol{r}_{W_2} &= \begin{bmatrix} l_F & -b_F/2 & 0 \end{bmatrix}^T \\ \boldsymbol{r}_{W_3} &= \begin{bmatrix} -l_F & b_R/2 & 0 \end{bmatrix}^T \\ \boldsymbol{r}_{W_4} &= \begin{bmatrix} -l_F & -b_R/2 & 0 \end{bmatrix}^T \end{aligned} \tag{A.5}$$

and R_i, the rotation matrix for each wheel

$$R_i = \begin{bmatrix} \cos\delta_i & \sin\delta_i & 0 \\ -\sin\delta_i & \cos\delta_i & 0 \\ 0 & 0 & 1 \end{bmatrix} \approx \begin{bmatrix} 1 & \delta_i & 0 \\ -\delta_i & 1 & 0 \\ 0 & 0 & 1 \end{bmatrix} , \tag{A.6}$$

if δ_i is assumed to be small. The wheel patch contact speeds now become

$$\boldsymbol{v}_{X_W} = \begin{bmatrix} v_X - b\dot{\psi}/2 + (v_Y + l_f\dot{\psi})\delta \\ v_X + b\dot{\psi}/2 + (v_Y + l_f\dot{\psi})\delta \\ v_X - b\dot{\psi}/2 \\ v_X + b\dot{\psi}/2 \end{bmatrix} , \tag{A.7}$$

when setting $\delta_1 = \delta_2 = \delta$ and $\delta_3 = \delta_4 = 0$ and $b_f \approx b_r = b$. Interesting to note is the speed difference left/right, $\Delta v_X^{\mathrm{L/R}} = b\dot{\psi}$ and front/rear $\Delta v_X^{\mathrm{F/R}} = (v_Y + l_f\dot{\psi})\delta$, which is of importance when transferring torque using speed control of the wheels.

A.3 Slip Angles

Similar to the wheel speed computation above we have in the wheel reference frame

$$\boldsymbol{v}_{Wi} = \boldsymbol{v}_{O'} + \boldsymbol{\Omega} \times \boldsymbol{r}_{Wi} = \begin{bmatrix} v_X \\ v_Y \\ v_Z \end{bmatrix} + \begin{bmatrix} 0 \\ 0 \\ \dot{\psi} \end{bmatrix} \times \boldsymbol{r}_{Wi} \tag{A.8}$$

From Eq. (A.8) to the slip angles are derived according the definition given in Eq. (2.2) as follows:

$$\boldsymbol{\alpha} = \begin{bmatrix} \delta - \tan^{-1}((v_Y + \dot{\psi} l_f)/(|v_X - \dot{\psi} b/2|)) \\ \delta - \tan^{-1}((v_Y + \dot{\psi} l_f)/(|v_X + \dot{\psi} b/2|)) \\ -\tan^{-1}((v_Y - \dot{\psi} l_r)/(|v_X - \dot{\psi} b/2|)) \\ -\tan^{-1}((v_Y - \dot{\psi} l_r)/(|v_X + \dot{\psi} b/2|)) \end{bmatrix} \tag{A.9}$$

A.4 Static load transfer

Given $m_s << m_u$, $m_u \approx m$:

$$\boldsymbol{F}_Z = m \begin{bmatrix} (l_R g - h a_X)/2l - (\gamma h_0 + h_{\varphi_F} l_R/l) a_Y/b \\ (l_R g - h a_X)/2l + (\gamma h_0 + h_{\varphi_F} l_R/l) a_Y/b \\ (l_F g + h a_X)/2l - ((1-\gamma) h_0 + h_{\varphi_R} l_F/l) a_Y/b \\ (l_F g + h a_X)/2l + ((1-\gamma) h_0 + h_{\varphi_R} l_F/l) a_Y/b \end{bmatrix}, \tag{A.10}$$

where γ is the ratio between the front- and total roll stiffness. See Section A.5 for more details.

The distance of the sprung mass to the roll axis, h_0, relates to the front- and rear roll centers, h_{φ_F} and h_{φ_R}, and h as

$$h_0 = h - ((h_{\varphi_R} - h_{\varphi_F}) l_F/l + h_{\varphi_F}) \tag{A.11}$$

A.5 Roll Dynamics

The pure roll dynamics (not considering the coupling between yaw and roll dynamics) can be expressed by the following dynamic equation:

$$(\bar{I}_{XX} + m_s h_0^2)\ddot{\varphi} + \frac{\partial M_X}{\partial \dot{\varphi}}\dot{\varphi} + \frac{\partial M_X}{\partial \varphi}\varphi = m_s h_0 (a_Y + g\varphi) \tag{A.12}$$

Rewriting as a state-space equation and taking he lateral acceleration, $[a_y]$ as the input vector, the above equation becomes:

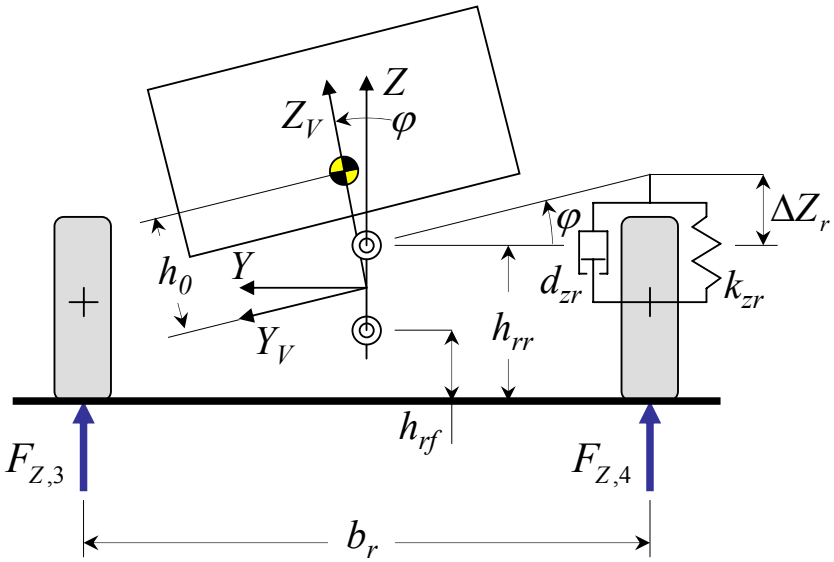

Figure A.1: Rear view of vehicle model including roll dynamics

$$\frac{d}{dt}\begin{bmatrix}\varphi\\ \dot{\varphi}\end{bmatrix} = \begin{bmatrix}1 & 0\\ 0 & \bar{I}_{XX}+m_s h_0^2\end{bmatrix}^{-1}\begin{bmatrix}0 & 1\\ m_s h_0 g - \frac{\partial M_X}{\partial \varphi} & -\frac{\partial M_X}{\partial \dot{\varphi}}\end{bmatrix}\begin{bmatrix}\varphi\\ \dot{\varphi}\end{bmatrix} + \frac{m_s h_0}{\bar{I}_{XX}+m_s h_0^2}\begin{bmatrix}0\\ 1\end{bmatrix}[a_Y] \tag{A.13}$$

At steady-state the lateral acceleration, $a_Y = v_X\dot{\psi}$ and the roll angle

$$\varphi = \frac{m_s h_0}{\frac{\partial M_X}{\partial \varphi} - m_s h_0 g} v_X \dot{\psi} \tag{A.14}$$

A.5.1 Roll Center Height

The front and rear suspensions are assumed to have a fixed roll center height, h_r, determined by the layout of each suspension. If h is height of the CoM above the ground, the height above the roll axis h_0 is computed as from the front and rear roll center heights as:

$$h_0 = h - ((h_{rr} - h_{rf})l_f/l + h_{rf}) \tag{A.15}$$

A.5.2 Roll Stiffness and Damping

Considering a linear spring stiffness k and damping coefficient d at the wheel center the roll stiffness and damping respectively of each axle can be computed. Usually each axle is also equipped with an anti-roll bar which roll stiffness k_φ is added to the contribution from the springs. If a roll moment, M_X is applied to the vehicle body, the reaction moment from the front and rear suspension can be expressed as:

$$\begin{aligned} M_X =& 2(k_{zf} \underbrace{\frac{b_f}{2}\varphi}_{\Delta Z_f} + d_{zf} \underbrace{\frac{b_f}{2}\dot{\varphi}}_{\dot{Z}_f})\frac{b_f}{2} + k_{\varphi f}\varphi + 2(k_{zr} \underbrace{\frac{b_r}{2}\varphi}_{\Delta Z_r} + d_{zr} \underbrace{\frac{b_r}{2}\dot{\varphi}}_{\dot{Z}_r})\frac{b_r}{2} + k_{\varphi r}\varphi \\ =& \underbrace{\left(\frac{k_{zf}b_f^2 + k_{zr}b_r^2}{2} + k_{\varphi f} + k_{\varphi r}\right)}_{\partial M_X/\partial\varphi}\varphi + \underbrace{\frac{d_{zf}b_f^2 + d_{zr}b_f^2}{2}}_{\partial M_X/\partial\dot{\varphi}}\dot{\varphi} \end{aligned} \tag{A.16}$$

The roll moment also has a small effect on the Z-axis of the vehicle due to the inclination of the roll axis which is neglected here.

Appendix B

Evaluation of lateral grip margin estimation

This chapter contains data obtained from a series of verification tests described in Chapter 4. The purpose of this was evaluate the various modeling effects which are not included in the theory developed in Chapter 3. First a fully detailed model was used; including the aero drag and rolling resistance; steer effects (off-direction forces projected due to steering of the front wheel); and lateral load transfer. The succeeding rows start with disabling all these effects, thereafter turning them on one at a time. The influence on the maximum lateral acceleration and the longitudinal acceleration are collected in Table B.1 and Table B.2. Conclusions are given in Section 4.1.

Asphalt ($\mu_0 = 1$)					
F_X^{IN}/m	**Drivline**	a_X^{lim}	a_Y^{max}	a_x^{max}	a_Y^{min}
Full model					
1,0	FWD	8,9	7,9	0,8	0,3
1,0	RWD	9,1	7,9	0,8	0,3
1,0	AWD	9,0	7,9	0,8	0,3
3,0	FWD	7,0	6,1	2,8	0,2
3,0	RWD	8,6	7,4	2,8	1,9
3,0	AWD	8,2	7,4	2,8	0,3
No lateral load transfer, steer effect or drag					
1,0	FWD	8,9	8,8	1,0	1,0
1,0	RWD	9,1	9,0	1,0	1,0
1,0	AWD	9,0	9,0	1,0	1,0
3,0	FWD	7,0	6,9	3,0	3,0
3,0	RWD	8,6	8,4	3,1	3,0
3,0	AWD	8,2	8,1	3,0	3,0
Lateral load transfer considered					
1,0	FWD	8,9	7,9	1,0	1,0
1,0	RWD	9,1	8,1	1,0	1,0
1,0	AWD	9,0	8,0	1,0	1,0
3,0	FWD	7,0	5,8	3,0	3,0
3,0	RWD	8,6	7,3	3,0	2,4
3,0	AWD	8,2	7,2	3,0	3,0
Effect of steering angle considered					
1,0	FWD	8,9	9,0	1,0	0,5
1,0	RWD	9,1	9,0	1,0	0,5
1,0	AWD	9,0	9,0	1,0	0,5
3,0	FWD	7,0	7,4	3,0	2,6
3,0	RWD	8,6	8,1	3,0	2,6
3,0	AWD	8,2	8,4	3,0	2,6
Aero drag and rolling resistance considered					
1,0	FWD	8,9	8,8	0,8	0,4
1,0	RWD	9,1	9,0	0,8	0,5
1,0	AWD	9,0	8,9	0,8	0,4
3,0	FWD	7,0	6,9	2,8	0,2
3,0	RWD	8,6	8,0	2,8	2,8
3,0	AWD	8,2	8,1	2,8	0,4

Table B.1: Verification of lateral grip margin estimation on a dry surface $(\mu_0 = 1)$. Units are [m/s^2], where applicable.

Snow ($\mu_0 = 0.4$)					
F_X^{IN}/m	**Drivline**	a_X^{lim}	a_Y^{max}	a_x^{max}	a_Y^{min}
Full model					
0,5	FWD	3,6	3,6	0,3	0,1
0,5	RWD	3,7	3,6	0,3	0,1
0,5	AWD	3,6	3,6	0,3	0,1
1,0	FWD	3,2	3,3	0,8	0,1
1,0	RWD	3,6	3,4	0,8	0,6
1,0	AWD	3,5	3,5	0,8	0,1
No lateral load transfer, steer effect or drag					
0,5	FWD	3,6	3,6	0,5	0,5
0,5	RWD	3,7	3,7	0,5	0,5
0,5	AWD	3,6	3,6	0,5	0,5
1,0	FWD	3,2	3,2	1,0	1,0
1,0	RWD	3,6	3,7	1,1	0,7
1,0	AWD	3,5	3,5	1,0	1,0
Lateral load transfer considered					
0,5	FWD	3,6	3,6	0,5	0,5
0,5	RWD	3,7	3,7	0,5	0,5
0,5	AWD	3,6	3,6	0,5	0,5
1,0	FWD	3,2	3,2	1,0	1,0
1,0	RWD	3,6	3,7	1,1	0,7
1,0	AWD	3,5	3,5	1,0	1,0
Effect of steering angle considered					
0,5	FWD	3,6	3,6	0,5	0,3
0,5	RWD	3,7	3,7	0,5	0,3
0,5	AWD	3,6	3,7	0,5	0,3
1,0	FWD	3,2	3,4	1,0	0,8
1,0	RWD	3,6	3,6	1,0	0,7
1,0	AWD	3,5	3,6	1,0	0,8
Aero drag and rolling resistance considered					
0,5	FWD	3,6	3,6	0,3	0,1
0,5	RWD	3,7	3,7	0,3	0,1
0,5	AWD	3,6	3,6	0,3	0,1
1,0	FWD	3,2	3,2	0,8	0,1
1,0	RWD	3,6	3,6	1,0	0,7
1,0	AWD	3,5	3,5	0,8	0,1

Table B.2: Verification of lateral grip margin estimation on a snowy surface ($\mu_0 = 0.4$). Units are [m/s^2], where applicable.

Appendix C

Vehicle Data

This chapter contains the technical data of the vehicle which was used for the various simulations and evaluations.

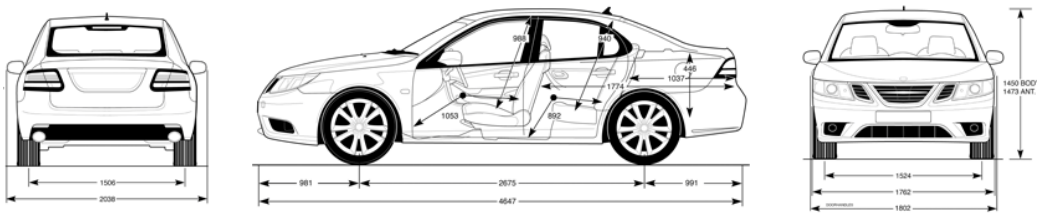

Figure C.1: Vehicle dimensions

Par.	Value	Unit	Description
ρ	1.204	[kg/m^3]	http://en.wikipedia.org/wiki/Density_of_air
g	9.81	[m/s^2]	Gravitational constant
μ	1.0	[-]	Friction coefficient

Table C.1: Environment

Par.	Value	Unit	Description
$v_X^{\max}$	220	[km/h]	Top speed (unconstrained)
$t_{0\rightarrow100}$	8.5	[s]	Acceleration 0 to 100 km/h
$t_{60\rightarrow100}$	8.5	[s]	Acceleration 60 to 100 km/h (4:th gear)
$t_{80\rightarrow120}$	12.5	[s]	Acceleration 80 to 120 km/h (5:th gear)

Table C.2: Vehicle Performance

Par.	Value	Unit	Description
m	1675	[kg]	Curb weight (full tank, no driver or pass.)
m^{payload}	450	[kg]	Maximum payload (driver not included)
$\boldsymbol{I}$	$\begin{bmatrix} 540 & 0 & 50 \\ 0 & 2398 & 0 \\ 50 & 0 & 2617 \end{bmatrix}$	[kg m^2]	Inertia matrix
l	2.675	[m]	Wheel base
l_F	$0.4l$	[m]	Distance along X-axis from CoG to front axle
l_R	$0.6l$	[m]	Distance along X-axis from CoG to rear axle
b_F	1.517	[m]	Track width front
b_R	1.505	[m]	Track width rear
h	0.50	[m]	Distance along Z-axis from CoG to ground
A_F	2.17	[m^2]	Front area
C_{D}	0.30	[-]	Air drag coefficient

Table C.3: Vehicle Body

Roll damping & stiffness

$$k_\varphi = k_Z b^2/2 + k^{\text{aux}} \tag{C.1}$$

$$d_\varphi = d_Z b^2/2 \tag{C.2}$$

Par.	Value	Unit	Description
m_{u}	185	[kg]	Unsprung mass all four wheels
k_{Z_F}	30.8·10^3	[N/m]	Front Susp. Ride Rate (w/o tire)/side
k_{Z_R}	29.9·10^3	[N/m]	Rear Susp. Ride Rate (w/o tire)/side
d_{Z_F}	4500	[Ns/m]	Suspension damping front, per side
d_{Z_R}	3500	[Ns/m]	Susp. damping rear, per side
k_F^{aux}	16.22	[N/rad]	Front aux. roll stiffness (w/o springs)
k_R^{aux}	7.837	[N/rad]	Rear aux. roll stiffness (w/o springs)
h_{φ_F}	4.49·10^3	[m]	Front roll center hight above ground
h_{φ_F}	0.101	[m]	Rear roll center hight above ground

Table C.4: Suspension

Par.	Value	Unit	Description
F_Z^0	4000	[N]	Force around which tire characteristics are linearized
μ_1	6.0·10^{-5}	[N^{-1}]	Friction versus normal load
c_0	21.3	[-/rad]	Normalized cornering stiffness
c_1	11.1·10^{-5}	[N^{-1}]	Normalized cornering stiffness vs. load
C_{RR}	0.0164	[N/kg]	Rolling resistance constant
$C2_{\mathrm{RR}}$	4.0·10^{-8}	[Ns^2/m kg]	Rolling resistance velocity squared term
L_Y	0.6	[m]	Tire lag to lateral force buildup
L_X	0.3	[m]	Tire lag to longitudinal force buildup
r_{dyn}	0.316	[m]	Static rolling radius of tire
J_ω	1.0	[kg m^2]	Spin inertia for one wheel + brake rotor

Table C.5: Tire Data

Par.	Value	Unit	Description
i_{S}	15.9	[-]	Ratio of steering gear
k_δ	115	[Nmm/rad]	Steering column stiffness
q	57.8	[mm]	King-pin lateral offset @ center
r	-0.58	[mm]	King-pin lateral offset @ ground
σ	0.23	[rad]	King-pin inclination angle
r_τ	14.6	[mm]	Castor trail @ ground
τ	0.057	[rad]	Castor inclination angle

Table C.6: Steering data & geometry

Gear	**Ratio [-]**
1st	3.385
2nd	1.760
3rd	1.179
4th	0.894
5th	0.660
Reverse	-3.166
Final	4.059
Power take-off unit (PTU)	2.782
Rear drive module (RDM)	2.769

Table C.7: Manual transmission, PTU and RDM ratios

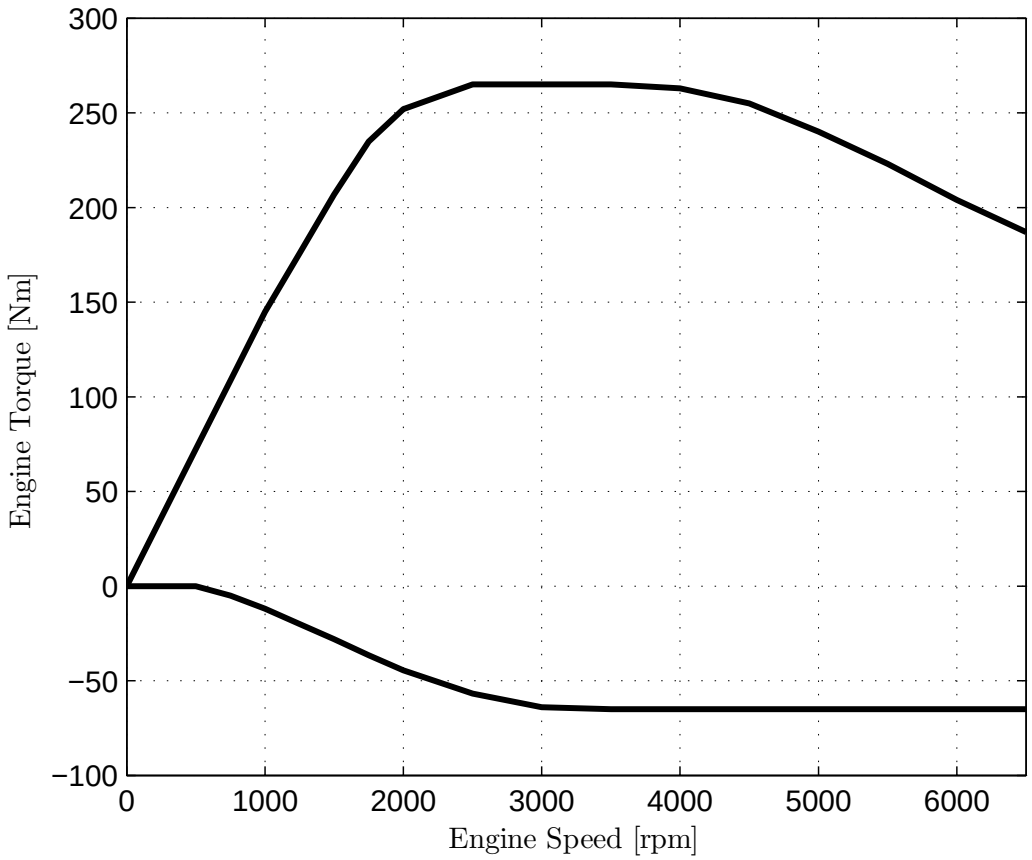

Figure C.2: Engine map for wide-open (WOT) and closed throttle

Appendix D

Gauss-Newton Solver

This solver[1] was used for solving of all the non-linear problems in this work.

```
% Purpose: Finds and returns an approximate solution X, within a given
%          error tolerance tol, of F(X(i-1)) - F(X(i)) ≤ tol
%          using Newtons metod starting from a given initial vector X0.
%          For over-determined systems, the solver gives the optimal
%          solution in a least-square sense.
% Usage:   [X,iter] = MyNewtonSysSolver(F, X0)
% Example: [X,iter] = MyNewtonSysSolver(@(x) [sin(x(1));x(2)-x(1)^2],[4;0])

function [X,iter] = MyNewtonSysSolver(F, X0)
h = 1e-8; gamma = 1; tol = sqrt(h); % Use a absolute tolerance
X = X0; dX = tol + 1; iter=0; d = length(X); e = eye(d);
dY = zeros(length(feval(F,X)),d); % Intialize Jacobian
while norm(dX) > tol && iter < 100
    Y  = feval(F,X);
    for i = 1:d
        dY(:,i) = (feval(F,X+h*e(:,i))-Y)/h; % Jacobian
    end
    c = rcond(dY'*dY); % Check how nice this matrix is...
    if (isnan(c) || c<eps), X=NaN*X0; return, end
    dX = - (dY'*dY)\(dY'*Y);
    X = X + gamma*dX ;
    iter = iter +1;
end
if iter == 100  % Terminate if the tolerance criteria has not been met
                                % after a set number of iterations.
    disp('Warning: not converged!')
    X = NaN*X0;
end
```

[1] http://en.wikipedia.org/wiki/Gauss-Newton_algorithm